A THESIS

entitled

THE EFFECT OF CRYSTALLITE SIZE ON THE MELTING POINT OF TIN.

by

Christopher R.M. Wronski B.Sc., A.R.C.S.

Submitted for the

Degree of Doctor of Philosophy

of the University of London.

Imperial College of Science and Technology,

London

1963.

A B S T R A C T

This thesis deals with size dependence of the melting point of small spherical tin crystallites. Transmission electron diffraction and electron microscopy methods were used to obtain a relationship between the melting point of a crystallite and its radius.

Specimens consisting of spherical tin crystallites were prepared in an electron diffraction camera by evaporating tin onto thin amorphous films. The melting point of a specimen was determined by observing the temperature at which the diffraction pattern rings consistent with the solid polycrystalline phase ceased to be visible. The mass distribution of the crystallites was found by examining micrographs of the specimen, obtained by means of an electron microscope. From these measurements, and from further experiments it was possible to determine the ratio of liquid to solid masses at which the sharp ring electron diffraction pattern became obscured. It was then possible to calculate the radius which was to be associated with the melting temperature of the specimen.

Lattice parameters were measured to investigate any possible change with size, in the structure and density of the crystallites. By using two different amorphous substrates (silicon monoxide and carbon) it was concluded that the type of amorphous base did not affect the results.

A theoretical treatment of the phase equilibrium between solid and liquid using thermodynamic methods is also given. Two models of melting are

discussed to obtain theoretical relationships between the melting point of the crystallites and their size. The theoretical results obtained are correlated with the experimental observations.

C O N T E N T S

ßßßßßßßßßßßßßßßßßß

CHAPTER I
INTRODUCTION

1. Surface Effects on Solid Phases.

When a phase of indefinite extent is in thermodynamic equilibrium, its properties are uniform throughout. However if the phase is not indefinitely extended so that there is a surface associated with the phase, there is a discontinuity in the uniform distribution of matter. This discontinuity results in the individual atoms in or near the surface having a different energy and being subject to different atomic forces from the atoms in the interior. The different physical and thermodynamic properties of the surface, therefore, must be considered in the general treatment of thermodynamic equilibrium between phases as Gibbs pointed out in his work on "The Equilibrium of Heterogeneous Substances". The surface effects are negligible when normal bulk properties of a substance are considered, and only become appreciable when the size of the substance is decreased sufficiently for the energy associated with the surface to become an appreciable fraction of the total energy of the system or when the different forces at the surface affect the stresses in the interior of the phase. These effects increase as the size decreases.

Since for a long time, the observation of surface effects was limited to optical methods, sizes at which surface effects on solids became appreciable could not be observed. However with the advent of X-rays, electron diffraction and electron microscopy, surface effects

on the physical properties of the whole solid particle could be measured. Nicolson (1950), using finely powdered magnesium oxide in X-ray analysis, observed a contraction in the lattice spacing of particles of mean size 600 Å which closely agreed with those expected from surface stress effects. Bublik and Pines (1952) found, by transmission electron diffraction on thin unsupported metal films of chromium, nickel, vanadium and cobalt, that the structure of the film depended on their mean thickness. They explained this change in terms of surface free energy effects.

2. Investigations of the Effect of Surfaces on the Melting-Point.

The effect of surface on solid-liquid phase change was investigated as early as the beginning of this century. Pavlov (1909) observed a lowering of the melting point of a solid in the form of a finely divided powder. Meissner (1920) made the same observation when the solid was in the form of thin layers of the order of one micron thick. The results however, due to experimental difficulties were insufficiently accurate for quantitative investigation of the effect of size on the melting point.

When electron diffraction became available as a means of observing the change from the solid to liquid state, the phase change of solid particles whose size was well below one micron could be investigated.

Although the transition from solid to liquid tin had been observed by means of electron diffraction by Jenkins (1935), Sayama (1941)

and Richter (1943), the first experiments which established that the melting point is lowered as the size of the crystallites is decreased were carried out by Takagi (1954). The melting point of thin evaporated films was detected by means of reflection electron diffraction. It was found that the melting point temperature decreased as the mean thickness of the film decreased. However, because of the low accuracy in the temperature measurements, and because the crystallite size was considered to be equal to the mean thickness of the film, no reliable correlation between the size of a crystallite and its melting point could be obtained (See Curzon (1960)).

By means of transmission electron diffraction, Blackman and Curzon (1959) investigated the melting point of tin crystallites which had been evaporated in vacuo onto carbon films to form thin layers. They observed, using an electron microscope, the sizes of the crystallites which constituted the layers. These experiments were the first attempt to correlate directly, the melting point of a given crystallite with its size.

In the experiments described in this thesis, the Blackman-Curzon technique was extended in an effort to obtain a detailed study of the dependence of the melting point of tin on crystallite size. Direct observation of the melting point of a specimen is not possible with an electron microscope, because the heating of the specimen by the intense electron beam prevents accurate measurement of the temperature.

So that the theoretical treatment of a spherical surface would be valid, the crystallites were prepared in such a way that they were spherical even when their radii were of the order of 1000 Å. Since the crystallites in an evaporated layer do not have an uniform size, different sizes of crystallites will melt at different temperatures because of their different surface effects. However the melting point of a given specimen can be determined, with reasonable accuracy, by observing the disappearance of the sharp rings in its transmission electron diffraction pattern. The diffraction pattern of a specimen composed of solid crystallites is shown in Figure 1, that of a specimen with some solid and some molten crystallites in Figure 2, and one of a specimen in which all the crystallites are molten in Figure 3. Experiments were carried out to give the crystallite radius which was to be correlated with the observed melting point of the specimen. In this way it was possible to assign a definite melting point to a single crystallite of a given radius.

In addition the possible effect of neutral substrates on the formation and melting temperature of tin crystallites was investigated by using the two different substrates, silicon monoxide and carbon.

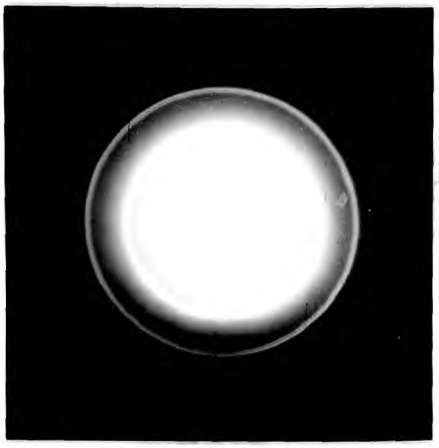

FIGURE 1. Transmission

Electron diffraction pattern produced by a tin specimen when all its crystallit are solid.

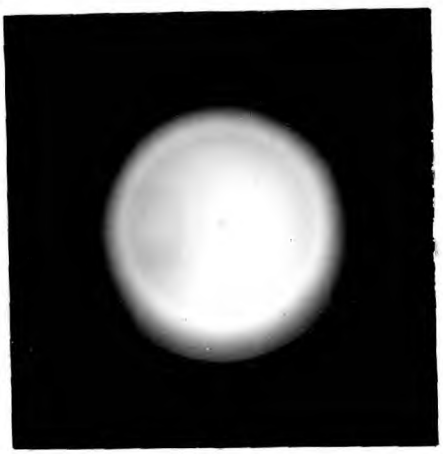

FIGURE 2. Transmission

electron diffraction pattern produced by a tin specimen where some of its crystallite are solid and some are molten.

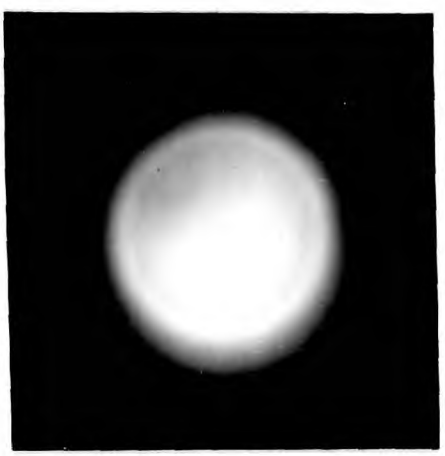

FIGURE 3. Transmission

electron diffraction pattern produced by a tin specimen when all of its crystall ites are molten.

CHAPTER II

APPARATUS.

1. General Arrangement of Diffraction Camera.

The experiments described in this thesis were carried out in a vertical diffraction camera designed by Kehoe and Newman (1956) which is shown diagrammatically in Figure 4. The camera could be evacuated down to a pressure of 10^{-5} mms.Hg. A conventional type of hot filament gun was used to produce an electron beam in which the electrons were accelerated to 45 K.V., which corresponds to a de Broglie wavelength of 0.0565 Å. The beam was focussed by a magnetic lens, B, onto a fluorescent screen, G. The specimen electron microscope grid A, 3 mms. in diameter, could be inserted into the camera by means of a specimen holder, D, which fitted into a large port in the side of the specimen chamber, C. An evaporator, E, was attached to a smaller port whose axis was level with, but perpendicular to, that of the specimen holder. This enabled in situ evaporation of tin onto the specimen grids so that experiments could be carried out on freshly prepared tin crystallites without exposure to the atmosphere. An evaporator shield, S, allowed the extent of evaporation to be controlled. A Faraday cage, F, at the same level as the specimen was inserted into the vacuum through another port. With this cage the electron beam intensity could be measured accurately and hence maintained

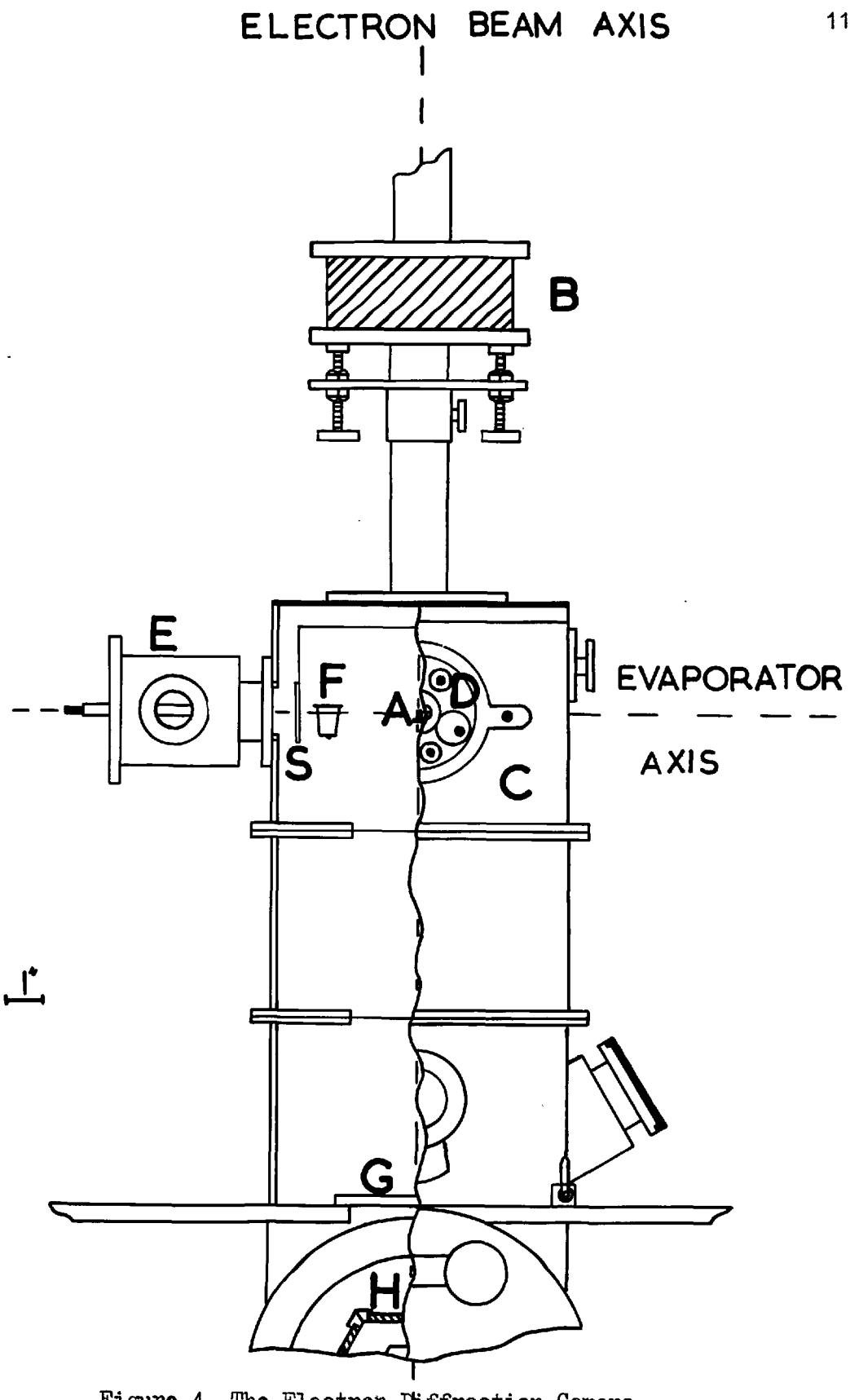

Figure 4. The Electron Diffraction Camera.

constant throughout different experiments. There were two windows for observing the inside of the specimen chamber which was illuminated internally. The diffraction pattern from the specimen could be observed on the fluorescent screen, G. Photographs of the diffraction patterns could be taken, either on photographic film or on plates at H, by raising the screen.

2. Specimen Chamber.

The general arrangement of the specimen chamber is shown in Figure 4. The evaporator, previously described by Kehoe, Newman and Pashley (1954), is shown diagrammatically in Figure 5. On the axis of the evaporator was a tightly wound molybdenum filament, F, so arranged that it could be rotated to have its apex horizontal or vertical. When the specimen was correctly positioned, the axis of the evaporator was perpendicular to the specimen, the distance between the filament and specimen being 15 cms. The filament was very tightly wound so that on heating, the molecular beam of tin travelled in the forward direction only, with a constant polar distribution (Holland (1956) p.146), and a collimator, C, was fitted onto the end of the evaporator to ensure that the molecular beam did not spread throughout the specimen chamber. When the shutter, S, was raised, a fixed fraction of the molecular beam of tin evaporated from the filament, condensed on the specimen grid. The filament was heated by a current

of up to 25 amps. A.C., the heavy current leads being led into the vacuum via robust porcelain-metal seals, L. The rate of evaporation was controlled by varying this current using a "Variac" transformer.

The specimen electron microscope grid was mounted inside the specimen heater previously described by Curzon (1960) which was incorporated in a specimen holder of the type described by Kehoe, Newman and Pashley (1954). The heater is shown diagrammatically in Figure 6. The specimen grid, S, fitted into the hollow copper cylinder, A, of internal diameter equal to the diameter of the grids. This cylinder A was open at one end and had a centrally placed aperture at the other. The grid was kept in a fixed position next to the aperture by the part B, the two parts being held together by means of a press fit. The specimen grid in this position was perfectly flat in a plane perpendicular to the axis of the cylindrical container, and in good thermal contact with both parts of the container. It can be seen from the diagram that when the molecular beam was incident along the axis of the cylindrical container, via B, it impinged without hindrance on the specimen grid. Also, if the electron beam was incident through the aperture, along the axis of A, a diffraction pattern of the specimen could be obtained.

The cylindrical container was brazed to the heater, H, on one side, and to a calibrated copper/constantan thermocouple junction, C, on the other. The heater elements consisted of nichrome wire wound on a mica

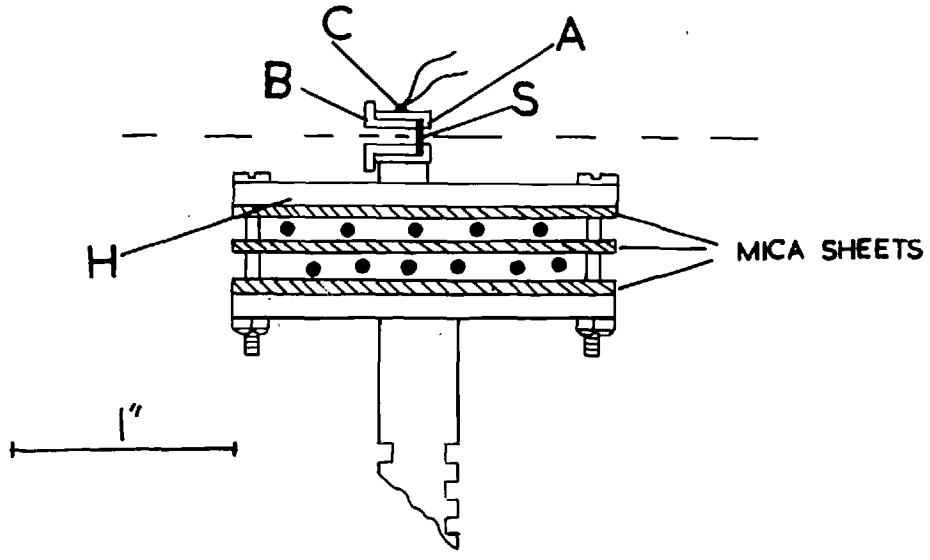

Figure 6. The Specimen Heater.

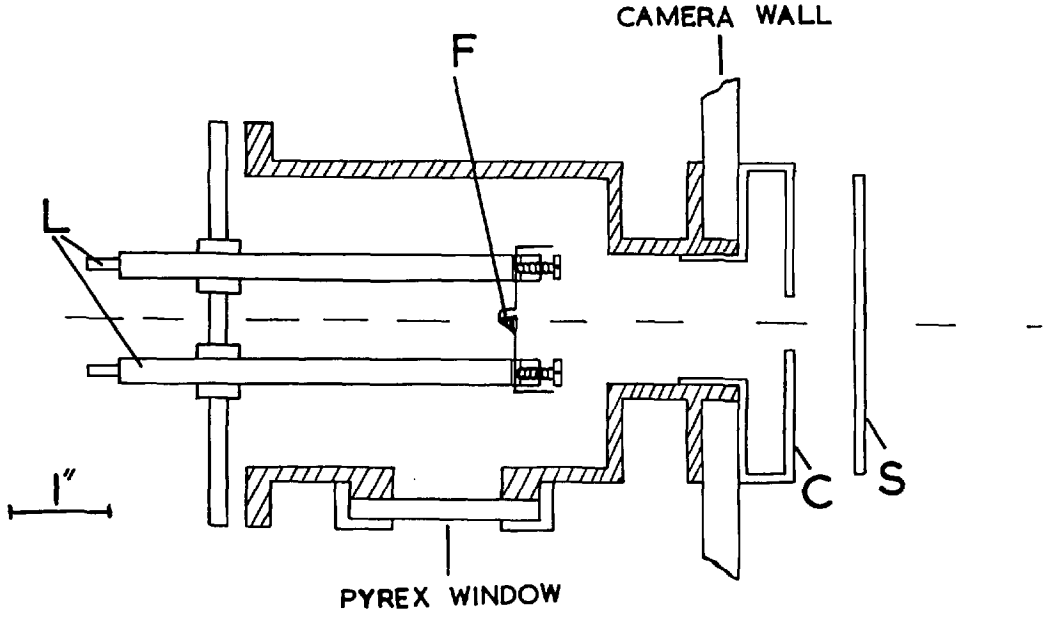

Figure 5. Horizontal Section through the Evaporator.

former and insulated from the metal parts of the heater by mica sheets. The rate of heating of the specimen could be controlled accurately by varying the current through the windings using a rheostat in series with a 24 volt D.C. supply. The temperature of the specimen was registered on a calibrated microammeter in the thermocouple circuit. When the maximum current of 3 amps was passed through the heater windings no deflection of the electron beam, was observed due to the magnetic field produced. The cylindrical parts of the container were made of "spec-pure" copper and the brazing material contained no volatile substances such as zinc, so that on heating up to 300°C no contamination of the specimen occurred.

The heater was mounted on the specimen holder as shown in Figure 7. The thermocouple and heater leads were led out of the camera via the insulated seals, D and E. When the specimen grid was inserted into the vacuum, part Q of the specimen holder was secured in a fixed position with bolts on the outside of the specimen chamber. In this position the axis Z-Z of the specimen holder was perpendicular to the evaporator axis, X-X, and to the electron beam, Y-Y. By means of controls F and G, indicated in the figure, two independent modes of motion of the heater, relative to the specimen, were attainable. The position of the specimen was so adjusted that it coincided with the intersection of the three axes. A greased O-ring between the parts P and Q enabled the specimen holder as a whole, to be rotated about the Z-Z axis. With the specimen in the specified position, the holder could be rotated so that the axis of the cylindrical

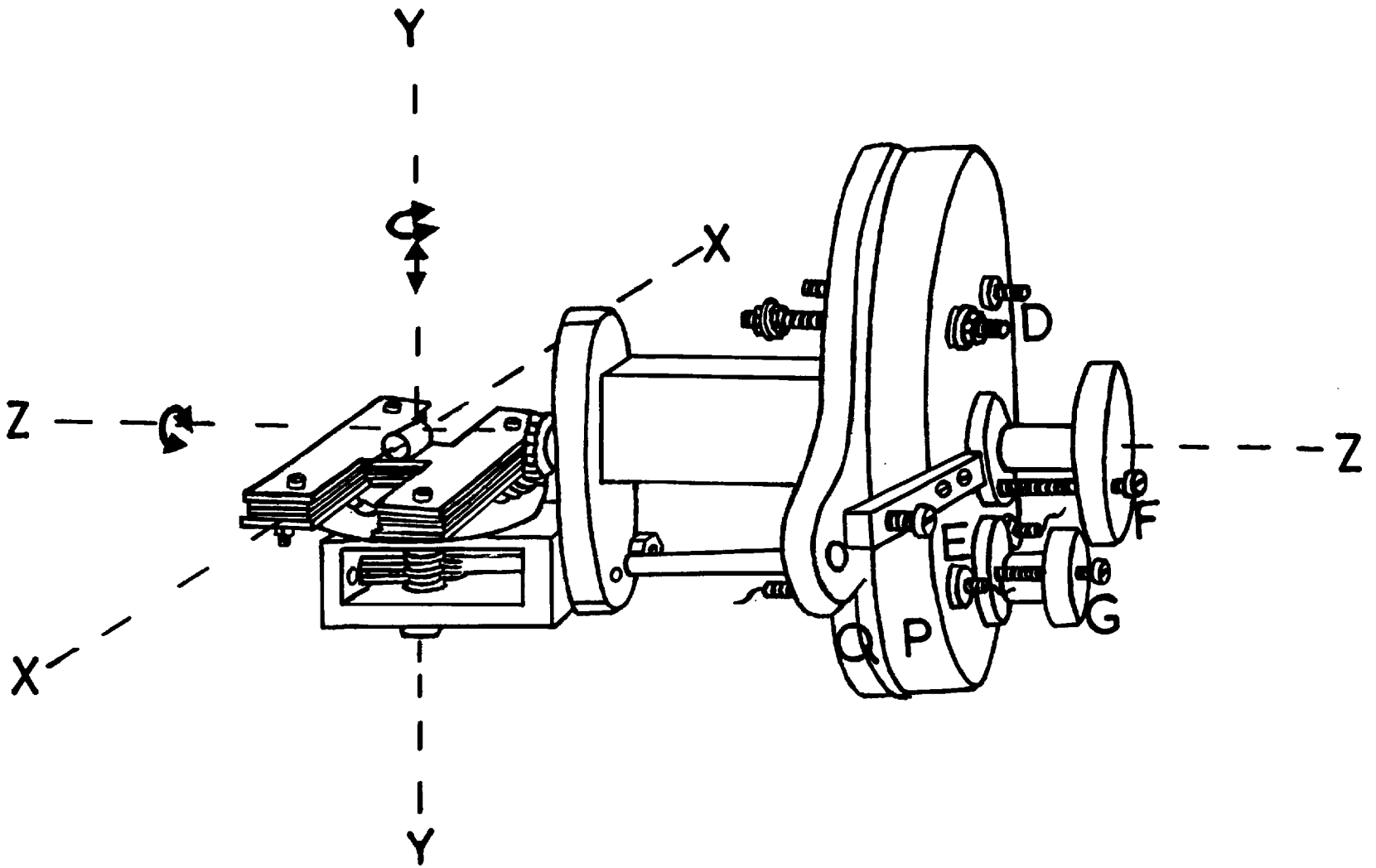

Figure 7. The Specimen Holder.

container coincided with the axis of the evaporator or with the electron beam, enabling the evaporation to be carried out with subsequent observation of the diffraction pattern. It was advantageous (and in some cases essential) for different specimens to be in exactly the same position with respect to the evaporator filament and the electron beam. For this purpose locking devices were incorporated in the controls of the specimen holder. The controls F and G were permanently locked and P clicked into the two specified positions by means of a rachet. This ensured that on extraction and subsequent replacement of the specimen holder into the vacuum, after changing the specimen grid, the same condition of evaporation was obtained and the electron beam incident on the specimen gave a diffraction pattern in exactly the same location.

3. The Electron Beam.

The electron beam was produced by a hot hairpin tungsten filament with a grid biased negatively with respect to the filament. The filament current was supplied by two accumulators, the bias by a dry cell, and the accelerating voltage by a stabilized supply. The emitted electrons were formed into a beam, accelerated by 45 K.V., and admitted into the rest of the camera through a small aperture in the anode. The intensity of the beam was controlled sensitively by varying the current through the filament and negative bias on the grid so that the same beam intensity was obtained repeatedly. By means of a magnetic lens (B in Figure 4), which was clamped

in a fixed position above the specimen chamber, the electron beam could be focussed on the fluorescent screen by having a definite current passing through the lens. The focussed beam could be moved in a horizontal plane by tilting the lens on the three levelling -screws in the clamp. The levelling-screws were adjusted so that the electron beam passed through the specimen when it was in the position for observation of the diffraction pattern. Two of these were locked permanently and the third was adjustable in such a way that it could be returned to exactly the same position, thus bringing the focussed beam back to exactly the same location on the screen. This enabled the beam to be deflected to a Faraday cage at the side of the specimen chamber for beam intensity measurements in different experiments.

The electron beam intensity was measured by means of this Faraday cage (Curzon 1960) connected to a sensitive moving coil galvanometer. The Faraday cage was in the horizontal plane of the specimen so that the beam diameter was the same in both positions. The beam entered the cage through a small aperture and the beam current was registered on a moving coil galvanometer of sensitivity of 8,000 mms. per μA. so that the electron beam intensity could be adjusted to any required measured value. As it was important not to have any effective heating of the specimen by the beam, a beam current intensity of 0.03μA. was used in the experiments which corresponded to $1 \cdot 0\ 10^{-5}$ A/cm^2. current density when the beam diameter in the plane of the specimen was 600 μs.

The diffraction patterns in the experiments determining the melting temperature of the crystallites were taken on photographic film. A continuous series of exposures at different temperatures could be taken. For the superimposition of patterns from different speciments and for those used in measurement of lattice spacings, photographic plates were used as these were more mechanically stable.

CHAPTER III

EXPERIMENTAL PROCEDURE

1. Preparation of Substrate Films.

The tin crystallites were evaporated onto substrate films of silicon monoxide and of carbon. To obtain a silicon monoxide film, glass slides were cleaned in chromic acid and washed in alcohol, coated with an evaporated layer of rocksalt, and then silicon monoxide was evaporated on top of the rocksalt. Both these evaporations were carried out without breaking the vacuum so that contamination during the evaporation of the different layers was minimised. There was a copper shield between the filaments so placed that the two filaments were shielded from one another, without obstructing the path to the slides of the molecular beam from either evaporation. Powdered SiO was mixed into a paste with distilled water and the molybdenum filament was filled with this paste. A small crystal of rocksalt was placed in the tungsten filament and the evaporating plant evacuated to a pressure of 10^{-5} mms. Hg. The rocksalt was evaporated quite rapidly so that a film was formed on the glass slides. The vacuum was allowed to recover and a current was passed through the molybdenum filament. This formed a silicon monoxide film on top of a rocksalt layer.

To strip the silicon monoxide film from the glass, the slide was immersed slowly and obliquely into distilled water in a petry dish, and as

the rocksalt dissolved,the silicon monoxide film floated off. The film was made into supports by transferring it onto copper electron microscope grids. Great care was taken to ensure that the film was spread uniformly over the centre of the fine mesh of the grid. To do this, the flattened end of a short piece of copper wire was bent over a small part of the edge of the grid. The end was pressed in sufficiently hard to keep the grid steadily fixed but could easily be bent back, and the grid could be released without any damage to the film on it. The other end of the wire was held in a pair of tweezers and the grid was submerged in the water and moved so that it was below the floating film and parallel to it. It was then raised slowly so that part of the film spread uniformly over the centre of the grid as it passed through the film.The film on the grid was then allowed to dry.

Silicon monoxide films of any required thickness could be produced, the thickness depending on the magnitude and duration of the current through the molybdenum filament. The film was made of a sufficient thickness to be able to withstand heating to 300^{o}C. and bombardment by the intense electron beam in the microscope without fracture, but at the same time thin enough to give a good tin electron diffraction pattern from very thin tin layers evaporated onto it. Once the optimum value for the thickness had been obtained, identical films could be made by reproducing the same conditions of evaporation, under which a current of 15 amps.passed through the molybdenum filament with the slides 12 cms. from it.

Samples of the silicon monoxide substrate films were examined under an optical microscope to ensure that there were continuous layers over the centres of the grids. Each specimen was examined by transmission electron diffraction, just prior to evaporation of tin, to check that there were no impurities on the substrate to give sharp rings which could be mistaken for those due to solid tin. A typical electron diffraction pattern of the silicon monoxide film is shown in Figure 8 and a photograph taken through an optical microscope of part of the coherent film on the electron microscope grid in Figure 9. It can be seen that the electron diffraction pattern consists of diffuse broad haloes showing that the silicon monoxide is in an amorphous state. If any sharp rings were observed the film was discarded as impure. A sharp ring pattern produced by crystallites of tin was clearly visible on these diffuse haloes, even when weak. This was of great advantage in determining the melting point of tin.

The carbon films were prepared as described by Bradley (1954) and Curzon (1960). This preparation was similar to that of the silicon monoxide films except that a carbon arc was used in place of the filament with silicon monoxide. The thickness was dependent on the size and duration of the current causing the carbon arc flash. Once the optimum thickness conditions had been determined, exactly the same carbon substrate films could be reproduced, giving halo diffraction patterns similar to those of silicon monoxide.

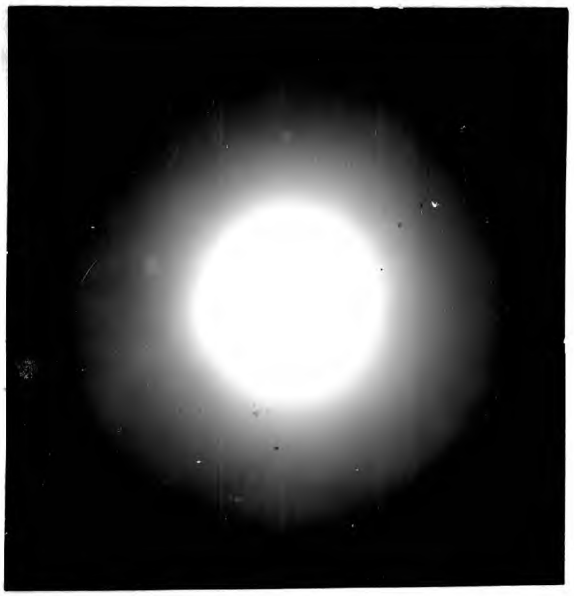

FIGURE 8. Transmission electron diffraction pattern produced by a silicon monoxide substrate film.

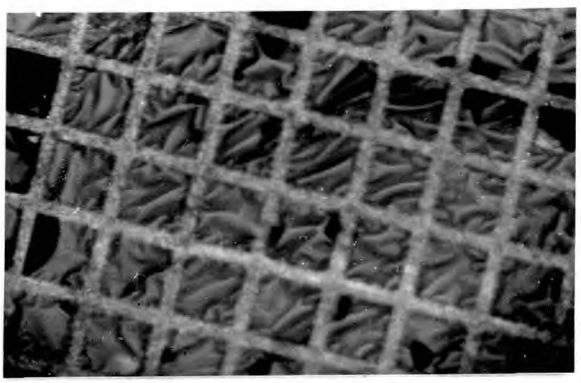

FIGURE 9. Photograph of a part of a silicon monoxide substrate film on an electron microscope grid.

2. Preparation of Tin Crystallites.

The tin films prepared on the two substrates were sufficiently thin not to form continuous layers but were composed of separate crystallites (Holland (1956) pp. 205-209) . As Spherical crystallites with a definite size distribution across the surface of the substrate were required, the special evaporation techniques described below were devised. A further discussion of the formation of these crystallites is carried out in Section 3.1 of Chapter V.

It was found during preliminary evaporations of tin in vacuo that different masses of tin gave different size distributions of crystallites on the substrate films (see also Curzon (1960)). However the increase of the mean size with the amount evaporated was not linear. With a high rate of evaporation, crystallites formed on the substrate at room temperature gave circular electron microscope images when masses up to 4 mgs.were evaporated from the filament. For larger masses the crystallites tended to lose their circular images and to coalesce. To overcome this, the temperature of the silicon monoxide or carbon base during these evaporations was raised through a series of temperatures up to 160°C. The rates of evaporation, pressure and position in the diffraction camera were kept as constant as possible for the different evaporations. By using masses of tin ranging from 1 to 20 mgs., a whole series of tin specimens were produced under these conditions of evaporation.

Tin was cut from a tin rod whose chemical and spectroscopic analyses

indicated that it was 99.996% pure tin with the main impurities being 0.002% lead and 0.001% antimony. A chipping was weighed on a micro-balance and cut down to the required weight. The weights were not distributed evenly over the range used, because the relation between the mean size of crystallites formed and the evaporated mass of tin was not linear. Many evaporations were carried out with weights of tin between 1 and 3 mgs. as, in this range, there was a rapid variation of mean size of the crystallites with mass evaporated.

The tin particle was placed in the evaporator filament, the axis of which was vertical. The silicon monoxide or carbon film onto which tin was to be evaporated was placed inside the cylindrical container of the heater, and the specimen holder was inserted in the position for observing an electron diffraction pattern of the film. The camera was evacuated to a pressure of 10^{-4} mms.Hg. and a current was passed through the molybdenum filament for a few seconds, sufficient to make it hot enough for the tin particle to melt and wet the filament. The temperature reached in this way was insufficient to evaporate any of the tin, so that on cooling down, the known weight of tin was fixed to the filament in the form of a sphere. The diffraction pattern from the silicon monoxide or carbon was examined to check that it had no impurities which would give rings on the diffraction pattern.

After the tin had cooled to room temperature air was admitted to the diffraction camera. The filament was rotated through 90 degrees so

it faced the position of the specimen grid and the grid was turned to the standard position for all evaporations (see Figure 7). In this position the uncontaminated substrate film was coaxial with the evaporator filament along X-X. The diffraction camera was then evacuated. In order to minimise the oxidation of the tin crystallites formed and to extract the water vapour from the long length of photographic film, the camera was pumped out continuously, with liquid oxygen in the trap above the diffusion pump, for several hours, so that a pressure of 10^{-5} mm. Hg. was attained.

The substrate was then heated to 300°C in order to evaporate the impurities, from the atmosphere and pumping system, which had condensed onto the substrate. This ensured that the formation of the tin crystallites was as uniform as possible over the whole of the substrate film. The evaporation of the tin was performed with the substrate films at a series of different temperatures. The specimens with mean radii greater than about 100Å had their substrates at temperatures between 180°C and 160°C, those below 100Å, at room temperature. The substrate was therefore allowed to cool to the required temperature, the evaporator shutter raised and the evaporation carried out. A current of 17.5 amps. was passed through the filament: this ensured rapid evaporation of the tin. The molecular beam which had condensed on the substrate film increased the mean thickness of the layer of tin crystallites at the rate of 200Å to 300 Å per minute, depending on the amount evaporated. When all the tin had evaporated the

heater was rotated so that the axis of the specimen was vertical and the diffraction pattern from the specimen could be observed. Before the melting-point experiments were carried out, the tin particles formed at higher temperatures were cooled to room temperature because they had formed in the liquid state.

3. Observation of the Melting of Tin Crystallite Specimens.

The specimen holder was rotated into the position for observation and photography of the diffraction pattern of the specimen. The electron beam was directed by means of the focussing coil onto the Faraday cage and the intensity was adjusted to a value of 0.03μA. Preliminary investigation had shown that the beam intensity did not change during an experiment, so it was only necessary to measure the intensity at the beginning and end of each of these experiments. The electron beam was then redirected onto the specimen so that the electron diffraction pattern of solid tin could be seen on the fluorescent screen. The pattern was photographed at room temperature and the specimen was then heated.

The current through the heater windings was adjusted to heat the specimen from room temperature to 100°C at a rate of 8-10°C per minute. The temperature of the specimen was read from the thermocouple microammeter and the temperature of the cold thermocouple junction was checked at regular intervals by means of a mercury-in-glass thermometer in thermal contact with the cold junction. When the specimen had reached 100°C the

increase in the heater current was adjusted to give a 1μA.per minute increase in thermocouple current - equivalent to a rise in temperature of 3-4°C per minute. When the tin crystallites had reached a temperature of about 150°C, photographs were taken of 1μA.increments of the thermocouple current up to the melting point of bulk tin. The electron beam intensity was so weak during these experiments that exposures of 10 seconds were required. However, the slow rate of heating ensured that the temperature rise during any exposure did not exceed 0.5°C. When the smallest crystallites were investigated ; photographs were taken at temperatures lower than 150°C. When the largest crystallites were investigated however, photographs were not taken untilabout 210°C and the rate of increase of temperature was halved so that exposures could be taken at increments of 0.5μA.

When the bulk melting point of tin had been reached, the specimen heater was switched off. When the specimen had reached room temperature, the recrystallised tin pattern was photographed, the specimen was transferred to the electron microscope and electron micrographs taken.

In certain cases a much longer film was placed in the camera so that double and triple heatings to 232°C and coolings to room temperature could be carried out on the same specimen.

4. Observation of Tin Crystallites in Specimen.

Electron micrographs of several regions of each tin specimen were obtained in an electron microscope. The microscope belonged to the Chemical Engineering Department, Imperial College, and the majority of the electron microscope work was carried out by Mr. H.I. Matthews. The micrographs were taken as soon as possible, most of the specimens being transferred directly from the camera to the electron microscope. The majority of the micrographs were taken at a magnification of 45,000 giving a resolution of 10-15Å. Great care was taken to have the microscope free from astigmatism and the magnification was continually checked.

To confirm that the tin crystallites studied in these experiments were spherical, certain specimens were shadowed by a heavy element (e.g. gold) and replicas of others were taken.

5. Super-position of Liquid and Solid Tin Electron Diffraction Patterns.

The relative intensities of the solid (sharp ring) and liquid (diffuse halo) electron diffraction patterns of tin were investigated in order to determine the mass of liquid necessary to suppress the diffraction pattern from a given mass of solid. The diffraction patterns from different specimens in which all the crystallites were solid were superimposed on patterns of specimens in which all the crystallites were molten and vice versa. Great care was taken to have identical conditions for every specimen when its diffraction pattern was photographed.

Silicon monoxide substrate films, thicker than those described in Section 1 of this Chapter, were prepared by increasing by 50% the duration of the evaporation of the silicon monoxide. These thicker films ensured that all the central apertures of the specimen grids were completely covered by a coherent film. Each grid was checked under an optical microscope for total continuity. The thicker amorphous substrate caused no appreciable increase in the background of any tin diffraction pattern - solid or liquid - but provided a continuous film over a large area. When the electron beam, which was 600 μ. in diameter, passed through a specimen, it defined a fixed area of silicon monoxide film covered by tin crystallites. If the substrate had not been perfectly continuous, so that regions of the grid were not covered by film, the effective area examined by the electron beam would not have been constant for different specimens.

A wide range of tin crystallite specimens was evaporated onto these substrates, the masses evaporated from the filament being divided into two groups, one from 1 to 2.5 mgs., the other from 10 to 25 mgs. The evaporations of tin were carried out as described in Section 2 of this Chapter, except that the silicon monoxide bases were at 160°C. throughout this series. The small masses were evaporated at this higher temperature so that the crystallites formed from a particular evaporated mass, would be as large as possible for a given mean thickness. The mean thickness was proportional to the mass evaporated and the constant of proportionality

was the same for all specimens since the substrate film was in the same position during each evaporation.

The liquid tin electron diffraction pattern of each specimen of large mean thickness was photographed at 232°C, to ensure that all the tin crystallites causing it were molten. The specimens of small mean thickness had their solid patterns photographed at room temperature, when all the crystallites were solid. To ensure that the conditions of exposure were identical, each specimen was in the standard position for observing the diffraction pattern; the electron beam, by virtue of the locking mechanisms on the focussing coil, could be returned to a fixed position on the fluorescent screen after it had been directed into the Faraday cage. The electron beam was carefully adjusted to 0.03μA. and checked before each exposure.

For each specimen, sets of five diffraction patterns were recorded on photographic plates. The plates were mounted so that each in turn could be rotated into exactly the same position for exposure, and diffraction patterns were then coincident on each plate. By different combinations of previously exposed plates, patterns from known specimens (liquid pattern on solid or solid pattern on liquid) were superimposed. These exposures were all the same since they were subject to the same beam intensity, voltage and time. When all the exposures required from the specimens had been taken, micrographs of some of the specimens were taken in the electron microscope.

6. Observation and Comparison of Structure of Tin Crystallites in Specimens.

Standard procedure was used for the determination of the structure and lattice spacings of tin crystallites. Two transmission specimens were mounted in the electron diffraction camera at the same distance from the photographic plate: one specimen was the polycrystalline layer of tin under investigation, and the other was a polycrystalline layer of thallium chloride formed by evaporation onto a silicon monoxide base. Both specimens were at room temperature.

The camera was then evacuated, and the high tension voltage supply and electron beam switched on and allowed several minutes to stabilize. The beam was orientated onto the tin specimen and the electron diffraction pattern produced was photographed on a photographic plate. The beam was then deflected by means of the focussing coil onto the thallium chloride and its diffraction pattern was photographed on another plate. This operation was carried out as quickly as possible in order to ensure that the voltage of the electron beam, and hence the electron wave-length, was identical for both photographs. Also, instead of the thallium chloride specimen, a tin specimen of a very different mean size of crystallites was used to determine whether the lattice parameters changed with size.

CHAPTER IV

MEASUREMENTS.

1. Determination of the Melting Point of Specimens.

Photographs of the diffraction pattern of the specimen had been taken as the temperature had been raised. The initial polycrystalline state gave a sharp ring pattern which remained unchanged over a large initial temperature rise except in the case of specimens with very small mean crystallite size. The sharp ring pattern of the solid tin began to change after a temperature rise of about a 100°C. The sharp rings then grew fainter, the background intensity increased, and haloes began to appear around the (200),(101) and (220), (211) inner rings. (Indexed polycrystalline patterns of tin are shown in Figure 33). As the temperature was increased further, the background intensity became so strong that the rings outside (301) disappeared; at the same time the intensity of the inner rings decreased and that of the haloes increased. On subsequent heating first the (301) then the (220),(211) rings disappeared and the remaining two rings became less and less distinct. At some temperature below the melting point of bulk tin, the intensities of the haloes had increased and those of the two innermost rings decreased to such an extent that only the halo pattern characteristic of liquid tin was visible. No further changes appeared to occur in the diffraction pattern on heating up to 232°C. The temperature at which this transition from sharp ring to diffuse halo pattern occurred depended on the size distribution of crystallites in the specimen. Those

specimens with the largest mean crystallite sizes had these transitions occurring over a range of several degrees, the range increasing to several tens of degrees as the mean size of the crystallites diminished.

All the crystallites were molten when the specimen was at 232°C , because this is the melting point of bulk tin, and at this temperature there were no sharp rings present on the diffraction pattern. The photographs of the diffraction patterns taken every 4°C or 2°C were compared visually with the photograph taken at 232°C in order to determine the melting point associated with the specimen. This is permissible since the eye is a sensitive detector of intensity gradients. Sharp rings could be observed in photographs of diffraction patterns, even when they were weak and the background intensity comparatively high. The melting temperature of the specimen, T_m , was taken as the mean temperature between two successive photographs so chosen that the first was distinguishable from the pattern of liquid tin but the second of which showed faint rings. The diffraction patterns, photographed during transitions of two specimens of quite different crystallite distributions, together with those taken at 25°C and 232°C, are shown in Figure 10(A,B,C,D,E) and Figure 11 (A,B,C,D,E). The transition in the latter specimen of larger mean size,is seen to be sharper.

The specimens which had very small mean crystallite size produced transitions with which it was extremely difficult to associate a definite melting point. The photographs of the diffraction patterns were taken

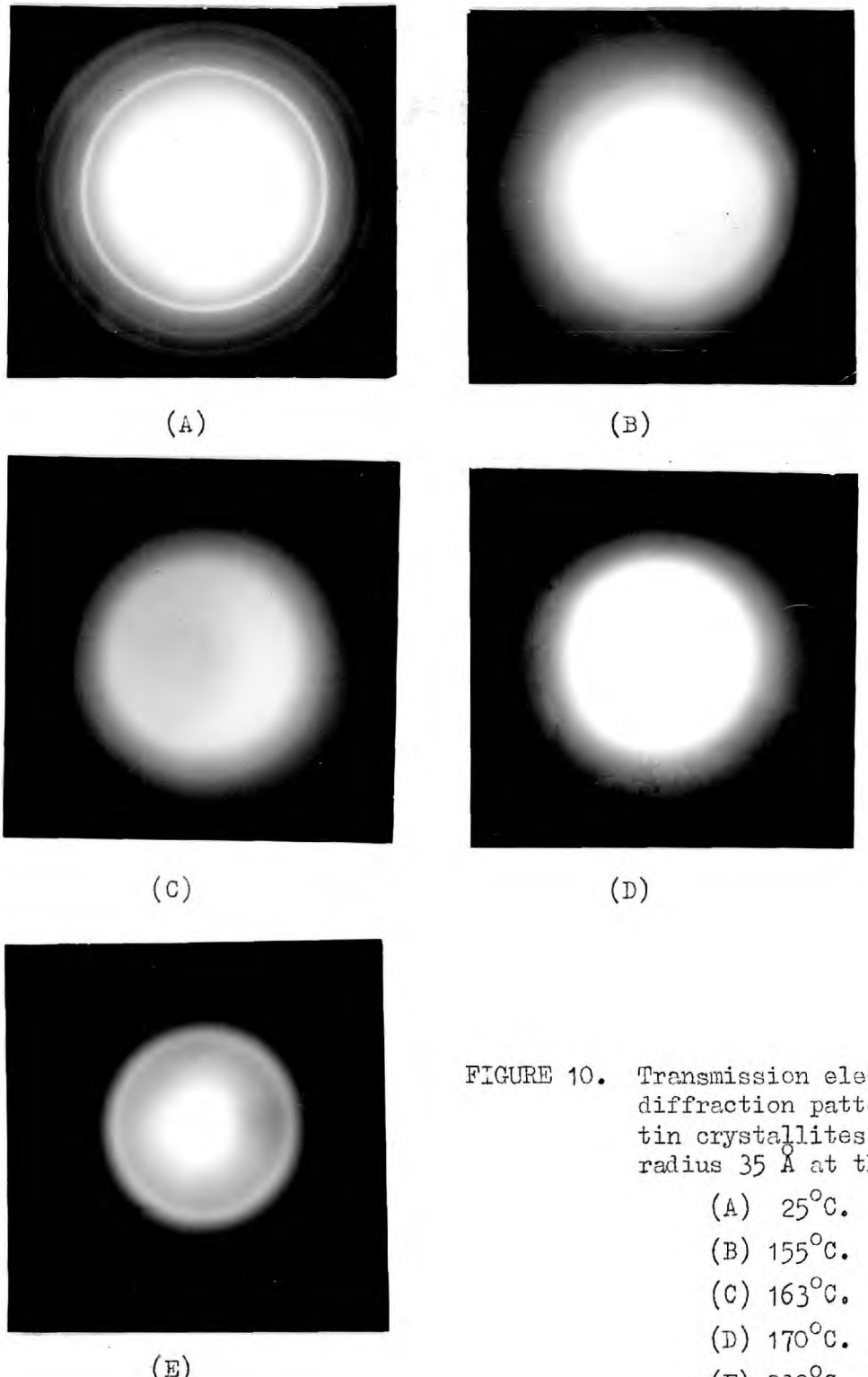

FIGURE 10. Transmission electron diffraction patterns of tin crystallites of mean radius 35 Å at the temperatures

(A) 25°C.
(B) 155°C.
(C) 163°C.
(D) 170°C.
(E) 232°C.

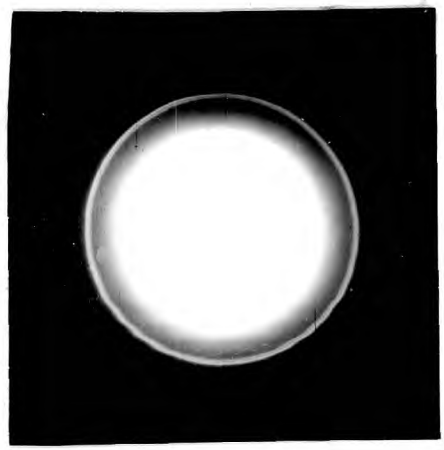

(A)

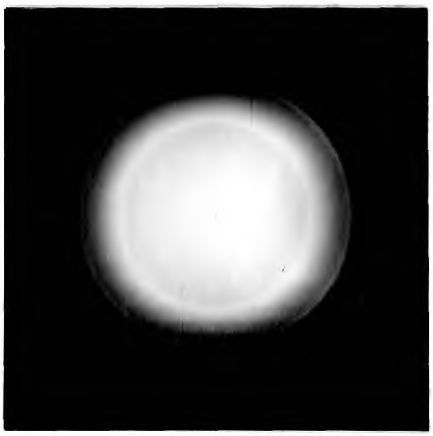

(B)

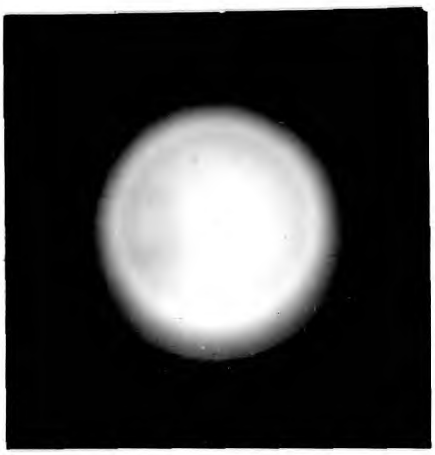

(C)

(D)

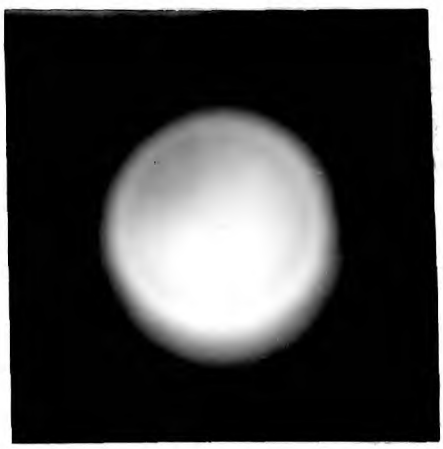

(E)

FIGURE 11. Transmission electron diffraction patterns of tin crystallites of mean radius 150Å at the temperatures.

(A) 25°C.
(B) 223°C.
(C) 225°C.
(D) 227°C.
(E) 232°C.

at room temperature, and then at intervals of 8 to 10°C because the transitions were so gradual. The transitions in the patterns were indefinite because the pattern produced by the solid crystallites was very weak and the polycrystalline rings had broadened out. The subsequent change in the diffraction pattern on melting was not so marked and in consequence the transition from solid to liquid was uncertain.

2. Determination of the Size and Mass Distributions of Crystallites in the Specimens.

In order to obtain the temperature at which a crystallite of given radius melted, it was necessary first to obtain the size, and then the mass distributions of crystallites in each specimen. Typical photographs of electron images of different specimens are shown in Figures 12 to 20. The images of the tin crystallites prepared in this series of experiments were circular, except for a few of the crystallites of several hundred Angstoms radius, which gave elliptical images. The diameters of crystallite images were measured in order to obtain the size distribution of the crystallites of a given specimen. In the case of the elliptical images the lengths of the two major axes were measured and their mean was taken as the equivalent diameter.

The resolving power of the electron microscope was 10-15 Å. The overall magnification of the crystallites was chosen to be 7.2×10^5 (i.e. 1 mm equivalent to 13.9 Å) so no loss of accuracy was incurred when a

millimetre scale was used for size determinations. Histograms of crystallite radii with a frequency interval of 6.95 Å were plotted. It was found that the smoothed-out shape of these histograms became constant when the number of particles measured from a specimen exceeded 500, provided the specimen did not contain crystallites with radii much greater than 100 Å. For specimens with crystallite radii larger than this, the spread of sizes was greater and hence a larger number of measurements of particles was required to obtain a smooth histogram. Consequently, for the specimens containing the largest crystallites an overall magnification of 3.6×10^5 was used.

The distribution function $n(r)$, of the crystallite sizes measured on a given specimen was given by the smooth curve through the histogram. Histograms of crystallite radii with the distribution functions superimposed, which were obtained for the specimens whose electron microscope photographs are shown in Figures 12,13,14 and 15, are shown in Figures 12a,13a,14a and 15a respectively. To minimise errors in the measurement of the crystallite sizes, micrographs of completely different parts of the same specimen were measured. Photographs of two other parts of the specimen shown in Figure 14 are shown in Figures 14',14". Their corresponding distribution functions are shown in Figures 14a',14a" respectively. It was found that the distributions of different parts of a carefully prepared specimen were identical within the experimental error. For each specimen, crystallites at two or more different parts were measured to give two distributions, and from these, the distribution

function of a given specimen was obtained. In a few specimens different parts gave distributions which differed by more than the experimental error; these were discarded.

Gaussian distribution functions of crystallite sizes were obtained from specimens for which the mean crystallite radius was less than approximately 60 Å . The mode and the mean coincided within the experimental error. When the specimens were such that the mean radius of the crystallites exceeded 60 Å, the distribution function obtained from high resolution micrographs showed marked peaks of unequal height with a well defined minimum between them. An example of this is shown in Figure 16a which is the size histogram for the specimen whose electron microscope photograph is shown in Figure 16. It can be seen that the crystallites whose radii were less than the radius of the minimum between the two peaks were much smaller than the mean radius of the shaded part of the histogram. Since the effects studied were proprotional to the cubes of the radii, these crystallites were ignored, and the distribution obtained from the histogram was still approximately Gaussian, as shown in the figure. Therefore this distribution would still be obtained from micrographs in which the smaller crystallites could not be resolved because of lack of contrast. Typical distributions for the larger tin crystallites are shown in Figures 17a, 18a, 19a, 20a; these were obtained from the specimens whose electron microscope photographs are shown in Figures 17,18,19 and 20. In these histograms the crystallites with radii

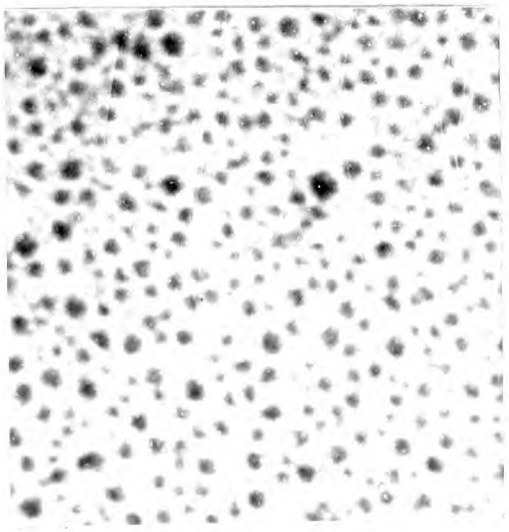

FIGURE 12. Electron microscope photograph of tin crystallites having mean radius 24Å. (x 360,000).

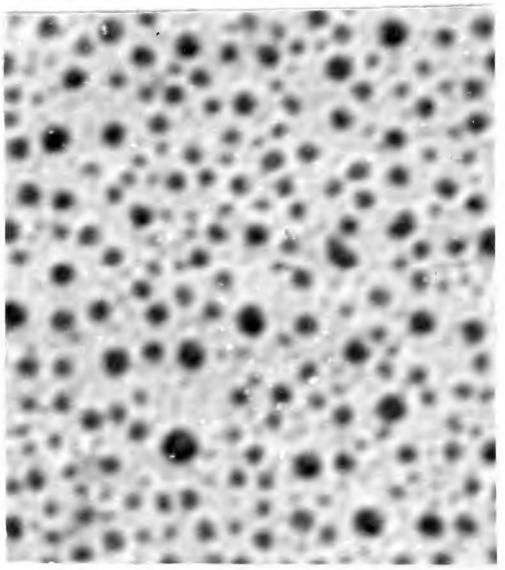

FIGURE 13. Electron microscope photograph of tin crystallites having mean radius 31Å. (x 360,000).

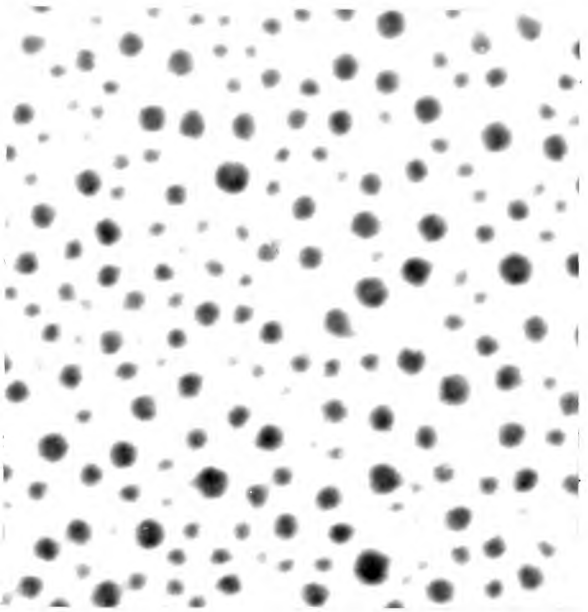

FIGURE 14. Electron microscope photograph of tin crystallites having mean radius 39Å. (x 360,000).

Figure 13a. Crystallite size distribution of Specimen shown in Figure 13.

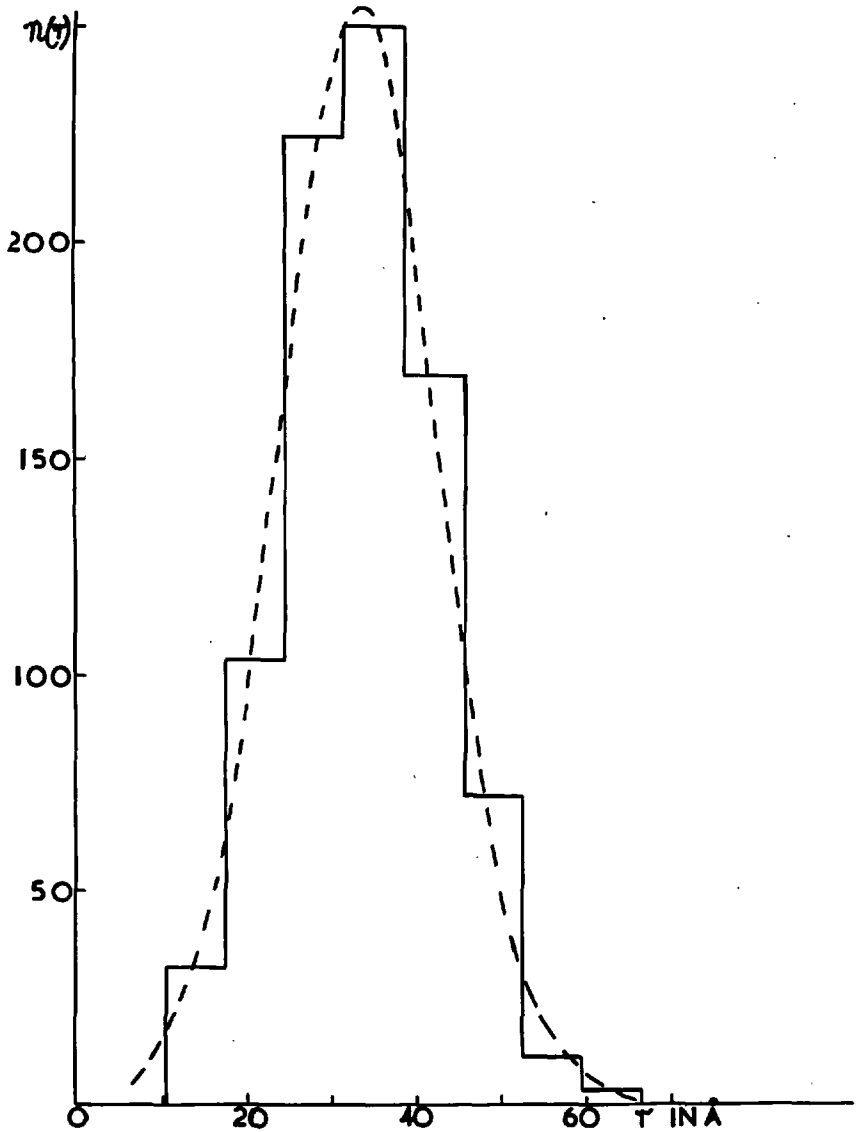

Figure 12a. Crystallite size distribution of Specimen shown in Figure 12.

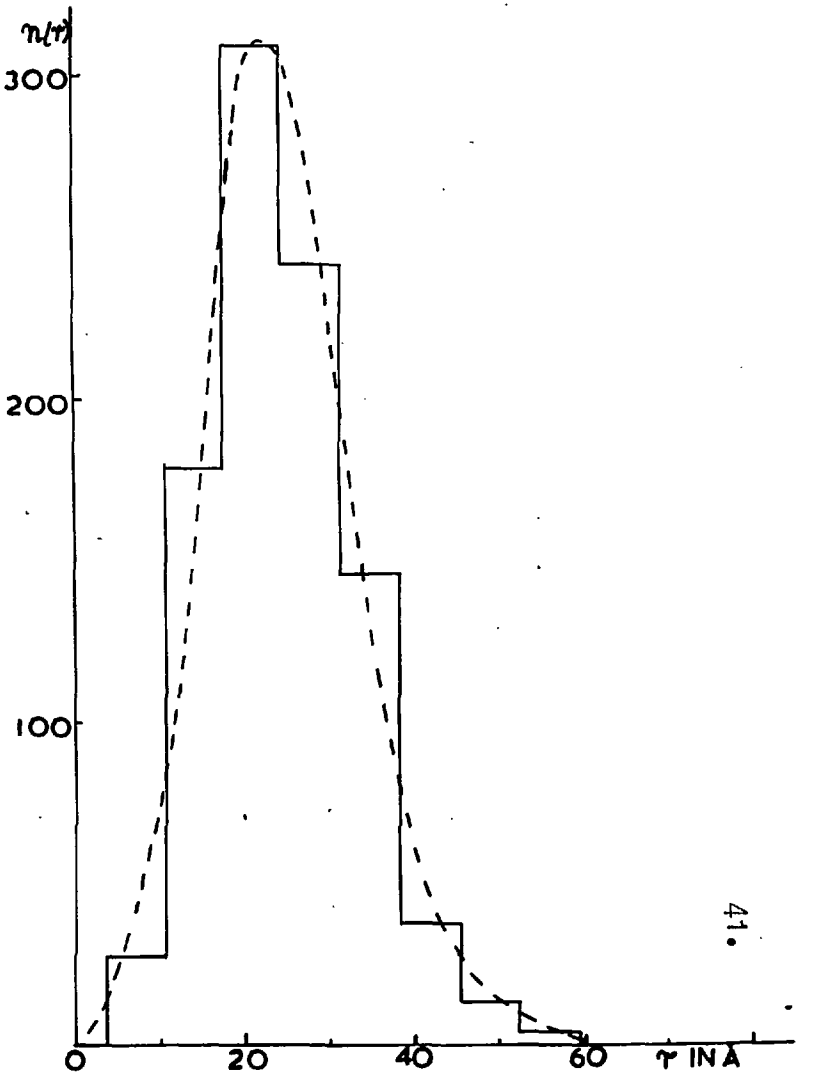

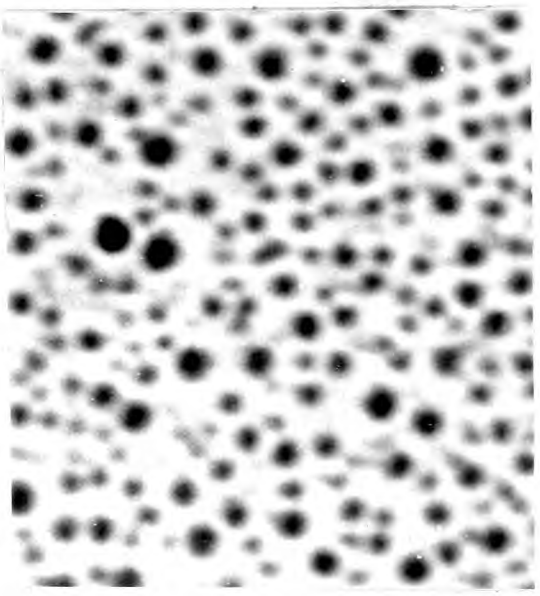

FIGURE 14!

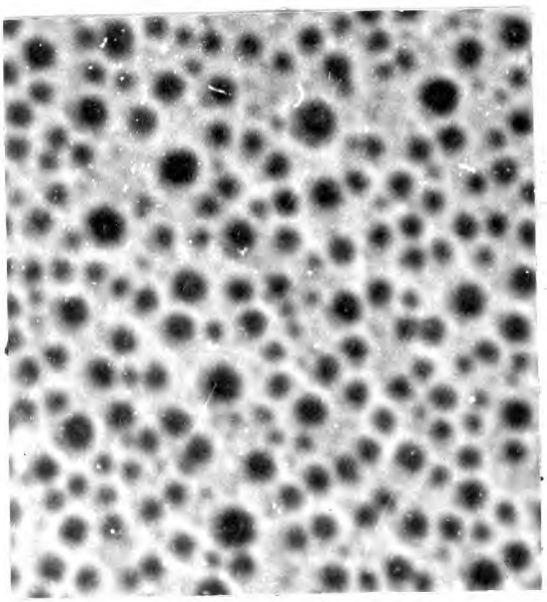

FIGURE 14"

Electron microscope photographs of tin crystallites, taken at widely separated regions, from the same specimen as Figure 14.

(x 360,000).

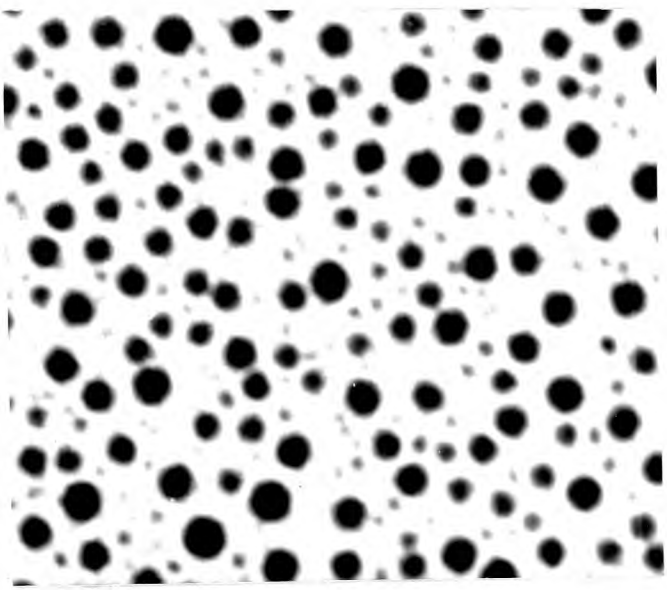

FIGURE 15. Electron microscope photograph of tin crystallites having mean radii 53 Å.

(x 360,000).

Figure 14a'. Crystallite size distribution of Specimen shown in Figure 14'.

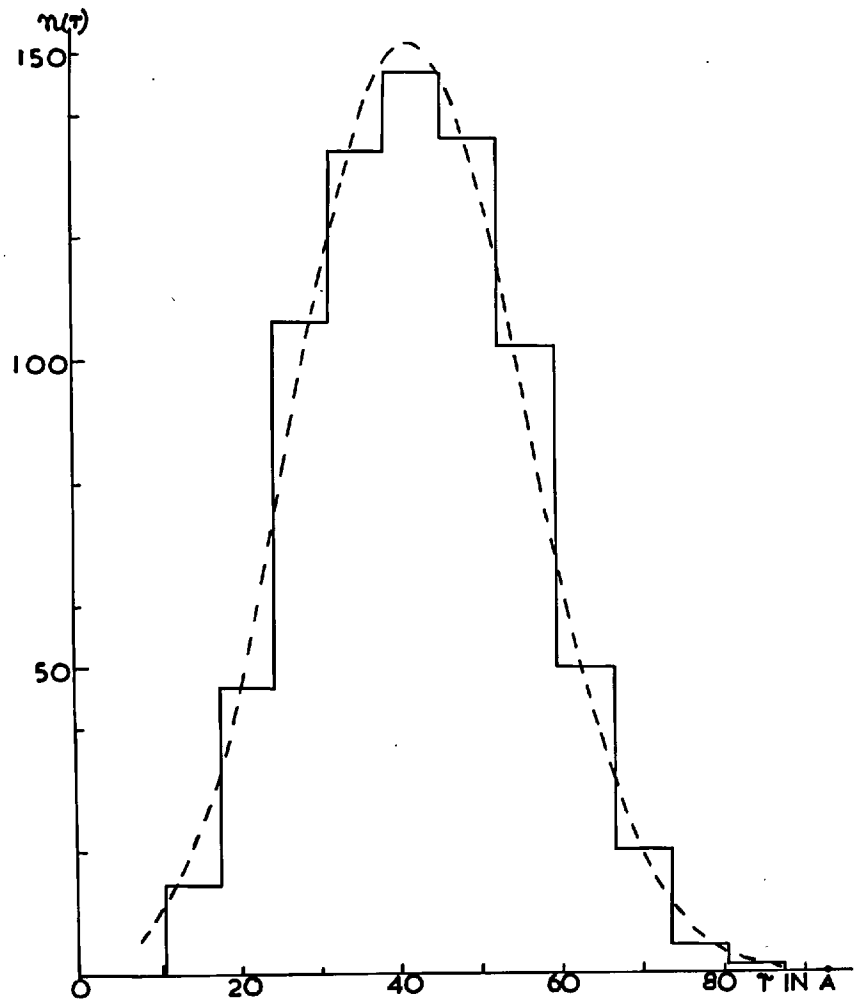

Figure 14a". Crystallite size distribution of Specimen shown in Figure 14".

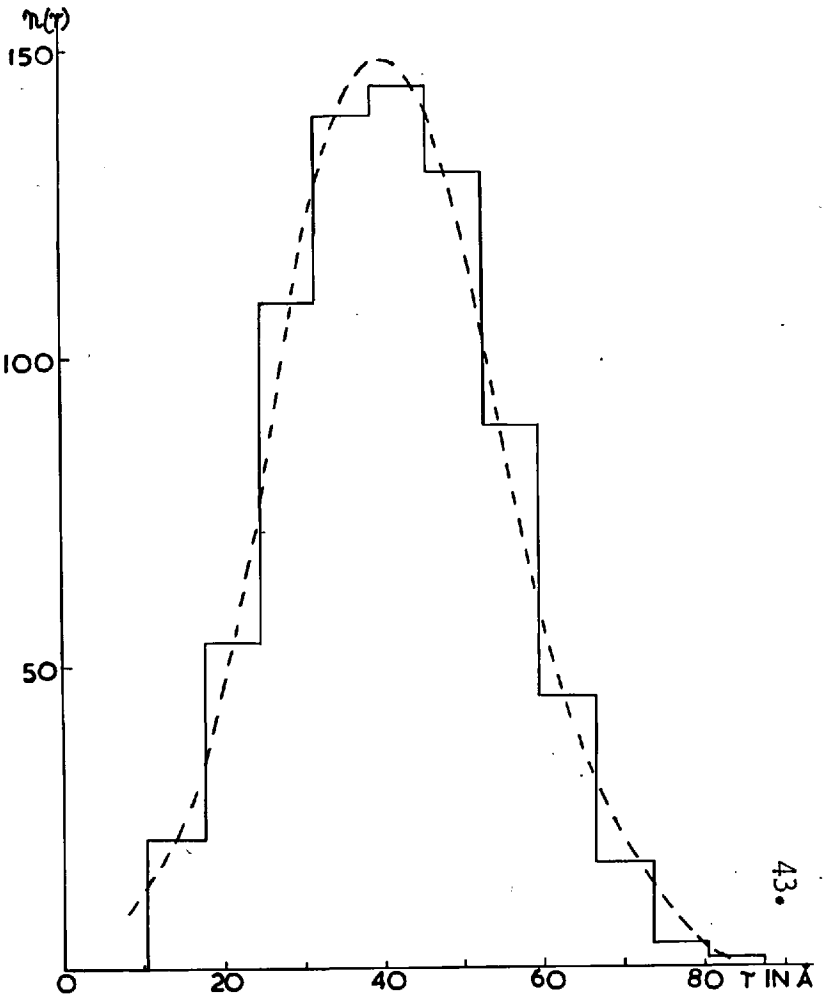

Figure 15a. Crystallite size distribution of Specimen shown in Figure 15.

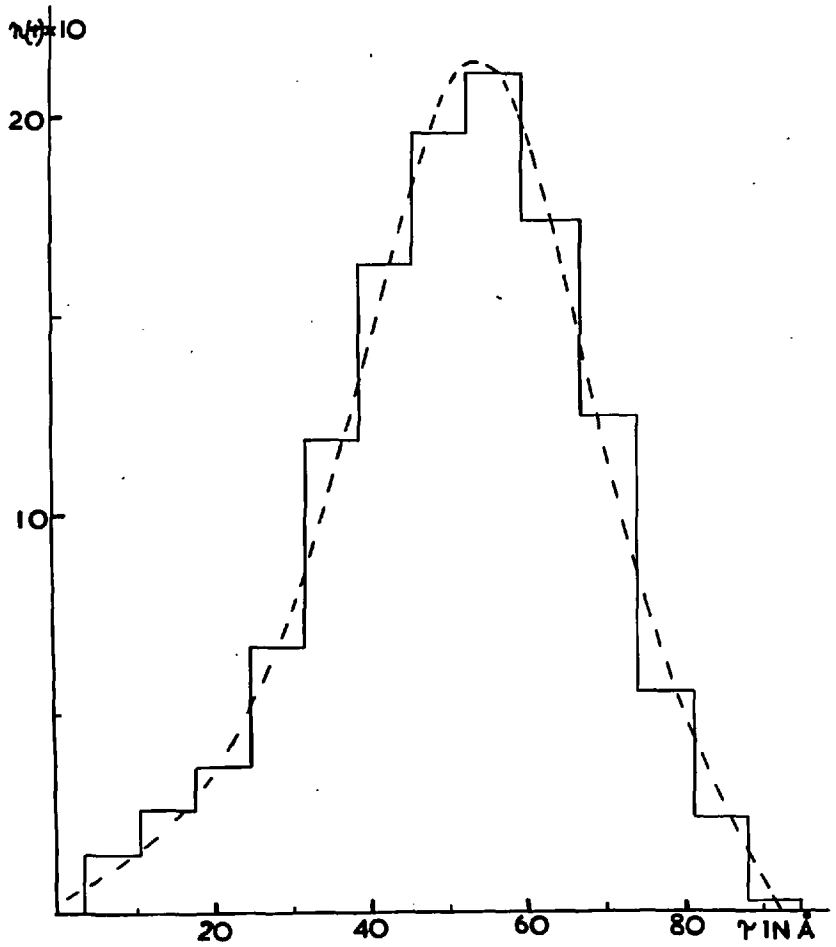

Figure 14a. Crystallite size distribution of Specimen shown in Figure 14.

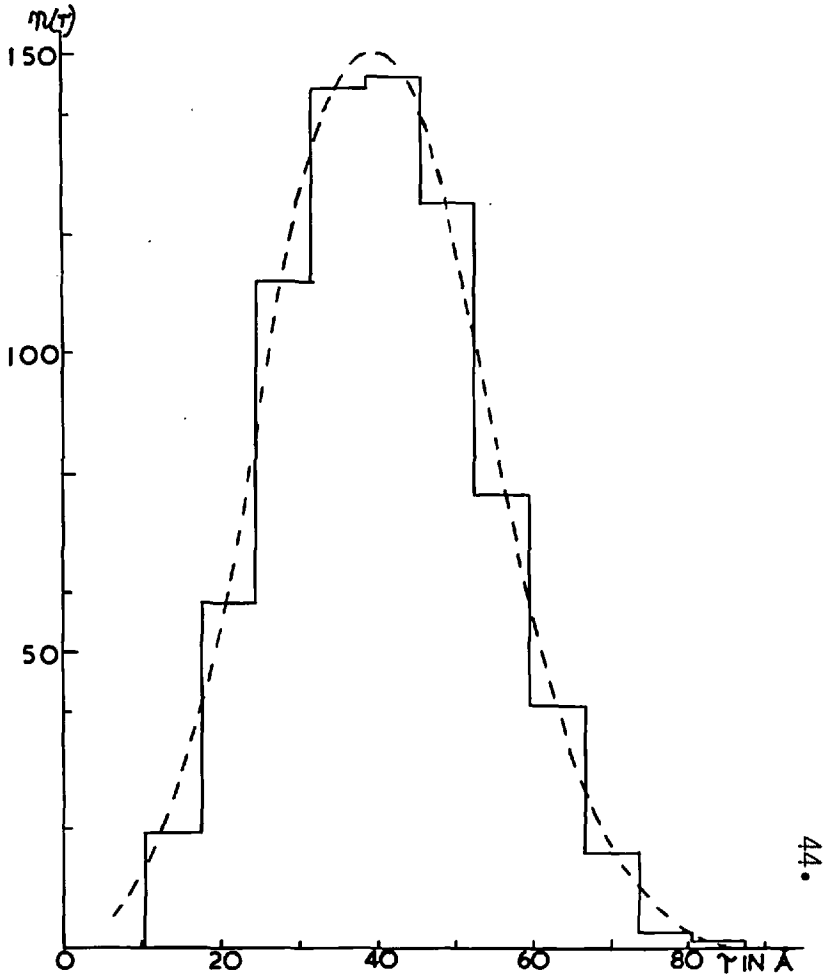

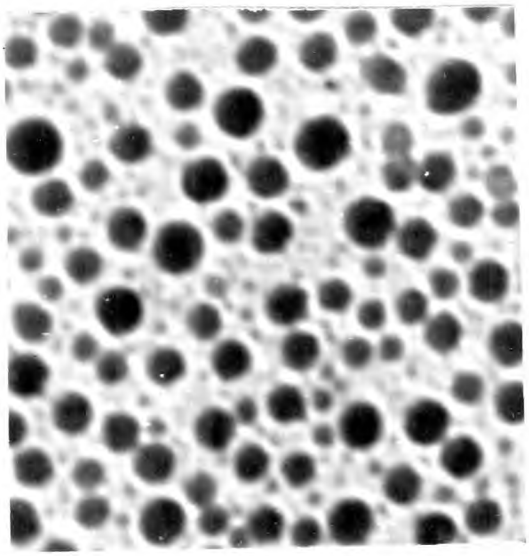

FIGURE 16. Electron microscope photograph of tin crystallites having mean radius 64Å. (x360,000).

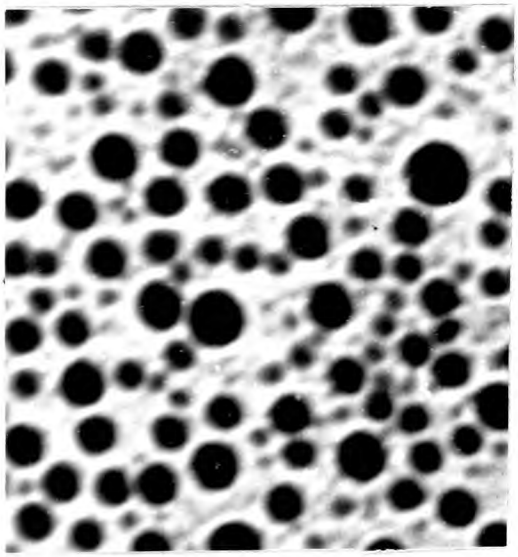

FIGURE 17. Electron microscope photograph of tin crystallites having mean radius 72Å. (x360,000).

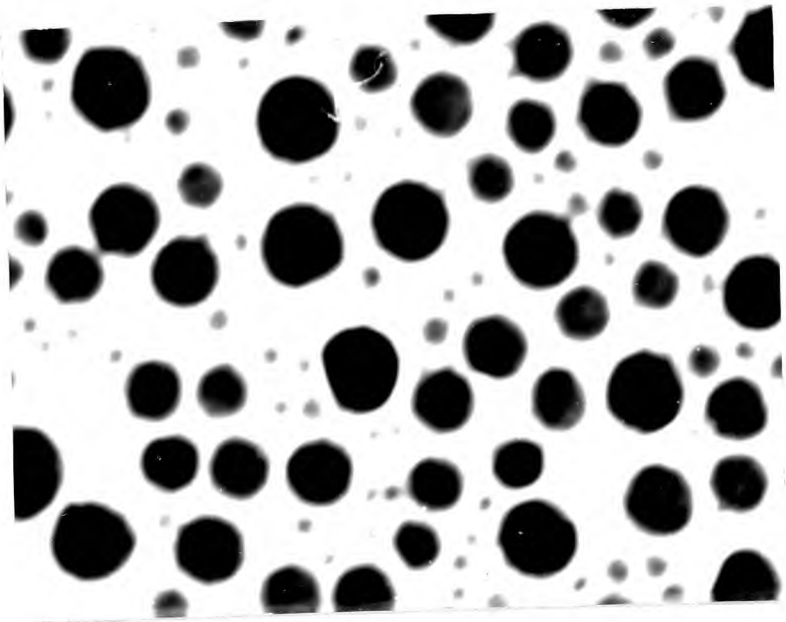

FIGURE 18. Electron microscope photograph of tin crystallites having mean radius 140 Å. (x 360,000).

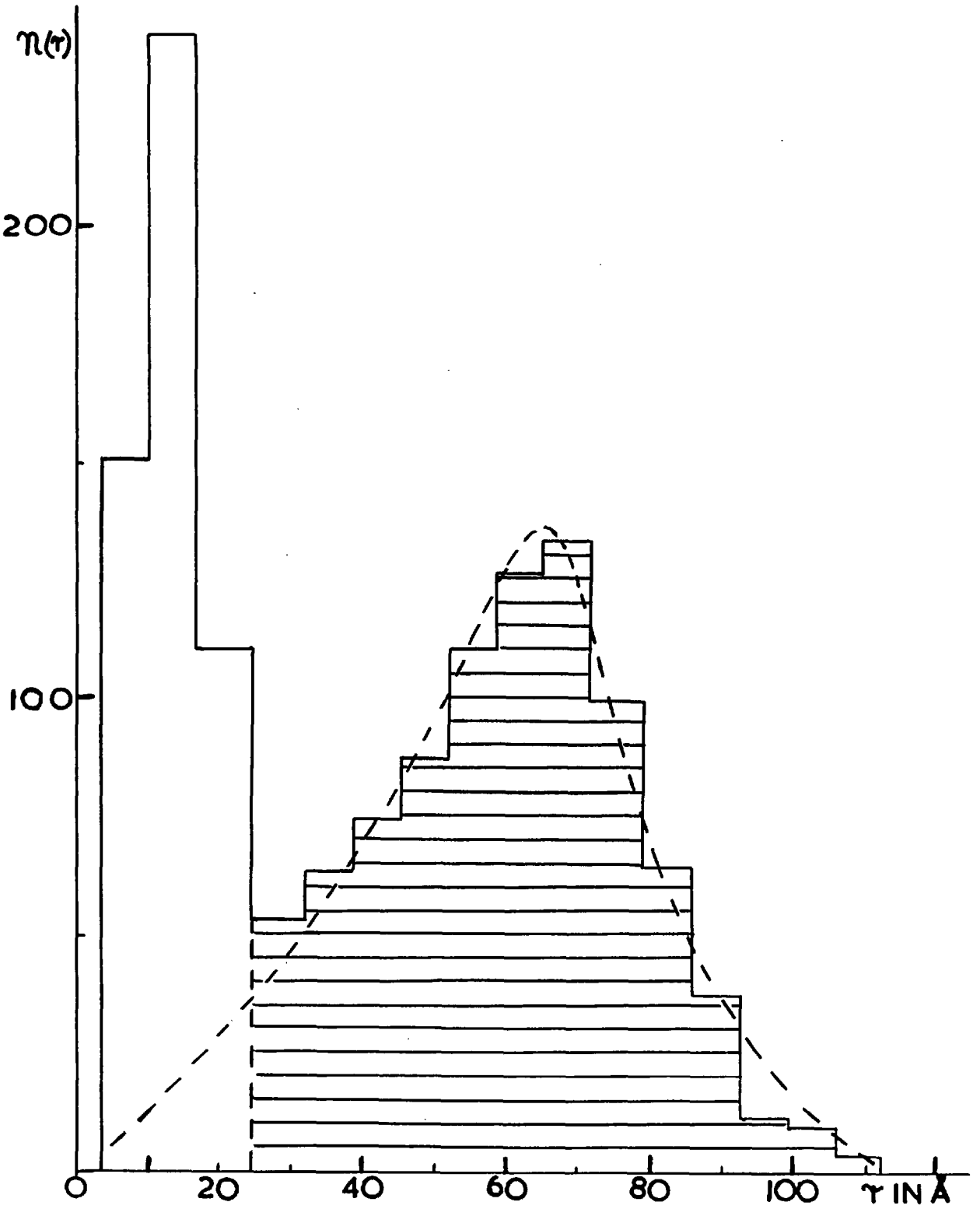

Figure 16a. Crystallite size distribution of Specimen shown in Figure 16.

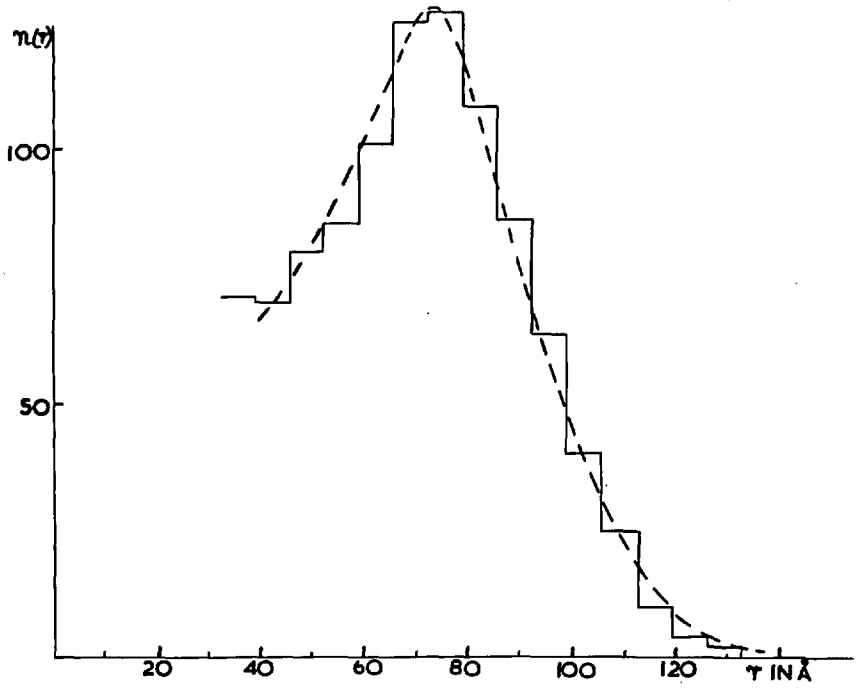

Figure 17a. Crystallite size distribution of Specimen shown in Figure 17.

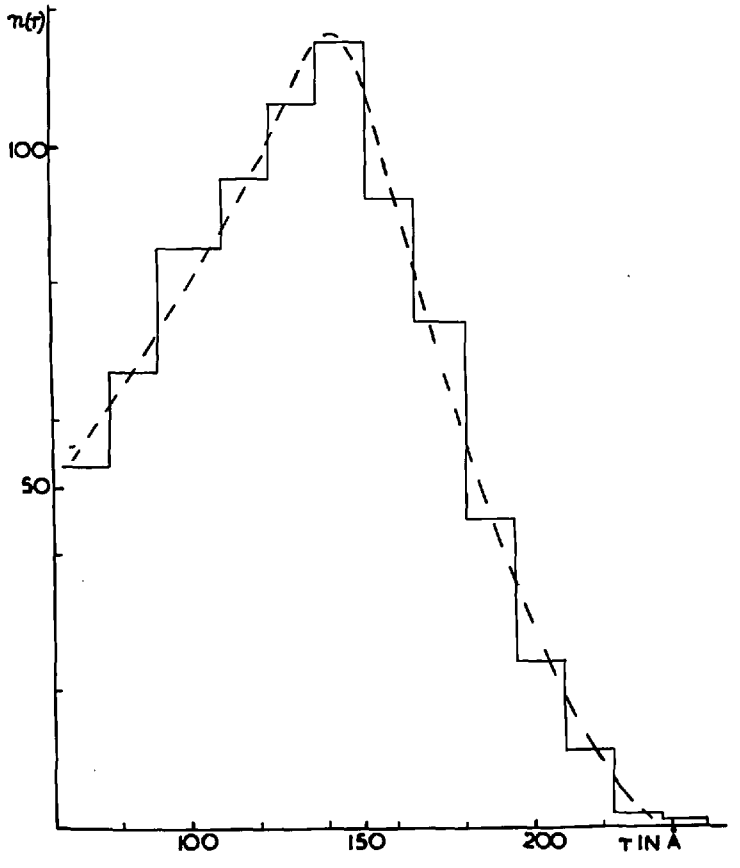

Figure 18a. Crystallite size distribution of Specimen shown in Figure 18.

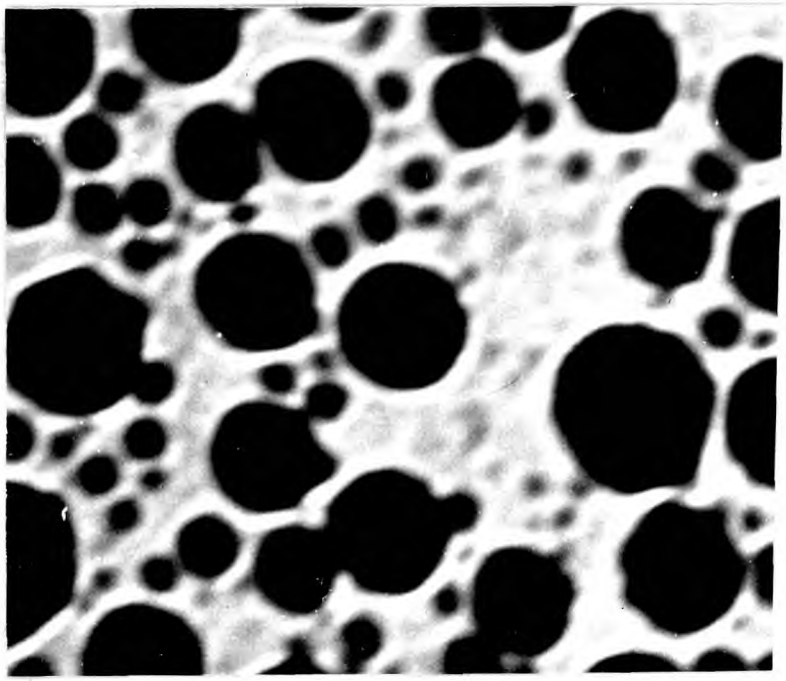

FIGURE 19. Electron microscope photograph of tin crystallites having mean radius 200 Å. (x 360,000).

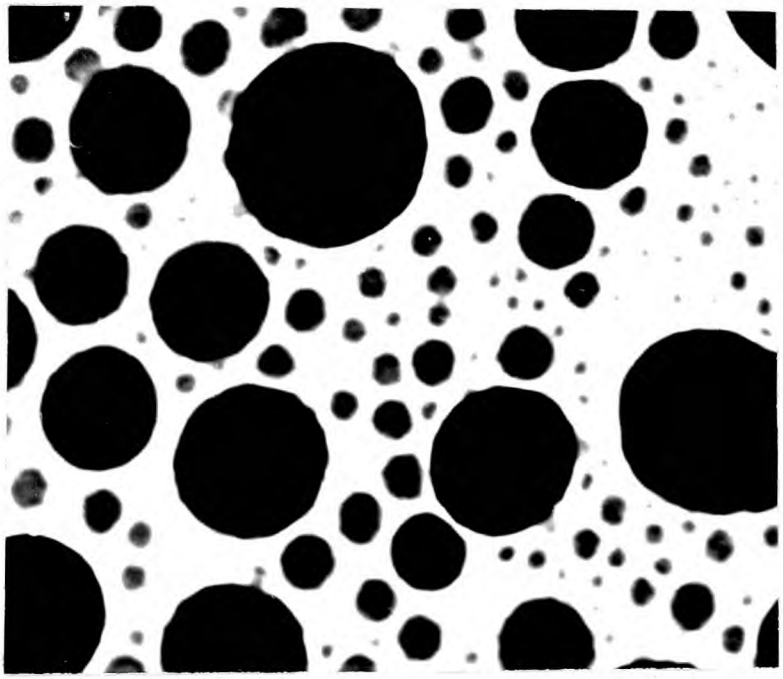

FIGURE 20. Electron microscope photograph of tin crystallites having mean radius 320 Å. (x 360,000).

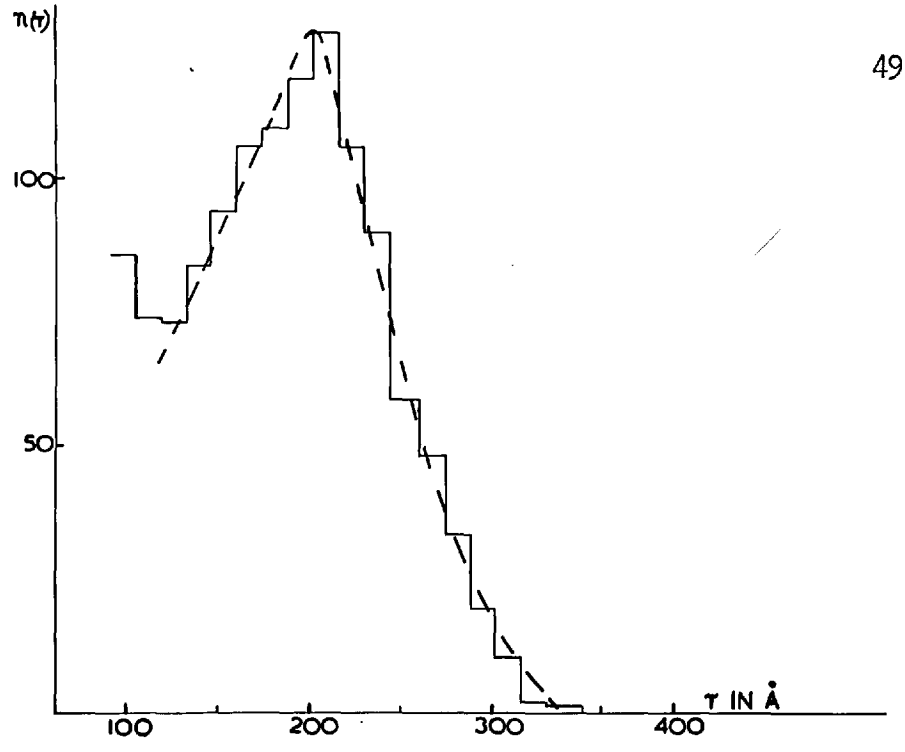

Figure 19a. Crystallite size distribution of Specimen shown in Figure 19.

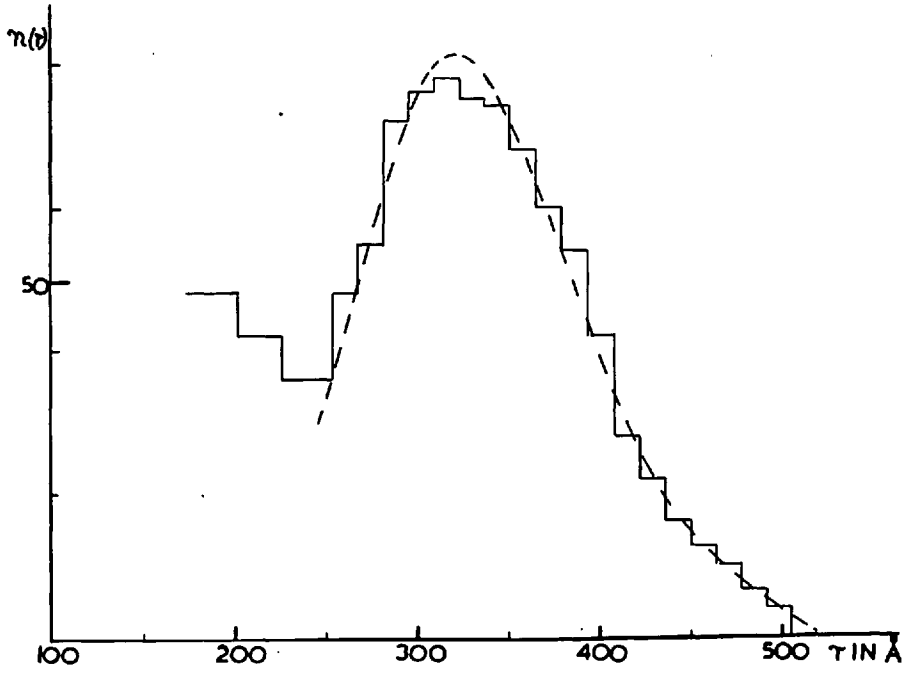

Figure 20a. Crystallite size distribution of Specimen shown in Figure 20.

to the left of the minimum of the distribution have been ignored.

From the histograms the corresponding mass distribution amongst the different crystallite sizes could be obtained. Since the crystallites were spherical the mass of a crystallite of radius r is m_r where

$$m_r = \frac{4}{3}\pi r^3 \rho = kr^3 \qquad (1)$$

$k = \frac{4\pi}{3}\rho$ and ρ = density of tin, assumed constant for all the crystallites studied. The total mass of tin, $M(r)$, in crystallites measured with radius r, is given by :-

$$M(r) = n(r)\, m_r \qquad (2)$$

where $n(r)$ = the number of crystallites measured with radius r. Therefore, from (1) :-

$$M(r) = n(r)\, kr^3 = km(r) \qquad (3)$$

where $m(r) = n(r)\, r^3$

The mass distribution histogram of each specimen was constructed by multiplying the determined values of $n(r)$ by r^3 and plotting this as ordinate against r as abscissa. (As the values required were only

relative, it was unnecessary to multiphy by k). The m(r) histograms of the specimens whose electron microscope photographs appear in Figures 12 to 20, are shown, with smooth curves drawn through them, in Figures 21 to 29. These distributions show that in the case of the larger crystallite specimens the contribution to the total mass of the specimen from the smallest crystallites is less than 1% of the total. Therefore when the crystallite sizes were measured no appreciable error was introduced by leaving outthe crystallites of radii smaller than the radius corresponding to the minimum between the two peaks of the size distribution. An example of the crystallites omitted is shown in the unshaded portion of Figure 16.

The distributions obtained for both masses and sizes were representative of the total specimen. The total mass of the specimen was proportional to th total mass in the histogram, the constant of proportionality, A, being the ratio of the total area of the specimen to the area used to construct the histogram. The total mass, M, in all the crystallites of the specimen is, therefore, given by :-

$$M = A \int_0^\infty M(r)\ dr = kA \int_0^\infty m(r)\ dr \qquad (4)$$

where the integration is carried out under the smooth distribution function. But

$$kA \int_0^\infty m(r)\ dr = kA \int_0^r m(r)\ dr + kA \int_r^\infty m(r)\ dr \qquad (5)$$

Figure 22. Crystallite mass distribution of Specimen shown in Figure 13.

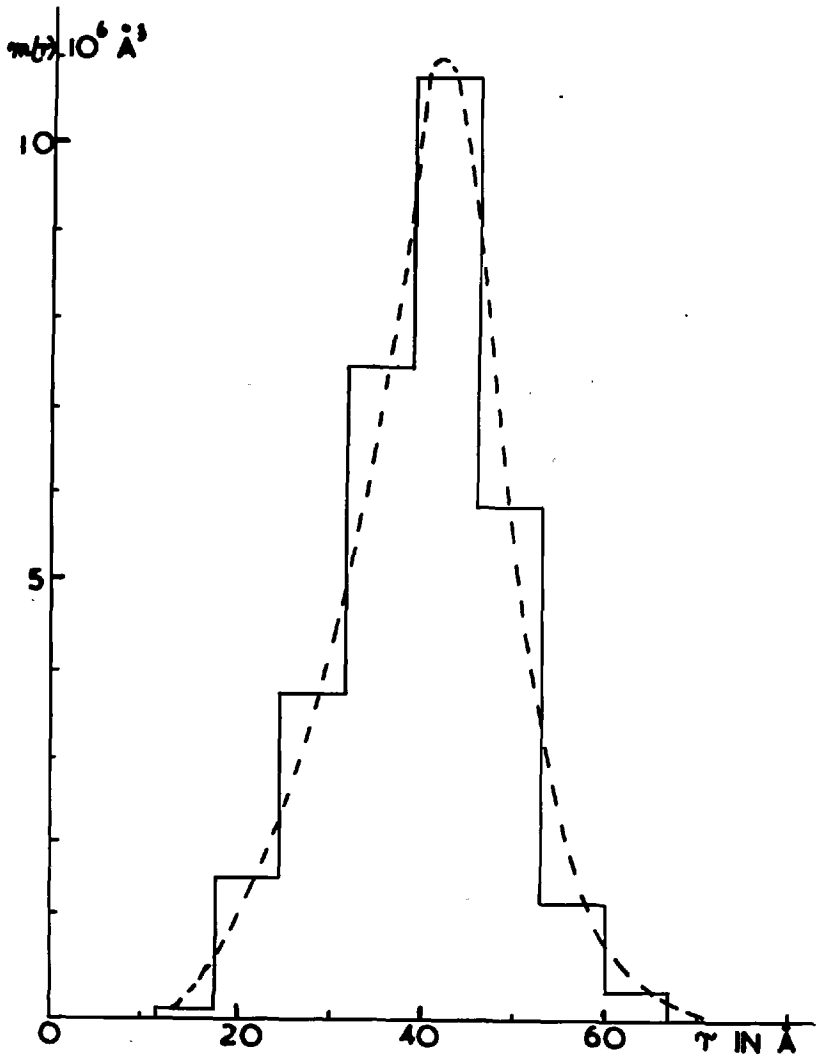

Figure 21. Crystallite mass distribution of Specimen shown in Figure 12.

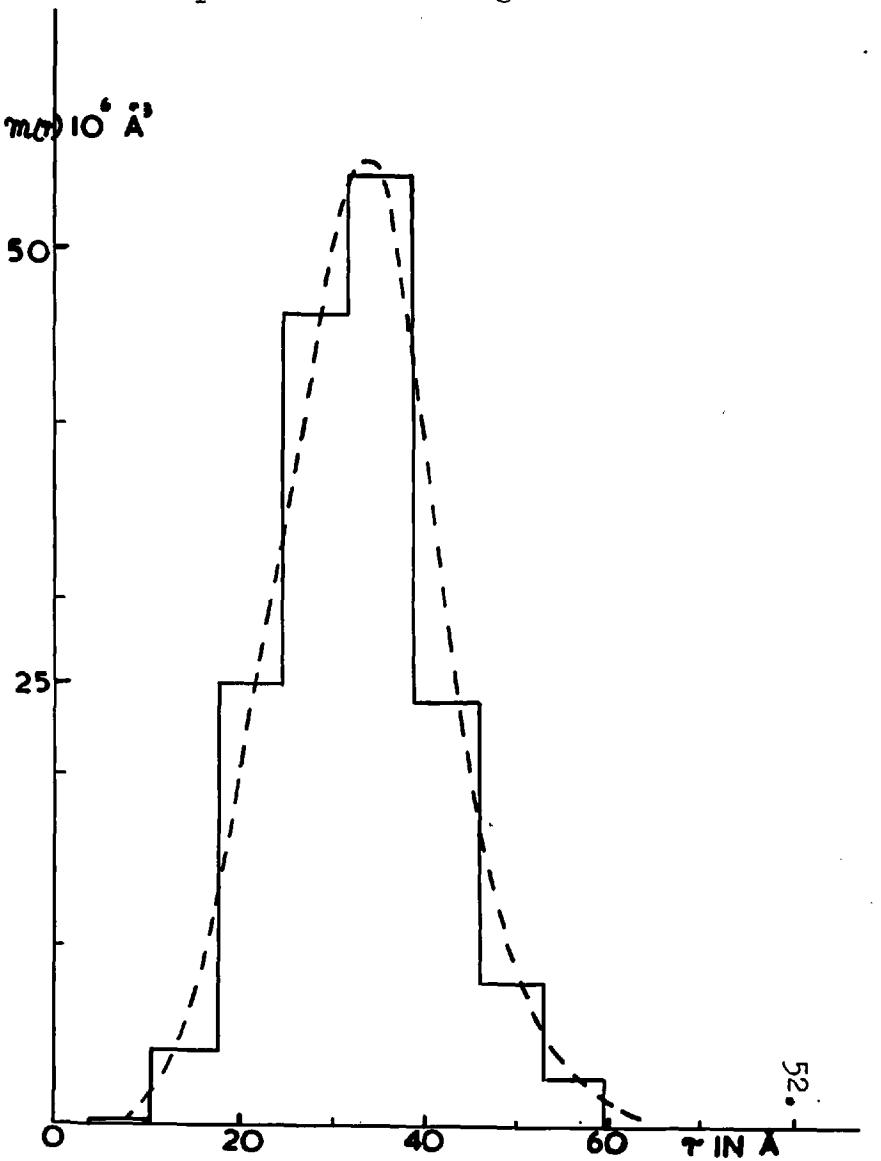

Figure 24. Crystallite mass distribution of Specimen shown in Figure 15.

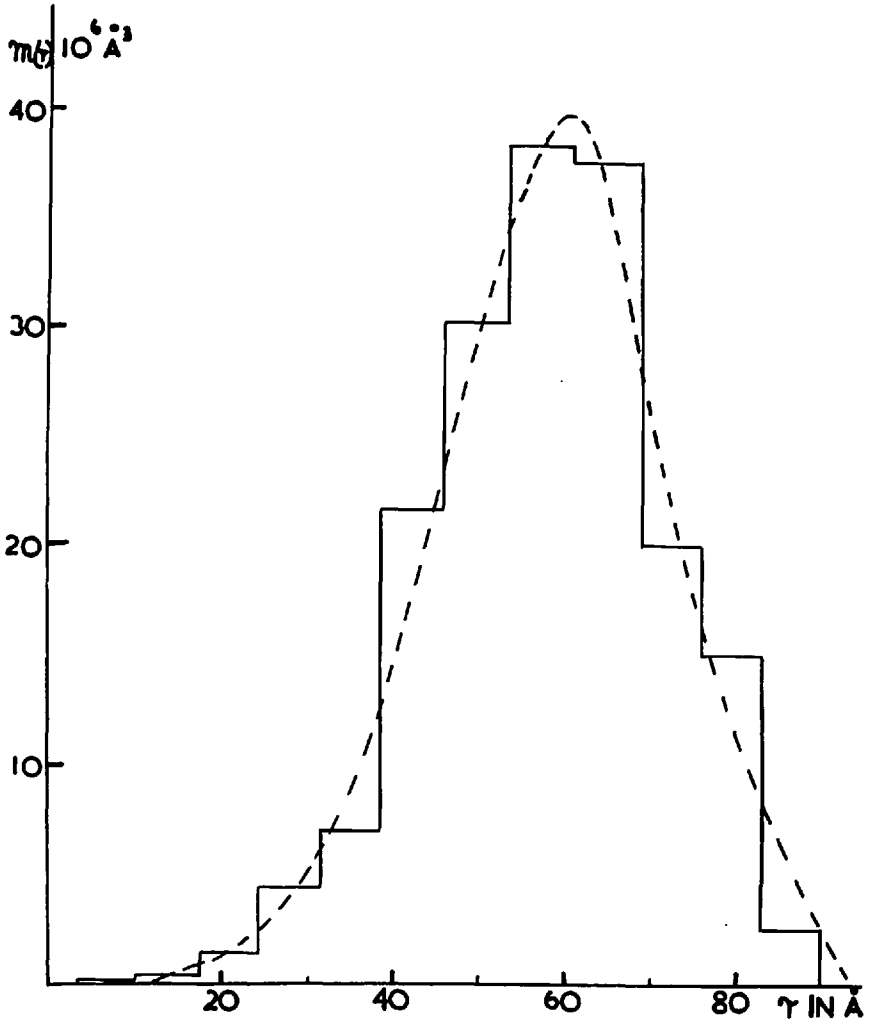

Figure 23. Crystallite mass distribution of Specimen shown in Figure 14.

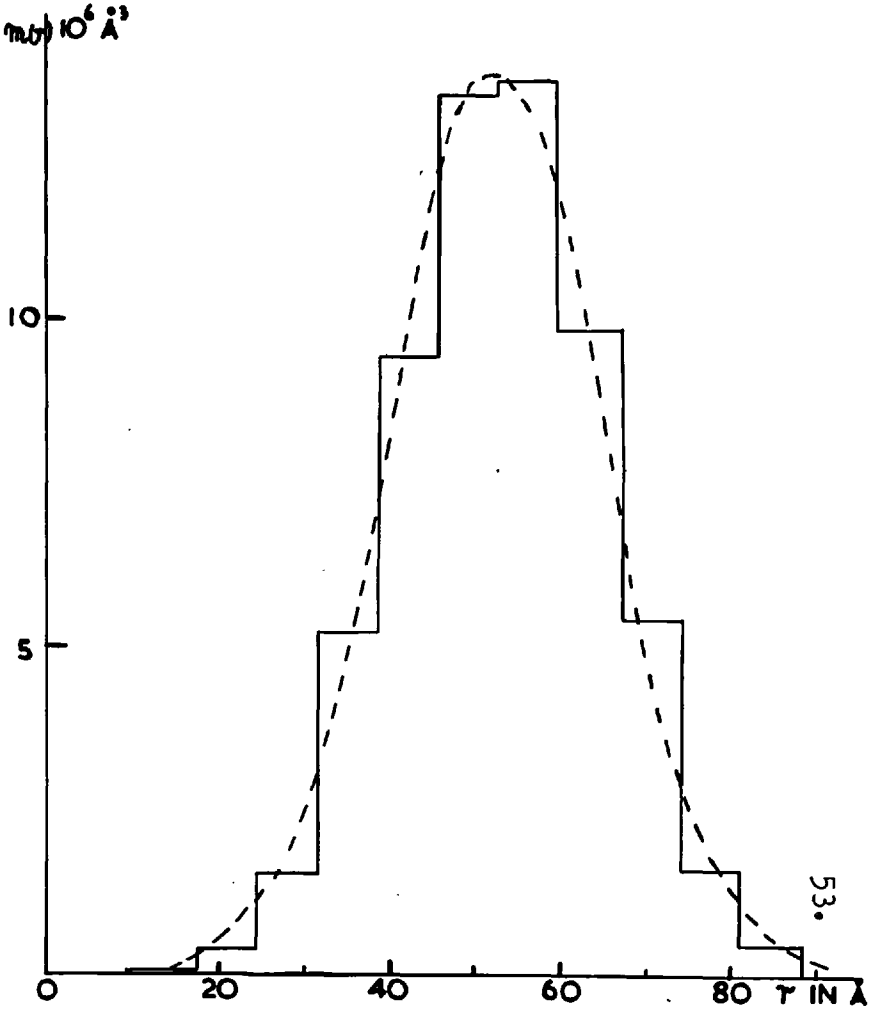

Figure 25. Crystallite mass distribution of Specimen shown in Figure 16.

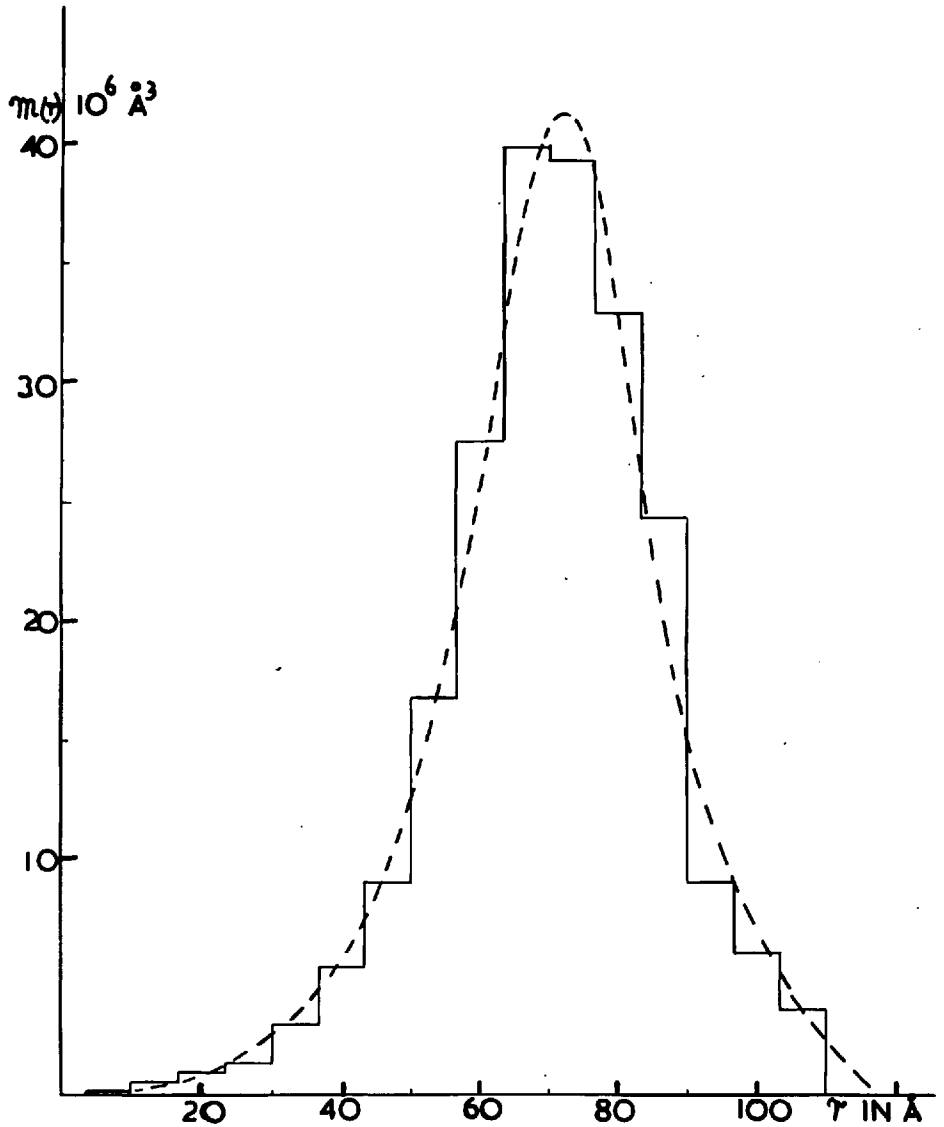

Figure 26. Crystallite mass distribution of Specimen shown in Figure 17.

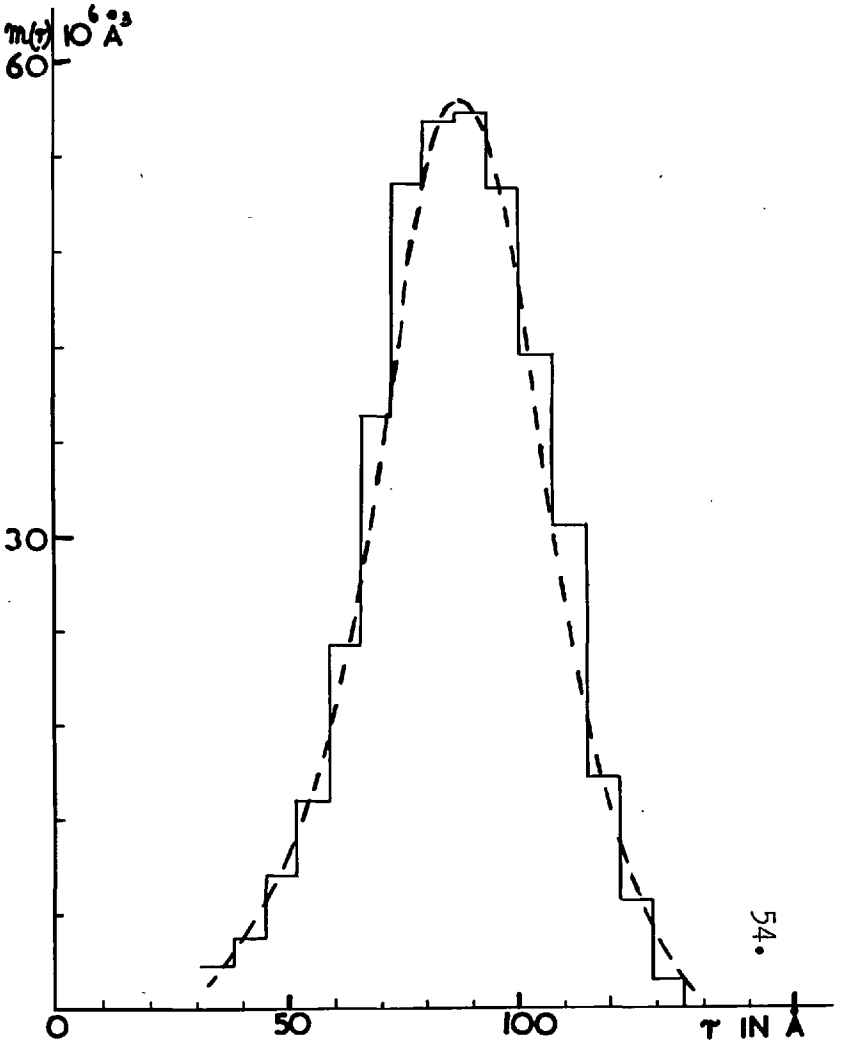

Figure 27. Crystallite mass distribution of Specimen shown in Figure 18.

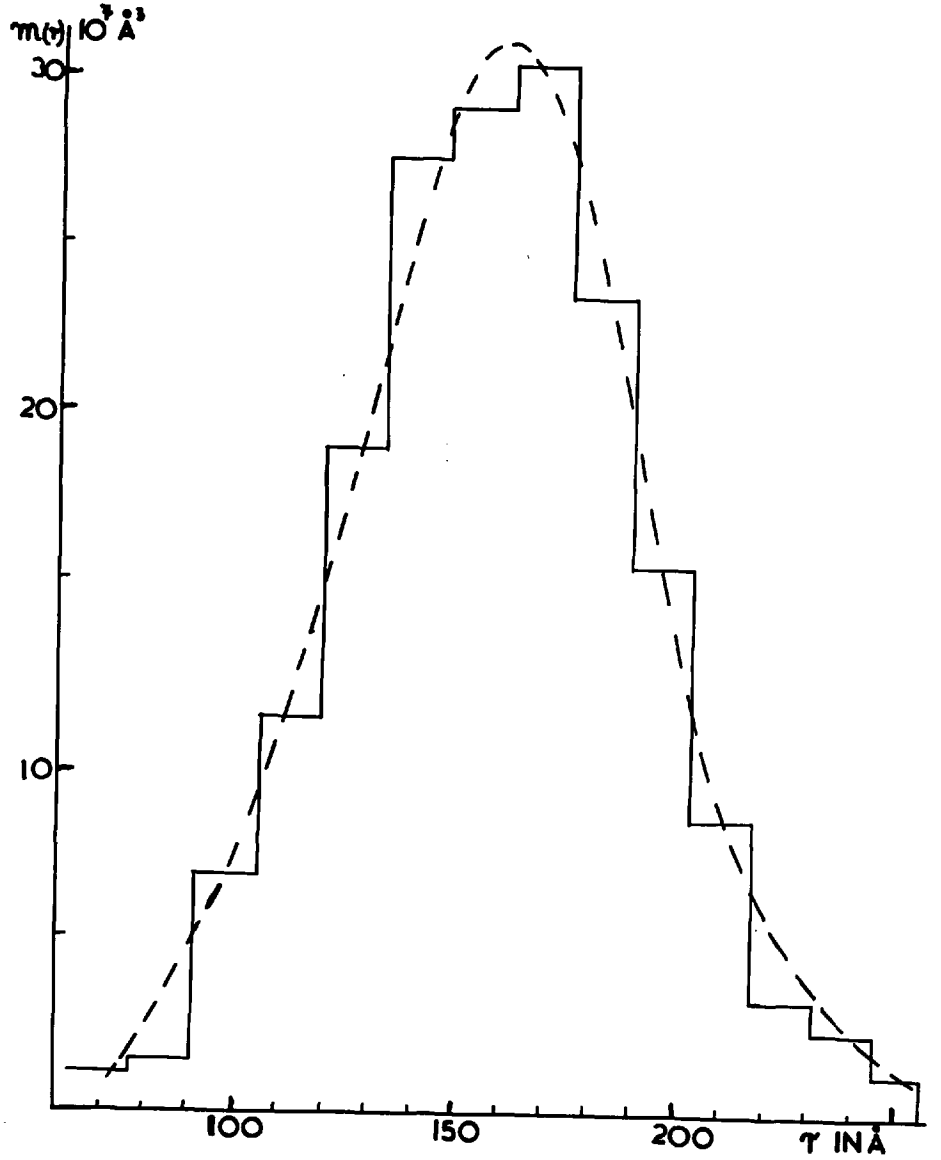

Figure 28. Crystallite mass distribution of Specimen shown in Figure 19.

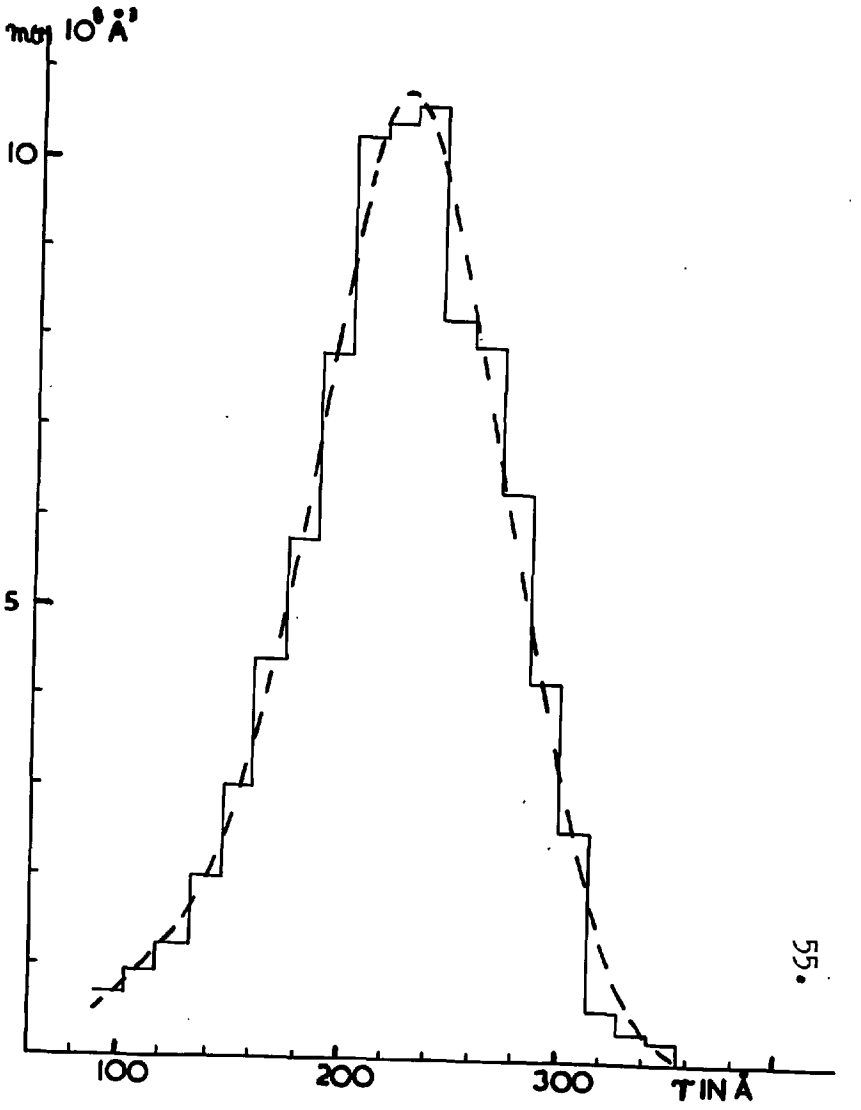

Figure 29. Crystallite mass distribution of Specimen shown in Figure 20.

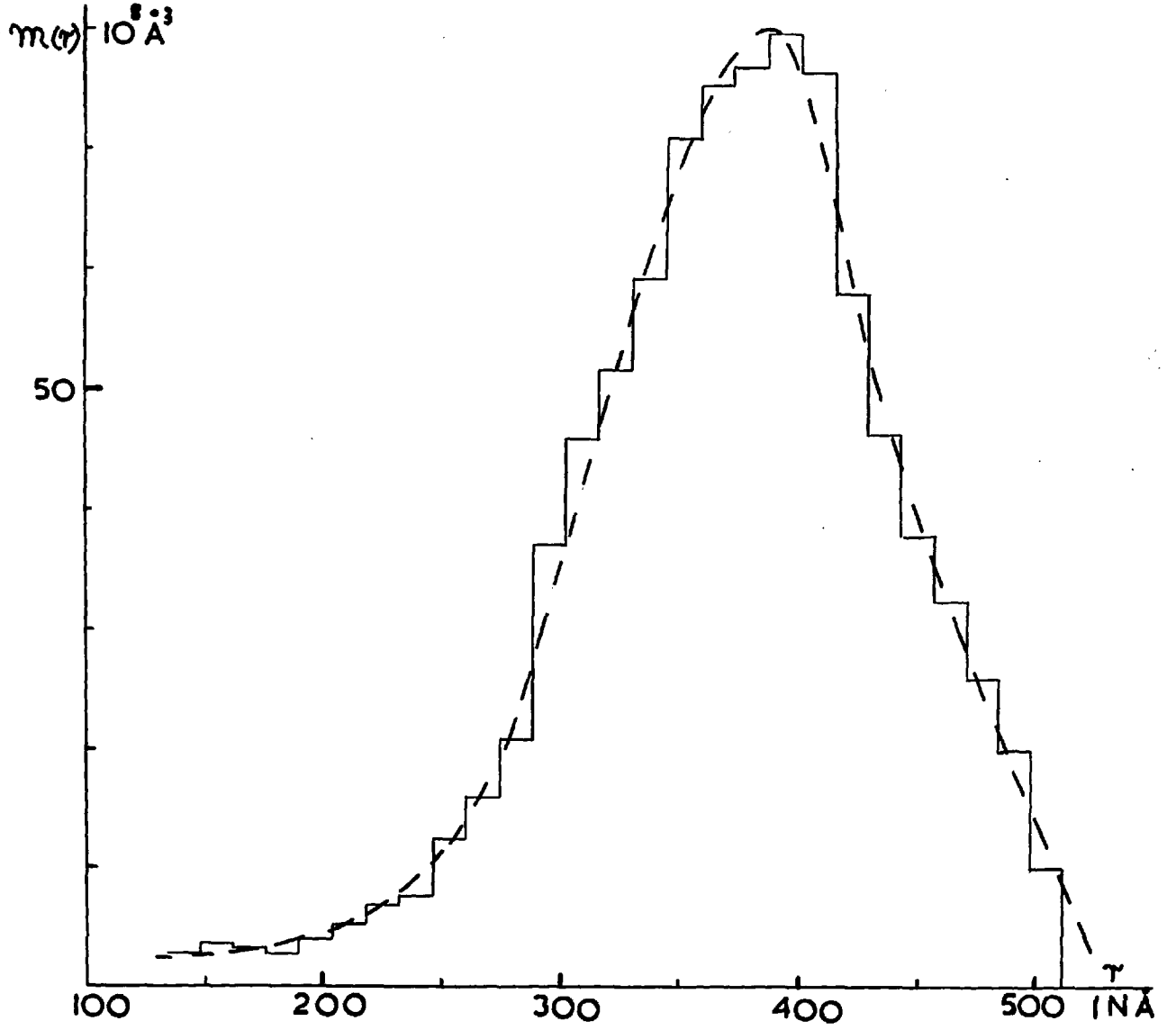

Therefore from the mass distribution functions m(r) and equation (5), it was possible to calculate the relative percentages of the mass of tin contained in crystallites with radii greater or less than any given r. This was essential for the determination of the melting point of a single crystallite.

3. Determination of the Melting Point of Crystallites of a Definite Radius.

In order to determine the effect of crystallite size on the melting point of tin it was, in principle, necessary to determine the melting temperature of a single crystallite of given radius. As the electron beam was 600 μ. in diameter at the level of the specimen, it passed through thousands of crystallites. Consequently, the electron diffraction patterns photographed at temperatures up to 232°C represented the resultant effect of all these crystallites. The specimens were prepared so that they had a definite uniform distribution of crystallites throughout. This made it possible to determine, by the method described below, the melting temperatures of crystallites of any given radius. The crystallites in a given specimen had different radii and hence different masses and surface to volume ratios. Because of the increase in the surface to volume ratio with decrease of radius, the smaller crystallites could be expected to melt at lower temperatures than the larger ones. As the temperature was raised, crystallites with progressively larger radii would melt, until at some temperature all the tin crystallites would have melted. This temperature would be below

232°C if there were appreciable surface effects in all the crystallites.

The change in the diffraction pattern described in Section I of Chapter IV is due to the crystallites melting in this way. However the sharp ring pattern would be expected to disappear before all the crystallites had melted because of the relative intensities of the liquid and solid patterns. The liquid haloes appeared in the same position as the (200), (101) and (220), (211) rings of the polycrystalline solid tin, so that when the liquid tin pattern reached a certain intensity relative to that of the solid, the sharp rings were no longer visible. The superposition experiments described in Section 5 of Chapter III, showed that there was a minimum mass of liquid necessary to obscure a ring pattern from a given amount of solid. Therefore, once the mass distribution of a specimen had been determined, the temperature at which its sharp ring diffraction pattern disappeared could be correlated with the sizes of the crystallites in it. Each crystallite produced its own diffraction pattern which depended on its size and temperature. The intensity of the pattern depends on the number of the scattering atoms causing it (Pinsker (1953) p.143) so that crystallites of different mass contribute different intensities to the total diffraction pattern. The variation with temperature of the intensity of a diffraction pattern, due to the thermal vibrations of the individual atoms, is small (Thomson & Cochrane (1939) p.105) so that the pattern of a solid crystallite can be considered as constant up to its melting point. At this temperature however the crystallite melts and there is a change in its diffraction pattern.

A large number of crystallites of the same size would produce a constant sharp ring pattern up to their melting point, when they would simultaneously melt and produce a diffuse halo pattern. The intensities of these patterns would depend on the number of crystallites and their masses that is $n(r)m_r \doteq m(r)$, where $m(r)$ is the mass distribution function. Crystallites with different radii would melt at different temperatures and their contributions to the solid pattern would cease, and there would be a corresponding increase in the intensity of the liquid pattern proportional to $m(r)$. The factor which therefore determines the type and intensity of the diffraction pattern of a specimen at a given temperature is the ratio of the solid to liquid crystallite masses, and not the relative numbers of solid and molten crystallites. The rate of transformation of the diffraction pattern would depend on the rate of heating and the size and mass distributions of the crystallites in a given specimen.

Suppose the effect of the size of crystallite on the melting point is such that a crystallite of radius r melts at a temperature T. Therefore at the temperature T all the crystallites with radii less than or equal to r are molten. For a given specimen, the liquid mass at temperature T is, $M_l = kA \int_o^r m(r)dr$ (from equation (5)) and similarly the solid mass at temperature T is $M_s = kA \int_r^\infty m(r)\, dr$, with $M_l + M_s = M$, the total mass of the specimen. As the temperature increases, M_l increases and M_s decreases, so that the value of r in the limits of the integrals changes.

The intensities of the liquid and solid patterns were respectively proportional to M_l and M_s so the resultant diffraction pattern became one characteristic of a liquid with the superimposed rings due to the solid becoming successively weaker. At a certain value of the temperature the rings were no longer visible. This temperature was identified as T_m (see Section 1 of this Chapter), so let the radius of the crystallites which melt at this temperature T_m be denoted by r_m. The specimen at this temperature has solid mass

$$M_s = kA \int_{r_m}^{\infty} m(r)\, dr \qquad (6)$$

and liquid mass

$$M_l = kA \int_{o}^{r_m} m(r)\, dr \qquad (7)$$

where M_l is sufficient to give a liquid pattern strong enough to obscure the solid pattern due to M_s. If the ratio of M_l to M_s for this to occur is found, the value of r_m may be obtained from the mass distribution of the specimen and hence the melting point of crystallites of given radius can be determined.

To determine which ratio of M_l to M_s would produce a diffraction pattern in which the solid rings had just ceased to be visible, the super-position experiments described in Section 5 of Chapter III were carried out. The areas of the specimens which produced the two seperate diffraction patterns were constant. Thus, as the mass distributions were uniform throughout each specimen, the intensities were proportional to the

total masses of tin on the specimens. Since the conditions during the evaporations were maintained constant, the condensed masses on any specimen were the same fraction of the evaporated masses. The super-position of the diffraction patterns produced by different masses of liquid and solid tin are shown in Figures 30,31 and 32. Since the masses producing the diffraction patterns of each specimen were a constant fraction of the masses evaporated, the ratios of these masses were the same for different specimens. Therefore the required ratio of the liquid mass to the solid mass could be determined from the appropriate masses evaporated. To check this, the size and mass distributions of equal areas were measured on different specimens and the ratio of the masses on these areas was found to agree, within the experimental error, with the ratio of the evaporated masses.

It was found from these experiments that when in a given mass of tin 15% was solid and 85% liquid, the solid sharp rings could no longer be seen on the liquid halo pattern of tin. This percentage was obtained for a whole series of total masses. The values of M_l, M_s defining r_m in a given specimen were therefore subject to the equations

$$\int_0^{r_m} m(r)\, dr = 0.85 \frac{M}{KA} \tag{8}$$

$$\int_{r_m}^{\infty} m(r)\, dr = 0.15 \frac{M}{KA} \tag{9}$$

where $\frac{M}{A}$ was the total mass of tin measured on the specimen. Therefore from the mass histogram of each specimen, the value r_m was determined by using equations (8) and (9), and this value was then correlated with T_m to give the melting temperature of a crystallite of a given radius.

FIGURE 30. A composite transmission electron diffraction pattern produced by tin crystallites from specimens with a weight ratio of solid to liquid of 1:3.

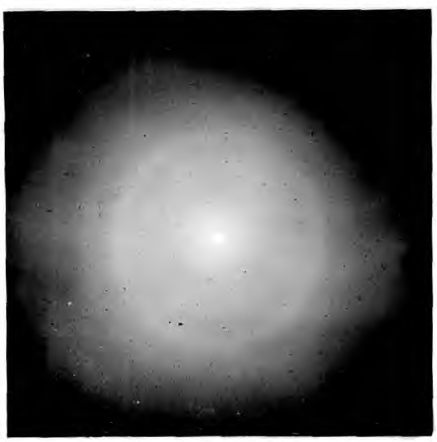

FIGURE 31. A composite transmission electron diffraction pattern produced by tin crystallites from specimens with a weight ratio of solid to liquid of 1:4.

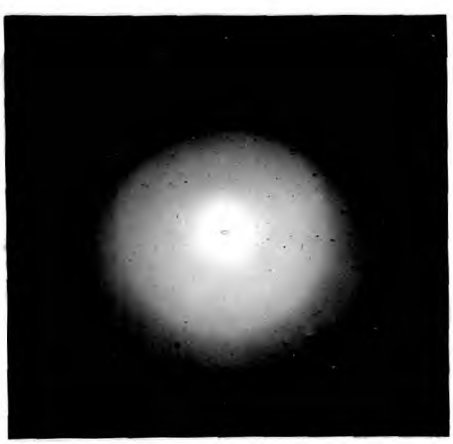

FIGURE 32. A composite transmission electron diffraction pattern produced by tin crystallites from specimens with a weight ratio of solid to liquid of 1:5.

4) Determination of Structure and Lattice Parameters of Tin Crystallites.

Two different structures occur in bulk crystalline tin, namely grey or α-tin and white or β-tin. Grey tin has a diamond type unit cell of side $a = 6.46$ Å (Bijl and Kolkmeijer 1918; 1919 a,b). White tin, which is stable at room temperature, has a tetragonal unit cell with dimensions

$$a = b = 5.82 \text{ Å} \quad c = 3.17 \text{ Å} \quad \text{at } 25\ ^{\circ}\text{C}$$

(Wyckoff, Chapter II, Text page 13, Illust. p.7; Jette and Foote, 1935, Koslapov and Trapeznikov, 1936; Jevins, Stramanis and Karlsons, 1938) The unit cell contains four atoms in the positions $0,0,0;0,\frac{1}{2},\frac{1}{4};\frac{1}{2},0,\frac{3}{4};$ $\frac{1}{2},\frac{1}{2},\frac{1}{2}$. The transformation temperature of grey tin into white tin is 13.2°C (Hedges and Higgs, 1952) therefore since in the experiments carried out the lowest temperature to which the crystallites were subject was approximately 25°C, if the crystallites had the structure of bulk crystalline tin, the white tin polycrystalline patterns should be observed. The bases beneath the crystallites were amorphous therefore they would not affect the structure of the crystallites. However as some of the crystallites had radii smaller than 30 Å, surface effects could affect the structure and produce a different unit cell from that of bulk tin. Bublik and Pines (1952) showed by electron diffraction methods that vanadium, which in bulk has a body-centred cubic structure, could be made

to form an unsupported film 60 Å thick with a face-centred cubic structure. Nicholson (1950) showed, using X-rays, that strain due to surface stresses in sodium chloride and magnesium oxide crystallites of mean size 600 Å induced changes in the lattice parameters of a fraction of a percent. Hence the experiments in Section 6 of Chapter III were carried out to see whether the surfaces of these small crystallites induced any change in the structure and lattice parameters of the crystallites in the specimens.

Two diffraction patterns were photographed in each experiment. One photograph was taken of the diffraction pattern from a specimen whose unit cell dimensions were known and the other from the specimen whose properties were investigated. A thallium chloride film had been prepared over 1000 Å thick so that surface effects on its unit cell were negligible. This has a cubic structure with sides of the unit cell $a = 3.842$ Å (Smakula and Kalnajas, 1955). A tin specimen was prepared, by the usual methods of producing spherical crystallites, of mean radius about 200 Å. The structure of this was analysed and its lattice parameters were determined. This specimen was then used to determine the structural properties of tin crystallites with small mean radii. Photographs of the diffraction patterns of crystallites of mean radii of about 200 Å and 25 Å are shown in Figure 33. with their rings indexed.

It may be shown to a first approximation (Pinsker (1953) p.86) that for an electron diffraction pattern produced by a polycrystalline

material

$$rd = L\lambda \quad . \qquad (10)$$

where r = radius a particular ring in the diffraction pattern.

d = the spacing of crystal plane which gives rise to the ring.

λ = electron wavelength.

L = distance of the specimen from the photographic plate.

In each experiment $L\lambda$ was exactly the same for the diffraction pattern photographs of both the standard and the specimen studied. The rings of the standard specimen were measured with a travelling microscope, and from the calculated plane spacings producing the rings, $L\lambda$ could be obtained.

For thallium chloride, the spacing in its cubic structure of a plane with Miller indeces h,k,l, $d_{h,k,l}$ is given by

$$d_{h,k,l} = \frac{3.842}{\sqrt{h^2+k^2+l^2}} \quad \text{Å} \qquad (11)$$

where 3.842 Å is the dimension of a side of the unit cell. This enabled accurate determination of $L\lambda$ using equation (10).

All the tin crystallite specimens were found to give the body centred tetragonal structure diffraction pattern of white tin. For tetragonal structure it can be shown (Thomson and Cochrane (1939) p.28)

that the spacing of planes with Miller indeces h,k,l is given by

$$d_{h,k,l} = \frac{1}{\sqrt{\frac{h^2}{a^2} + \frac{k^2}{a^2} + \frac{l^2}{c^2}}} \qquad (12)$$

where a,c are the sides of the unit cell. Using the values of a,c for bulk tetragonal tin,

$$d_{h,k,l} = \frac{1}{\sqrt{\frac{h_1^2 + k^2}{33.79} + \frac{l^2}{1.005}}} \qquad (13)$$

From the determined value of $L\lambda$, the lattice spacings of a specimen with mean radius $\sim$ 200 $\mathring{A}$ were determined by measuring the radii of its diffraction rings. The calculated spacings of planes giving rise to the main rings, together with the calculated values for bulk crystalline white tin are tabulated in Table I. The values agree to within the experimental error of $\pm$ 0.5%. This tin specimen was then used as a standard when smaller crystallite specimens were investigated. As the mean size of crystallites decreased, fewer rings could be observed on the diffraction pattern. However it can be seen from Figure 33 that the (211) ring is intense and its measurement was used in the comparison of lattice constants of the different specimens.

The radius of the (211) ring from the standard specimen was compared with that of the specimen under investigation and in no case was a change in the lattice parameter observed, to within the experimental accuracy of 0.5%.

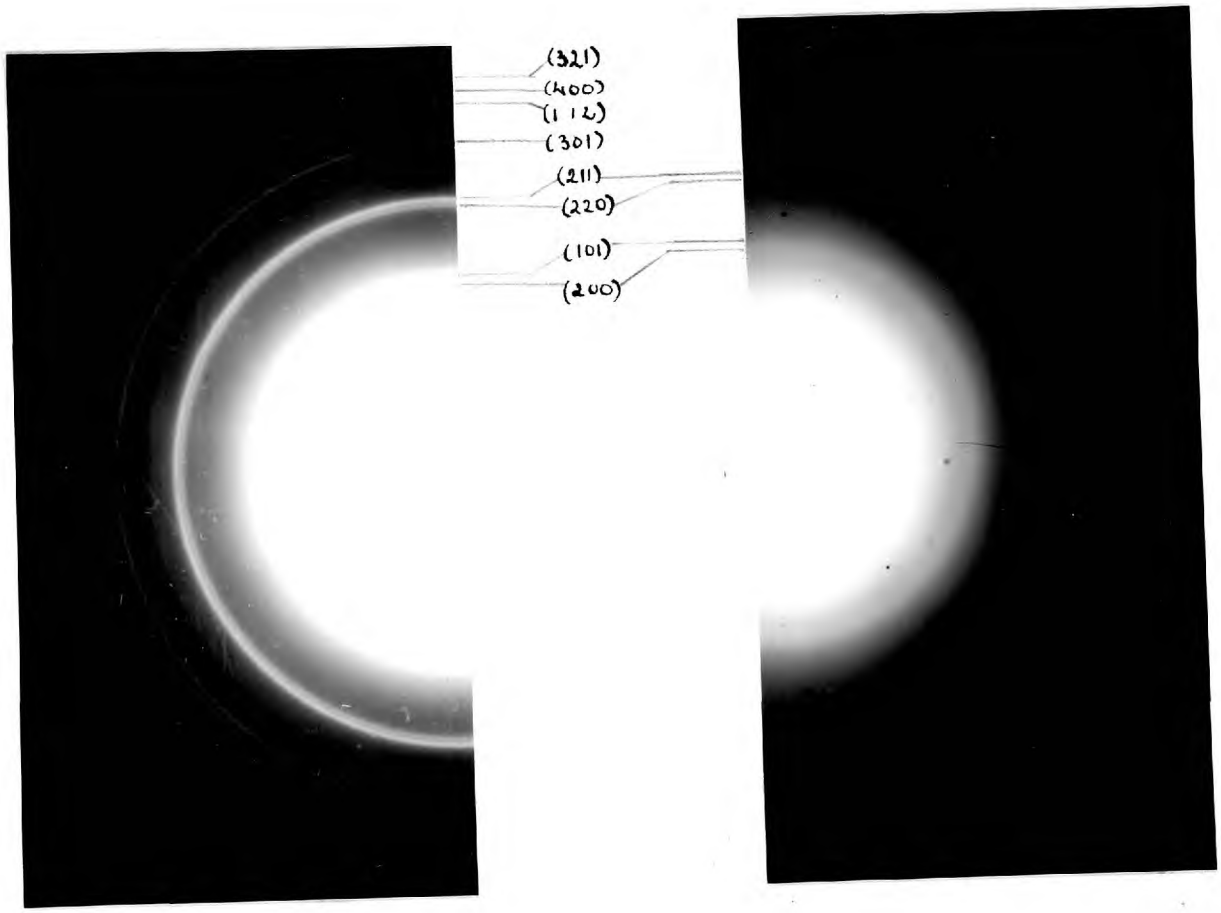

(A) (B)

FIGURE 33 Transmission electron diffraction patterns produced by tin crystallites.

(A) Crystallite mean radius $\sim$ 200 Å.

(B) Crystallite mean radius $\sim$ 25 Å.

TABLE I

MAIN RINGS OF THE DIFFRACTION PATTERN PRODUCED BY TIN CRYSTALLITES OF MEAN RADIUS $\sim$ 200 Å.

$$L\lambda = 2.257 \text{ Å}.$$

(h,k,l)	r in cms	d in Å	d_{calc} in Å
200	0.775	2.913	2.906
101	0.815	2.773	2.777
301	1.096	2.059	2.055
211	1.122	2.011	2.007
301	1.367	1.655	1.652
420	1.736	1.300	1.300

r = the radius of the ring in the diffraction pattern of tin

d = the measured plane spacing, calculated from r using equation (10).

d_{calc} = the calculated plane spacing for the (h,k,l) plane in tetragonal tin using equation (13).

CHAPTER V

Results and Discussion of the Experiments.

From previously explained measurements carried out on each specimen the two quantities T_m and r_m were determined - these being respectively the melting point of the specimen, and the radius defined from the mass distribution by the crystallites which contain 85% of the total mass of tin in the specimen. These two values can be identified with the melting point of a single tin crystallite of given radius $R = r_m$ melting at temperature $T_r = T_m$.

1. Tin Crystallites on Silicon Monoxide Substrates.

The results obtained from the specimens in which the tin crystallites under examination were on silicon monoxide are shown in Table II. The crystallite radius, R, was studied over a range of 40 to 400 Å, with a corresponding range for the melting point, T_R, of 150 to 230°C. The majority of values of R and T_R were determined for $R < 120$ Å, as the variation of T_R with R was found to be much more gradual for crystallites with radii larger than about 100 Å. The resultant graph of ΔT_R against R for tin crystallites on silicon monoxide bases is plotted in Figure 34 and that of T_R against $1/R$ in Figure 35.

2. Tin Crystallites on Carbon Substrates.

The results obtained from the specimens in which the tin crystallites studied were on carbon substrates are shown in Table III. The range of crystallite radii was extended to try to obtain melting points for tin

crystallites with radii less than 40 Å, but because of the lack of contrast in the electron microscope photographs, the accuracy of determination of the radii decreased for the smaller particles. In addition, the errors in the radius, R, and temperature, T_R, were larger for these small crystallites, since the rings from the solid crystallites had broadened out, the diffraction patterns had become weaker, and the transition of the diffraction patterns of the specimen on melting had become more gradual. For tin crystallites on a carbon base a graph of ΔT_R against R is plotted in Figure 36 and that of T_R against $^1/R$ in Figure 37.

The results obtained for carbon and silicon monoxide bases were the same within the experimental error.

3. Discussion of Experiments.

The information obtained from the experiments carried out on each specimen was analysed in terms of two parameters R and T_R for each individual tin crystallite. It would perhaps be advisable to consider the justification for this procedure and the errors involved in these parameters. The crystallites, whose formation and nature will be discussed, were from many different specimens, and were prepared and investigated under conditions as identical as possible. The experimental procedure followed was the same in all cases and the errors that arose in the different parts of this procedure must all be incorporated into the total error.

TABLE II

T_R °C	ΔT_R °C	R. Å	T_R °C	ΔT °C	RÅ
148±5	84±5	41±4	206±2	26±2	78±4
155±3	77±3	48±4	209±2	23±2	86±4
159±3	73±3	44±4	210±2	22±2	93±4
163±3	69±3	48±4	211±2	21±2	91±4
169±3	63±3	51±4	212±2	20±2	102±4
170±3	62±3	51±4	215±2	17±2	115±4
172±3	60±3	50±4	216±2	16±2	107±4
172±3	60±3	52±4	217±2	15±2	125±4
175±2	57±2	55±4	217±2	15±2	120±4
188±2	44±2	65±4	218±2	14±2	114±4
190±2	42±2	64±4	224±1	8±1	175±8
196±2	36±2	70±4	225±1	7±1	191±8
200±2	32±2	73±4	226±1	6±1	198±8
200±2	32±2	77±4	227±1	5±1	233±8
204±2	28±2	76±4	229±1	3±1	275±8
204±2	28±2	80±4	230±1	2±1	373±8

T_R = Melting temperature of tin crystallite.

R = Radius of tin crystallite

$\Delta T_R = T_B - T_R$

where $T_B = 232^{\circ}C$ - the melting point of bulk tin.

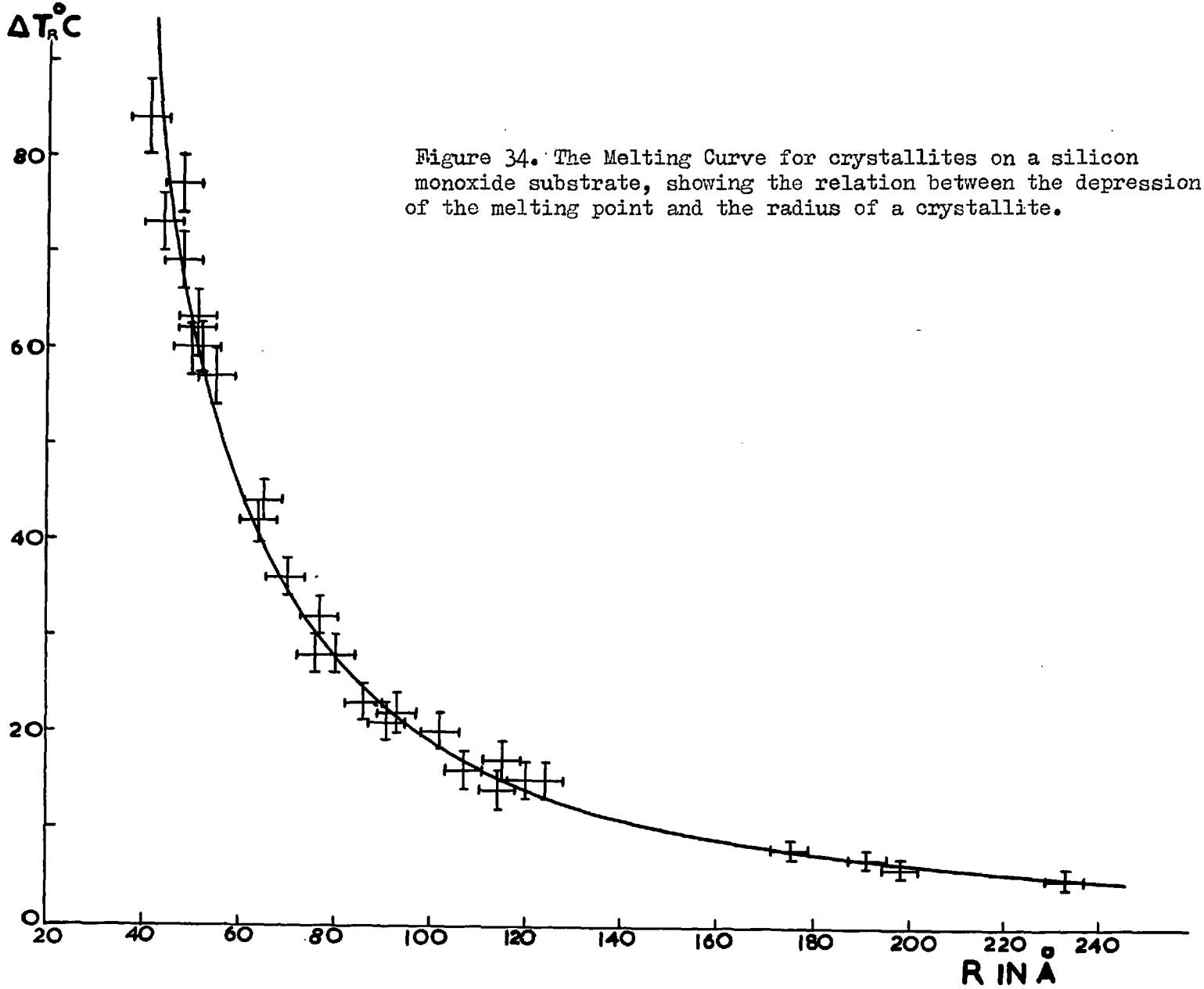

Figure 34. The Melting Curve for crystallites on a silicon monoxide substrate, showing the relation between the depression of the melting point and the radius of a crystallite.

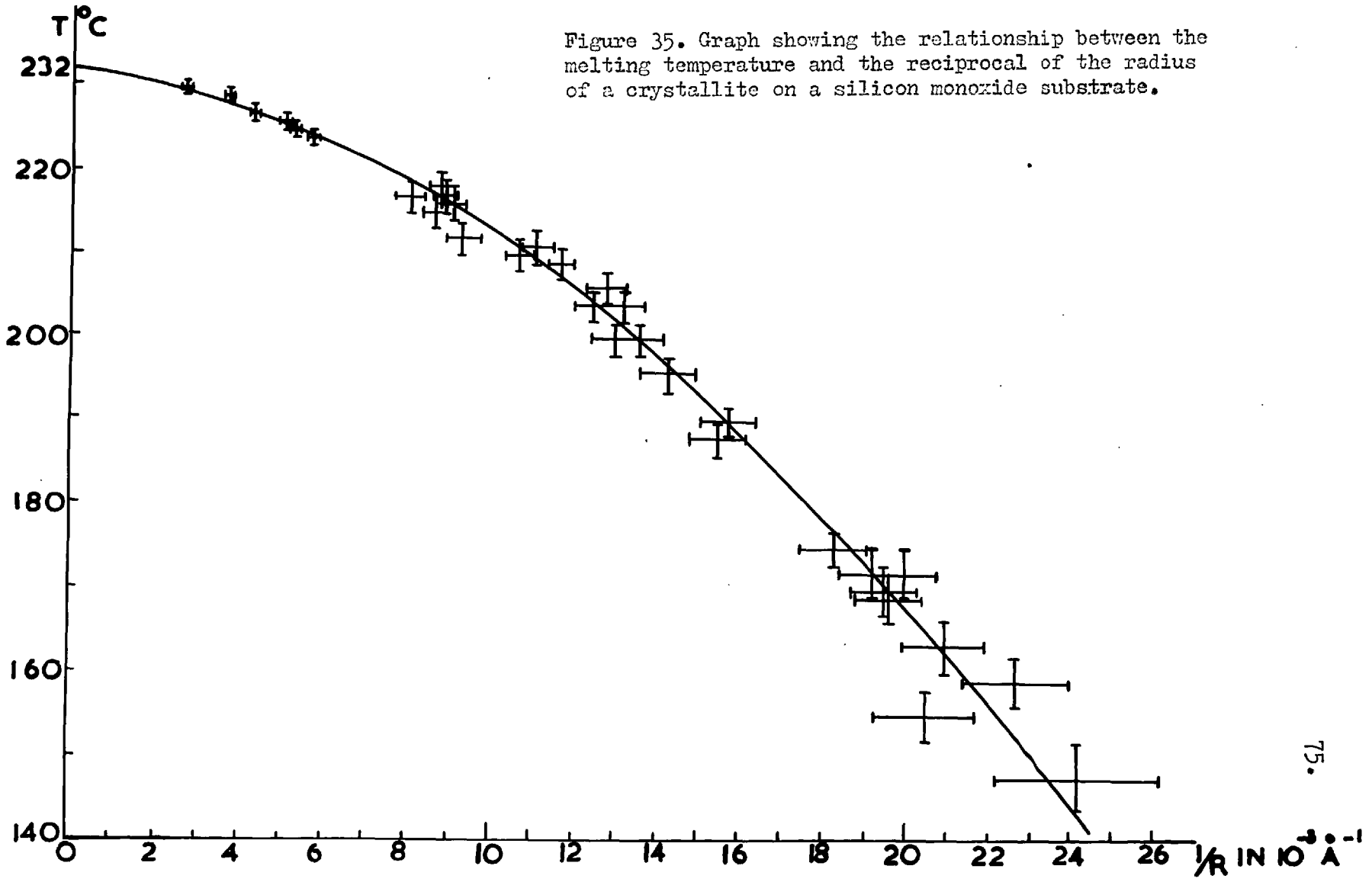

Figure 35. Graph showing the relationship between the melting temperature and the reciprocal of the radius of a crystallite on a silicon monoxide substrate.

TABLE III

T_R °C	ΔT_R °C	R Å	T_R °C	ΔT °C	R Å
60±20	162±20	30±5	187±2	45±2	63±4
100±10	132±10	36±5	191±2	41±2	68±4
115±8	117±8	42±4	196±2	36±2	66±4
127±8	105±8	38±4	202±2	30±2	71±4
135±5	97±5	40±4	202±2	30±2	74±4
140±4	92±4	40±4	204±2	28±2	78±4
158±3	74±3	48±4	205±2	27±2	81±4
165±3	67±3	52±4	212±2	20±2	104±4
166±3	66±3	53±4	215±2	17±2	103±4
177±2	55±2	59±4	225±1	7±2	181±8

T_R = Melting temperature of tin crystallite.

R = Radius of tin crystallite.

$\Delta T_R = T_B - T_R$

where T_B = 232°C - the melting point of bulk tin.

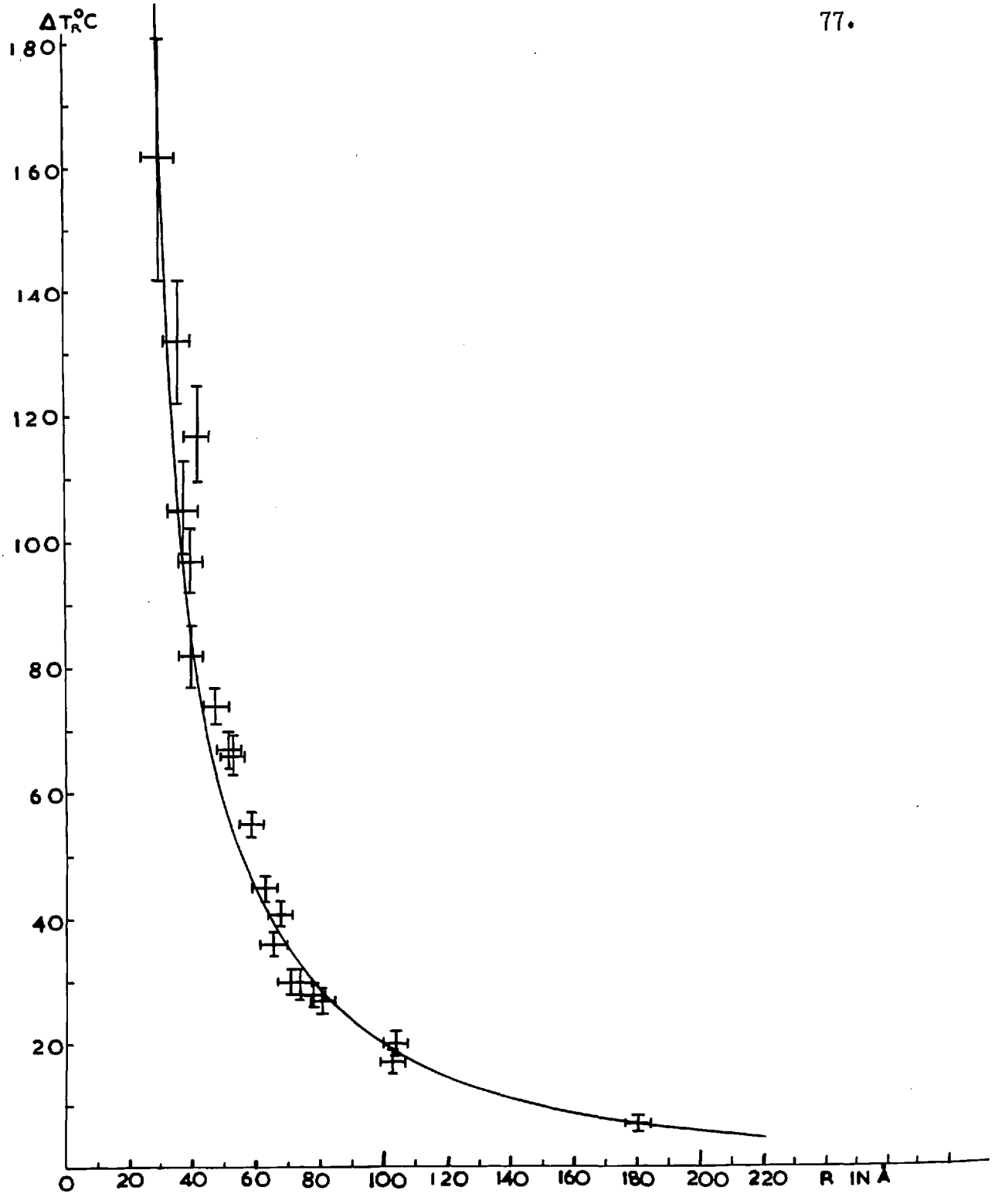

Figure 36. The Melting Curve for crystallites on a carbon substrate, showing the relation between the depression of the melting point and the radius of a crystallite.

Figure 37. Graph showing the relationship between the melting temperature and the reciprocal of the radius of a crystallite on a carbon substrate.

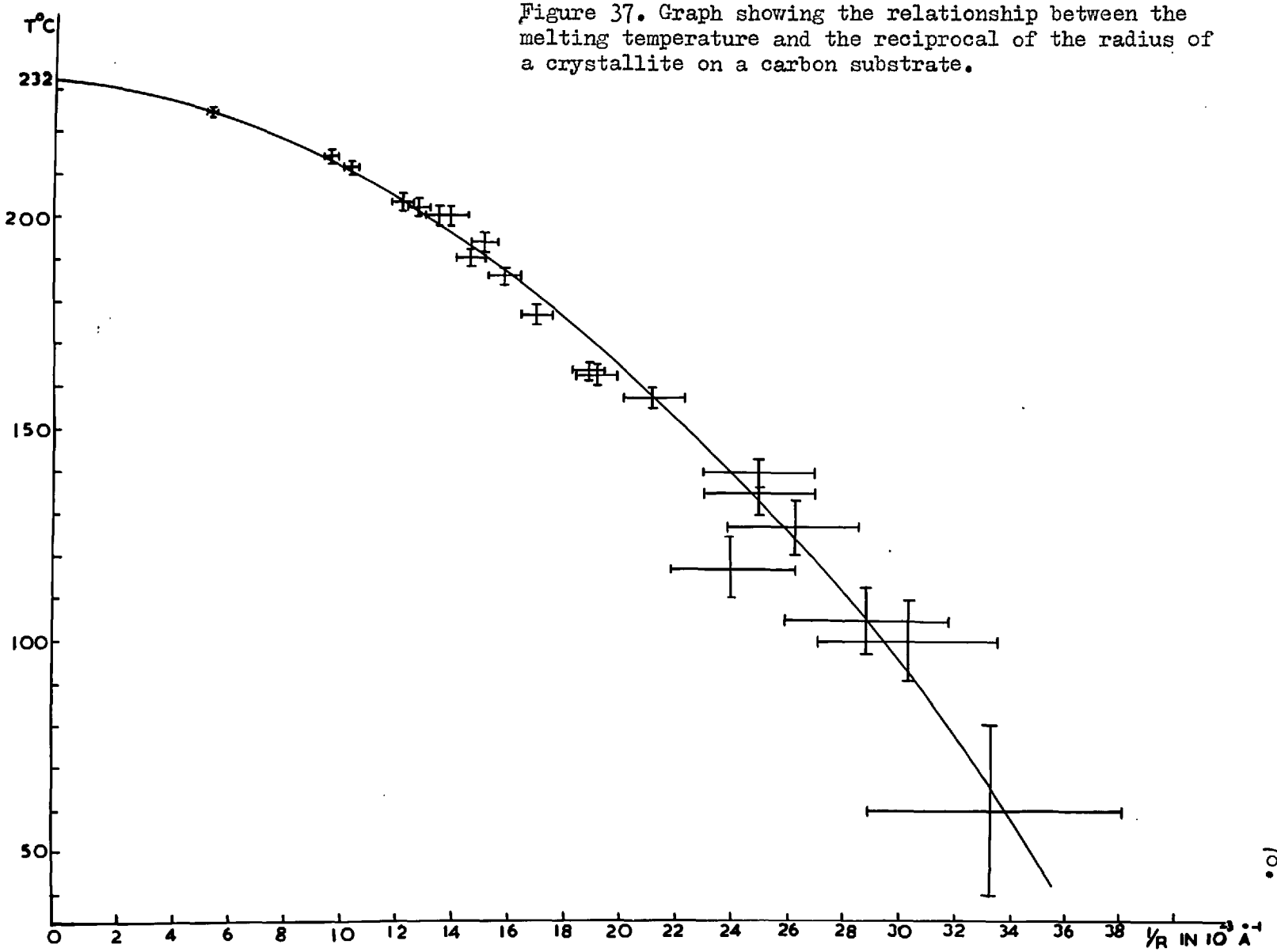

3.1 Tin Crystallites.

In principle, the determination of the effect of the surface of a crystallite on its properties would involve the observation of a single crystallite whose dimensions could be measured and whose properties studied directly. However the crystallite sizes studied were so small that it was experimentally impossible to deal with a single crystallite, and so a group of crystallites was studied simultaneously. In order to be able to determine their size easily, and in order to get as uniform a melting of each crystallite as possible, spherical crystallites with no sharp edges were required. Also, the theoretical considerations are simpler in the case of spherical crystallites. In order to determine the behaviour of a single crystallite from the results of observations on a specimen consisting of a whole range of crystallite sizes, it was necessary to have a uniform size distribution over the entire surface of the specimen. With this condition, an electron micrograph of a particular area of a specimen was representative of the whole specimen. Since each crystallite produces a circular electron microscope image, it is possible to find its mass and radius.

The nature of a thin metal layer, formed by condensation from a molecular beam, depends on the type and temperature of the substrate, the rate of evaporation, and the atmosphere in which the evaporation is carried out. Silicon monoxide and carbon substrate films were used because

their structure consists of randomly arranged atoms. These substrates are considered to be neutral, having little effect on the formation, structure and orientation of the crystallites deposited on them. (Pinsker (1953)p.196), so that layers of tin crystallites of uniform distribution could be obtained. With crystalline bases, preferential nucleation in surface imperfections could occur so that a non-uniform distribution might be obtained. The structure of thin films deposited onto a solid substrate may be stable either in the form of uniform dispersed monolayers or as agglomerates of atoms. In these experiments separate crystallites were required. The deposited metal film will be produced in the form of agglomeratesif the deposited atoms have a lower latent heat of evaporation from the surface of the substrates than from the metal itself (Appleyard 1937). Since the substrates were neutral the metal atoms had a comparatively small heat of evaporation from them and separate crystallites were formed.

In order to ensure a rapid growth of separate crystallites with the minimum loss of condensed atoms, the method described in Section 2 of Chapter III was used. Langmuir (1917) confirmed earlier experiments by Kundsen (1909) and Wood (1915,1916) which indicated that there is a critical temperature of the substrate above which condensation of a metal vapour beam will not occur. He also showed that the value of this critical temperature increases with the intensity of the vapour stream striking the substrate surface and he concluded that the phenomenon occurring on the surface was not one of reflection, but one of condensation

and re-evaporation with the incident metal atoms remaining on the surface for a finite period of time. If the average lifetime of a condensed metal atom on the surface is made sufficiently long for it to collide with another atom from the beam, the probability of re-evaporation is considerably decreased. Therefore, increase in the beam intensity allows a higher critical temperature for condensation and also raises the number of metal atoms remaining on the substrate surface, with a corresponding increase in the probability of nuclei being formed. Sennett, MacLauchlan and Scott (1952) by continuous observations on the formation of metal deposits evaporated in the specimen chamber of an electron microscope, found that volatile metals, such as Cd and Zn, simultaneously formed particles as large as 200 Å once the vapour beam had reached a certain intensity.

The formation and subsequent growth of nuclei can also be augmented, however, by migration of the condensed metal atoms over the surface of the substrate. The temperature and type of substrate are the principal factors influencing the mobility of adsorbed metal atoms on a solid surface. (Lennard-Jones (1937), Appleyard (1937)). The condensed atom is held by a field of force in the surface, which has pockets of low potential. At low temperatures any deposited atoms will vibrate about the minima of these pockets and will only combine with atoms colliding with them from the vapour beam. However, if the atoms are given sufficient kinetic energy to surmount the potential energy of the barrier, they may move over the surface provided they retain this energy. Since neutral substrates have

little effect on the condensed atoms, the metal atoms can move freely when their kinetic energy is much less than that required for evaporation from the surface. Consequently, a large migration of metal atoms can occur on these amorphous bases at temperatures far below those needed to re-evaporate the atoms, so that there is a formation and a subsequent growth of nuclei due to collision of atoms already on the surface.

If the rate of evaporation and the substrate temperature are sufficient to form a large number of randomly distributed nuclei, the mechanisms described above ensure fast growth. The size to which tin nuclei can grow once they are formed depends on the amount of tin condensed on the substrate and hence on the mass evaporated. Thus the sizes of crystallites were found to increase as the larger masses were evaporated onto the substrates. However when the crystallites grown from the original nuclei reach a certain size, a new mechanism of growth can be expected to take place. The nuclei originally formed can come together to form large crystallites, with a consequent disappearance of the smaller ones. This effect was observed by Basett, Mentner and Pashley, (1959) in their studies of the nucleation and subsequent growth of gold films on rocksalt at 270°C.

In the present series of experiments the electron micrographs of the crystallites showed not only elliptical images but sometimes two or more quite distinct circular images joined together. In Figure 19 the largest

crystallites can be seen to have regions around them which are perfectly clear of small crystallites since they have been "swallowed up".. The distribution was Gaussian for the crystallites formed from random nuclei. However, as these nuclei grew and came together, the second stage of growth i.e. the coalescence, would account for the crystallites greater than ~ 50Å. This could explain the new peak observed in the distribution curves. (See Chapter IV, Section 2).

The residual gases present during evaporation may have important effects on both the structure and purity of the condensed substance. Oxidation may occur whilst the metal is travelling from the evaporator to the substrate, or during condensation (Wagner (1943), Stahl (1949). The adsorbed gas and the impurities on the substrate surface will affect the purity and the structure of the metal films. The oxidation of the metal in the molecular beam will not occur if the mean free path of atoms in the beam is much greater than the distance from the evaporator filament to the substrate film. However, during the film formation, gas molecules striking the substrate may combine with the condensed phase to form a chemical compound (usually an oxide in the case of tin). Therefore the more rapid the formation of the metal layer, the fewer the gas molecules able to combine with the metal atoms and in consequence the purer the layer of metal formed.

The equilibrium shape of solid crystalline particles is the one which, for a given amount of matter, minimises the quantity $\Sigma_i \sigma_i A_i$ (Gibbs (1928);

Curie (1885)) where σ_i = surface free energy per unit area of the ith face

A_i = area of the ith face.

$\sum_i$ is the sum over all faces.

This expression applies to crystals with surface planes where the free energy of the edges is negligible. The shape of the crystal can be conveniently specified by drawing vectors from a point P inside the crystal, normal to each face, where h_i is the normal to the ith face. The shape thus defined will be directly proportional to σ_i (Wulff (1901)) or $h_i = \lambda \sigma_i$ where λ is a constant depending solely on the size of the crystal. The thermodynamically stable crystals of a given substance should therefore be geometrically similar polyhedra. The equilibrium shape will occur if the mechanisms necessary for change of shape during formation of the particle can take place sufficiently rapidly. In an extensive treatment of equilibrium shapes of solid particles Herring (1950 ;1952) has shown the different equilibrium shapes possible for cystals and amongst these, there are crystals in which finite plane regions are joined by smoothly curved regions. In this treatment,edge and corner effects, as well as variation of σ_i with curvature, have been ignored. As the size of the crystal is decreased however, these effects become more and more appreciable and must be considered. Since the edge and corner effects involve a higher free energy then a smooth surface does, there will be a

tendency to smooth out the surface of the crystal. This would tend to produce continuous smooth surfaces, and if the crystallites were small enough the interatomic forces could make the surface nearly isotropic so that spherical crystallites would be formed.

The rapid evaporation and the raised temperature of the substrate enabled a fast crystallite growth to be obtained.

The condensation from the beam, and the migration of the condensed atoms simultaneously, produced a mechanism by which the shape of the crystallite could change sufficiently rapidly for equilibrium to occur. The stability of the equilibrium of the crystallites formed was investigated by heating some specimens to the melting point of bulk tin two or three times in succession. In each case the same melting point of the specimen was observed, the crystallites obtained by the above method of preparation were found to be randomly oriented and their shapes gave circular images on the electron micrographs, even when specimens with a crystallite mean size of several thousand Angstroms were prepared. Several replicas of these large crystallite specimens were taken, and they showed that the crystallites appeared to be spherical with a small area of contact with the substrate. The largest crystallites had hemispherical shapes, but these were much larger than those studied in the melting point experiments. An electron micrograph and a photograph of a replica of these thousand Angstrom crystallites are shown in Figure 38 and Figure 39 respectively. It is therefore safe to assume that the crystallites which were smaller by more than an order of magnitude had spherical shapes. The tendency

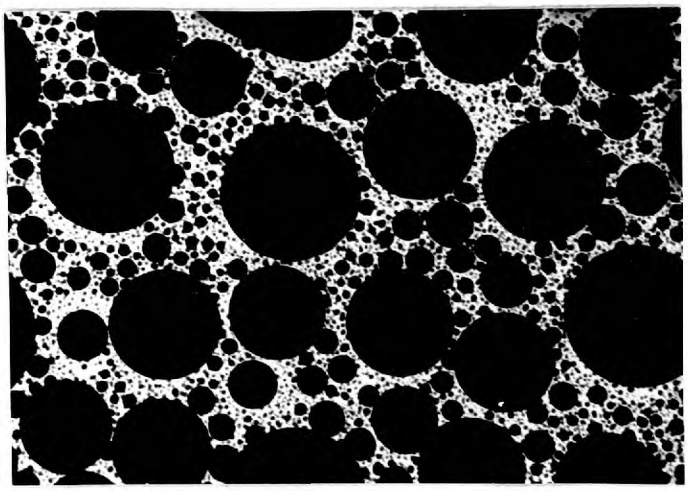

FIGURE 38. Electron microscope photograph of tin crystallites having a mean radius of several thousands Angstroms. (x30,000).

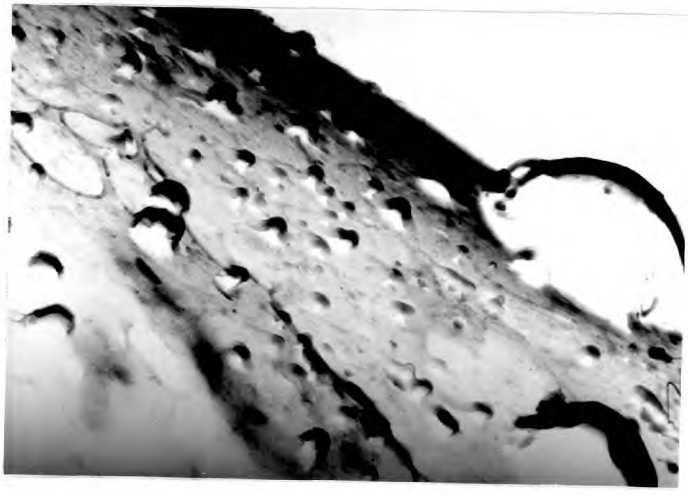

FIGURE 39. Electron microscope photograph of a replica taken of tin crystallites having a mean radius of several thousands Angstroms (x30,000).

to smooth out the surface by interatomic forces would have erased the small facets that were visible in the micrographs of the largest crystallites. Several specimens were photographed in the electron microscope before and after being heated in the diffraction camera to 232°C. No change in the size distribution of the specimens was observed after all the crystallites had melted and recrystallised, indicating that the crystallites were separate stable entities. Therefore the same distribution of crystallite size will be obtained irrespective of whether the measurement is made before or after melting.

3.2 The Melting Point Temperature T_R.

The errors in the measurement of T_R arose from the errors in the determination of T_m for the tin specimen. These errors were minimised by the following means: great care was taken to have the specimen in good thermal contact with the thermocouple so that the temperature registered was the true temperature of the specimen the temperature was raised slowly so that any possible temperature gradient effect was minimised, the electron beam current was adjusted to a value less than or equal to 0.03μA., so that there should be no heating of the tin crystallites by the beam. The current density corresponding to the maximum beam current used was $1.0\ 10^{-5}$ A/cm^2. and this was much less than the value of $1.5\ 10^{-5}$ A/cm^2 quoted by Winkelmann(1956) as the maximum density he could use without heating his gold-copper alloy thin films. Repeated melting point

measurements were made on the same specimen with electron beam currents ranging from 0.01 to 0.06 μA. No change in the melting point was observed so that no measurable heating of the specimen by the electron beam occurred.

The specimens contained crystallites of different sizes which melted at different temperatures. This gave rise to a gradual transition in the diffraction pattern so that difficulty was found in assigning a unique value to T_m. Although the number of crystallites which had melted may have increased rapidly with rise in temperature of the specimen, the mass of liquid, which determines the intensity of the halo pattern, increased comparatively slowly because the crystallites melting first were the smallest ones. The largest crystallites melted last and since the diffraction pattern from a crystallite is proportional to its mass, the solid diffraction pattern would still be visible at a temperature where all but a small percentage of the crystallites had melted.

The transition in the diffraction pattern of the smaller crystallite specimens were much more uncertain than the transitions of the larger specimens, with consequently larger errors. This may be explained by the following considerations. The rate of transformation of the diffraction pattern depended on the rate of heating, which was kept fairly constant in all the experiments, on the size distribution and also on the dependence of the melting point on the crystallite size.

If a crystal of radius r melts at a temperature T, when the temperature goes from T to $T + dT$, crystallites with radii r to $r + dr$ melt.

This results in a transfer of mass from the solid to the liquid state which is proportional to $m(r)\,dr$ (Chapter IV, Section 2). Therefore, the increase in intensity, dI, of the liquid pattern and the corresponding decrease in the intensity of the solid pattern is proportional to $m(r)\,dr$. Now the rate of change of the intensity of the liquid diffraction pattern with temperature is $\frac{dI}{dT}$, where $\frac{dI}{dT} \propto m(r)\frac{dr}{dT}$ i.e. $\frac{dI}{dT}$ does not only depend on $m(r)$ but also on $\frac{dr}{dT}$. By examining the graphs in Figures 34 and 36, $\frac{dr}{dT}$ can be seen to increase with an increase in r, therefore $\frac{dI}{dT}$ also increases with r. This means that the melting transitions in films containing the larger crystallites will be sharper. The above argument has neglected the effect of ring breadth which would affect the transition of the smallest crystallites by making the patterns even more diffuse.

Because of these effects the frequency with which the photographs were taken was sufficient to show all visible changes in the diffraction patterns. With the majority of specimens T_m could be registered to within $\pm 2^{\circ}C$. With the largest specimens it was possible to determine the melting point to within $\pm 1^{\circ}C$. In the smallest crystallite specimens studied, all the crystallites were smaller than 50 Å. The half width of a ring produced by solid crystallites is inversely proportional to their dimensions (Thomson & Cochrane (1939) p.77; Pinsker (1953) p.89) so that the smaller crystallites produce broader rings than the larger ones. As the crystallites get smaller, the rings become more diffuse and therefore,

become more difficult to see against the background of a liquid pattern. This effect led to a further inaccuracy in the determination of the melting point of the small crystallites, so that the total errors become $\pm$ 10^{0}C or more.

3.3. The Radius of Crystallite Melting at Temperature T_R.

The determination of the radius R of the crystallite melting at the temperature T_R, may be considered in two parts. The first part consisted of determining the size and mass distribution of a specimen for which T_m had been obtained. The second part consisted of the determination of the value of r_m to be associated with a specimen of given size distribution.

The magnification of the electron microscope used in the investigations of crystallite sizes was regularly checked by means of a specimen of pleurasigma angulatum supplied by the National Physical Laboratory. A micrograph of this was taken at the magnification used in the experiments on tin and the absolute magnification of the electron microscope was determined accurately from the known spacings of the di-atom.

Measurement of the magnified electron microscope image was subject to errors on the part of the observer in determining the actual diameters of the images which were not always sharp. To minimise this subjective error and to make sure that the distributions obtained were typical of the whole specimen, measurements on at least two different parts of the same specimen were carried out by two different observers. The resultant of

these distributions was then considered to be the distribution of the whole specimen. The likely error in the size distributions was obtained from photographs of the crystallite images from completely different parts of the specimen taken with different exposures so that the contrast of the images against the background was quite different. With the over and under-exposed photographs the extremes of any crystallite image size were obtained. Photographs of crystallite images from three different parts of the specimen under these conditions are showin in Figure 40 and their distributions in Figure 41. It can be seen that the error of the mean radius is less than 4 Å, the half-width of the histogram frequency, so that 4 Å can be taken as the error in the measurement of any radius in the distribution. The contrast of the images, however, tended to decrease with decreasing crystal size, causing loss of definition. The errors were, however, kept to $\pm$ 5 Å by measurement of a large number of crystallites at different parts of the specimen

Since $m(r) = n(r)\rho$, the mass distribution calculation from $n(r)$ was not subject to further errors, for ρ was found to remain constant to within the order of 1% for all the crystallites studied.

For the determination of r_m from the different diffraction patterns of a given specimen, an absolute criterion was obtained from the super-imposed solid and liquid diffraction patterns obtained from different specimens of known mass ratio. Although precisely the same condition could not be obtained in the super-imposition experiments as in the melting point determination ones, the same range of masses was evaporated in both cases.

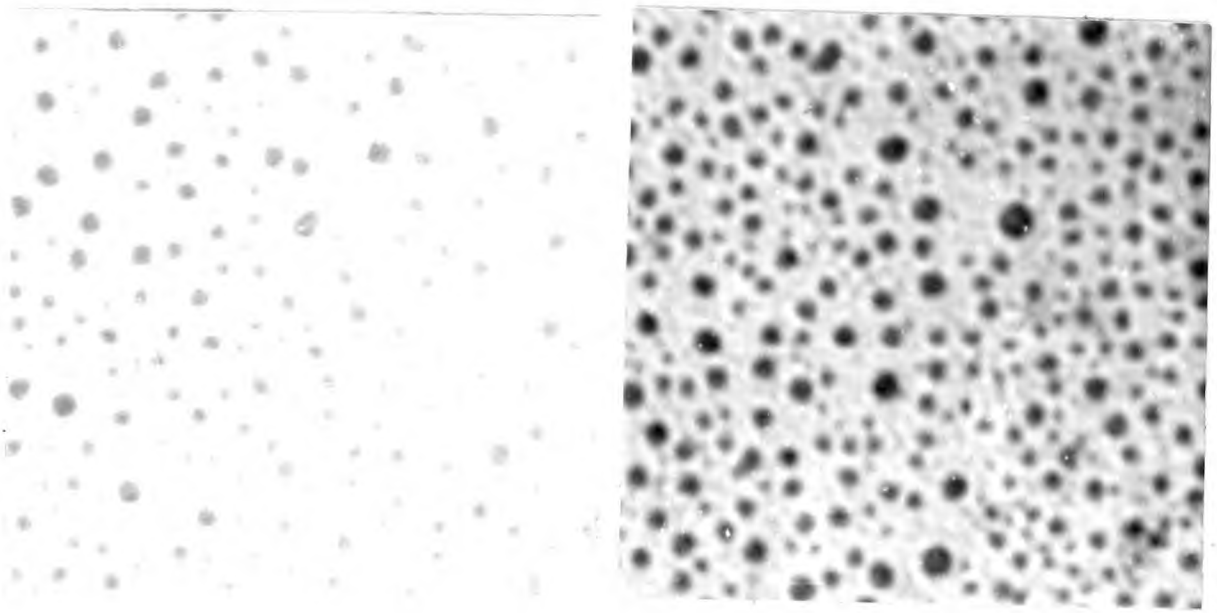

(a) (b)

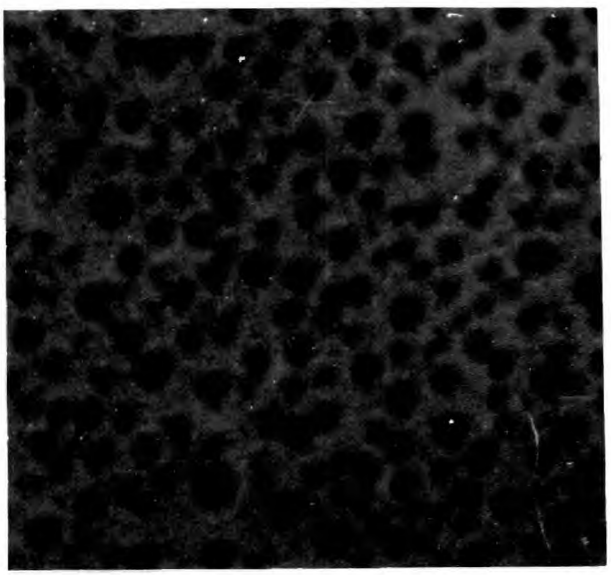

(c)

FIGURE 40. Electron microscope photographs of tin crystallites, taken at widely separated regions of a specimen and at different exposures. (x 360,000).

Figure 41. Crystallite size distributions obtained from the electron microscope photographs shown in Figure 40.

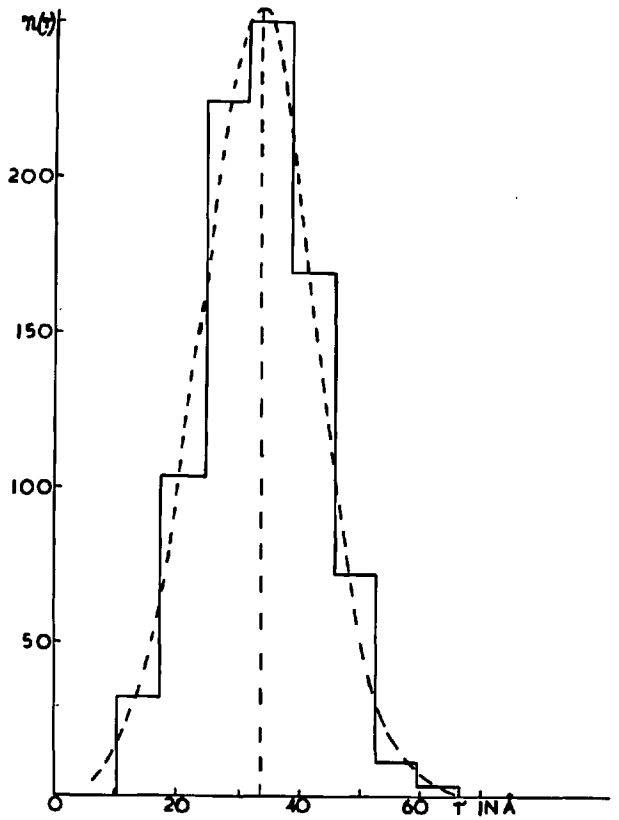

(a)

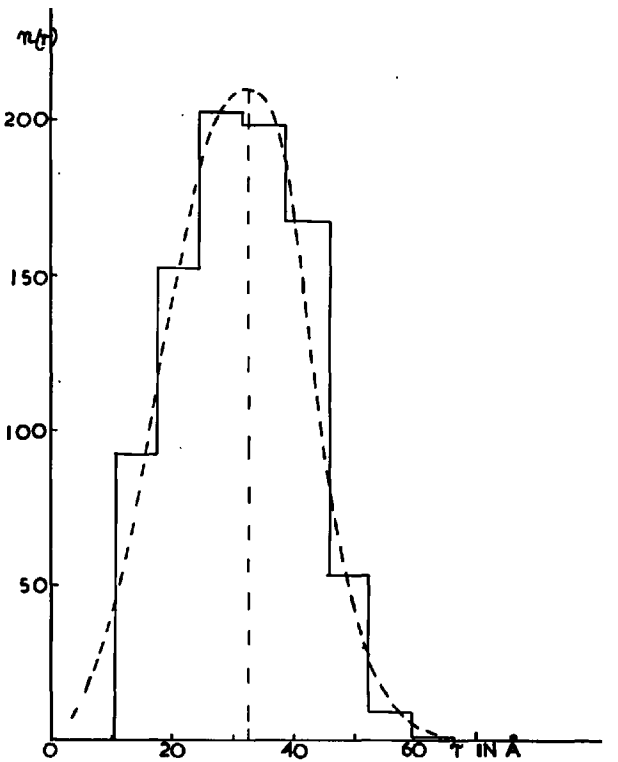

(b)

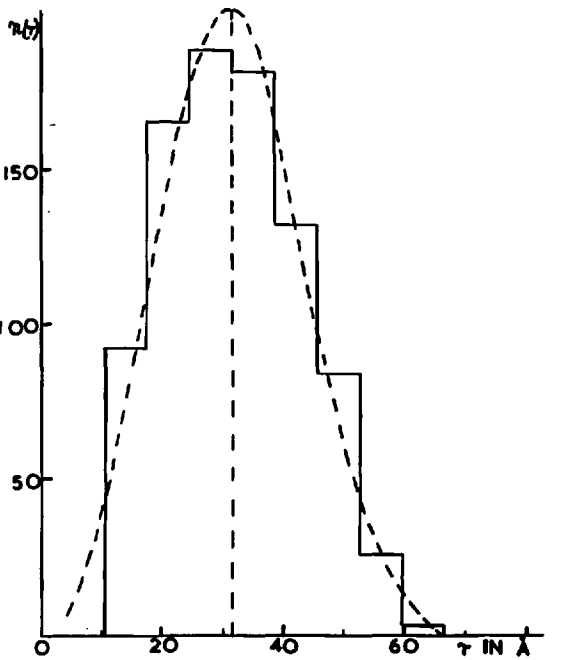

(c)

There were two differences between the superimposed patterns of solid and liquid crystallites and the pattern given by a single specimen on melting. The temperatures of the solid and liquid patterns were different in the former whereas with the latter both contributions were at the same temperature below the melting point of bulk tin. However, the effect of thermal vibrations of the individual atoms on the intensity of the diffraction pattern would be expected to be small (Kosita (1934); Coster and Van Lanten (1939) , so that the method used offered a good visual criterion.

In the single specimen diffraction pattern all the crystallites contributing to the solid ring pattern were larger than those contributing to the liquid haloes. In the superimposition experiments, the liquid crystallites could not all be made smaller than the solid ones since larger evaporated masses were used to produce the liquid pattern. An effort was made to make the crystallites producing the solid pattern as large as possible, but part of the liquid pattern was always produced by crystallites.

Since only 15% of the mass remained solid at T_m the errors involved in calculation of r_m were mainly due to the errors in obtaining the size distributions. The error in R is taken as 4-5 Å when the overall magnification of $7.2\ 10^5$ was used and 8 Å in the largest crystallites, where a magnification of $3.6\ 10^5$ was used. These errors were never exceeded when evaluation of r_m from mass histograms of different parts of the specimen were carried out.

3.4. Oxidation of the Tin Crystallites.

Precautions were taken to minimise oxidation of specimens during their formation so that pure tin crystallites would be obtained. No tin oxides were detected in the specimens used in the melting point experiments, pure tin diffraction patterns being observed throughout.

Stannous and stannic oxides both have tetragonal crystal structures (Wyckoff Chapter III Table p.27 Chapter IV Table p.15). Both these would produce sharp ring patterns, with more rings than the solid tin pattern, even at 232°C, because both melt at much higher temperatures than pure tin. Their presence would affect the determination of T_m because of the continual presence of sharp ring pattern throughout the transition of the tin diffraction pattern. Oxidised tin layers studied by transmission electron diffraction showed that the stannous oxide form was more likely to be formed, but it was never detected on the specimens used in the melting point experiments. A form of tin oxide which gives an amorphous diffuse halo diffraction pattern also exists (Richter (1943), Hart (1952)). This form of oxide would be difficult to detect unless the tin crystallites were extensively oxidised, since its halo pattern would only contribute to the background in the same way as the substrate film's amorphous pattern.

Reflection electron diffraction is a very sensitive detector of chemical attack on thin films. Newman (1955) evaporated very thin layers of tin onto silver in an electron diffraction camera and did not observe any oxide rings on his reflection diffraction patterns. Neither did Sayama (1941). Bublik and Pines (1954) and Takagi (1954) in their

reflection electron diffraction studies of molten thin tin films. This was in agreement with Stahl (1954) who concluded from his investigations of oxidation of films, that the substrate temperature must exceed 300°C for tin specimens to oxidise. Curzon (1960) did not detect any oxide in his thin tin layers, even after the tin film had been at a temperature of 232°C for several hours. Since in these experiments the specimens used did not show tin oxide diffraction patterns, it may be concluded that if there was any oxidation the rate was either extremely slow or that a protective layer of oxide formed on the outside of the crystallites stopped further oxidation. In either case, since no layer was observed, it must have been only a few Angstroms thick.

CHAPTER V

THEORETICAL TREATMENT OF THE MELTING OF SPHERICAL TIN CRYSTALLITES.

There are two possible approaches to the treatment of the melting equilibrium of small crystallites, namely statistical mechanics and thermodynamics, in which consideration to the possible effects of crystallite size can be given.

So far no satisfactory detailed model of fusion has been proposed, although attempts to prove that a solid becomes unstable at a definite temperature have been proposed (e.g. Lindemann (1910), Born (1939), Furth (1941) , Bofiglioli, Ferro and Montalenti (1952)). Alternative approaches using different models have been made by Lennard Jones and Devonshire (1939 (a,b)), Fowler and Guggenheim (1939) and others. Temperley (1956) gives an account of the difficulties associated with the statistical mechanical approach to fusion. Furthermore the treatment of surfaces by statistical mechanics is complex, as may be seen from the works of Fowler and Guggenheim (1939 p.445-50) and Kirkwood and Buff (1949). It is felt therefore that the statistical mechanical approach to fusion and the possible effects of surface on this is likely to be extremely difficult and will not be considered here.

General thermodynamic principles will, instead, be applied to investigate the possible effects of surface on the equilibrium of solid and liquid phases, and two models will be used to obtain from this, a relationship between the melting point of a spherical tin crystallite and its size.

The theoretical relationships derived on the basis of these models will be compared critically with the experimental results given in the last chapter. Although macroscopic concepts are used to obtain the equilibrium conditions, atomistic ideas will also be considered, since these not only give a deeper insight into the nature of the thermodynamic variables, but also suggest new macroscopic concepts which might not otherwise be noticed.

The effect of surface on the equilibrium conditions between two phases has aroused interest for some time. The foundations of this subject were laid by Gibbs (1875-7) and a brief historical review of the work done on this topic by thermodynamic methods is given by Curzon (1960). In addition to the authors mentioned by Curzon, important work on this subject has also been done by Tolman (1948,1949 (a,b)) and by Herring (1950 ., 1952).

1) Thermodynamic Treatment of Surfaces.

In the treatment of bulk phases where the effects of surfaces are ignored, the phases are considered as extending homogeneously up to a mathematical surface which determines their volumes. When two phases are in equilibrium there is a physically inhomogeneous region where transition takes place from the uniform distribution of matter in one phase to that in the other. In obtaining a thermodynamic treatment of surfaces, Gibbs (1928) called this region "the region of discontinuity" but pointed out that this term did not imply that the discontinuity was absolute. However, because of the short range of the atomic forces, this region would have a very small dimension in one direction, and he proposed to replace this physical non-homogeneous, three dimensionsal region by a "dividing surface" which is a surface in the strict geometrical sense. This dividing surface coincides with the physical surface of discontinuity to within the accuracy with which the latter is localised, but has a precisely defined position. It passes "through all points which are similarly situated with respect to the condition of the adjacent matter". Different choices of the nature of these points will lead to different dividing surfaces all parallel to one another, but displaced from one another in a direction normal to the surface, so that some convention is necessary to complete the definition. The two conventions used by Gibbs will be given later, but the following discussion is valid for any choice of a dividing surface.

Once a dividing surface has been chosen to represent the discontinuity, then energy, entropy and other extensive quantities can be associated with it. To obtain these extensive quantities let us consider a portion of a transition layer between two single component phases (1) and (2), the extent of the transition layer being defined by the two parallel surfaces which mark the limits of homogeneity of the two phases (ABCD, EFGH in Figure 42). Phase (1), below ABCD and phase (2), above EFGH extend with homogeneous properties. The volume ABCDEFGH, equal to ν, has physical and thermodynamic properties which are intermediate to those of the two phases. However this volume ν has a definite amount of internal energy = ε entropy = η, and mass = m, depending on the phases (1) and (2) and the volume ν. Let a surface KLMN, of area s, parallel to and between the surfaces ABCD and EFGH, divide the element of the transition layer into volumes ν' = ABCDKLMN and ν'' = KLMNEFGH. The extensive quantities associated with a dividing surface element KLMN- namely internal energy, ε^s, entropy, η^s, and mass, m^s, - are defined by the difference between the extensive properties in the volume ν and the value of these quantities when the uniform homogeneous phases extend up to the dividing surface. Let the internal energy entropy and mass per unit volume of the bulk homogeneous phase (1) and (2) be ε_1, ε_2, η_1, η_2, m_1 and m_2 respectively. Since we have already assigned the values of the extensive quantities in this element, the values of ε^s, η^s, m^s are

given by :

$$\varepsilon = \varepsilon_1 \nu' + \varepsilon_2 \nu'' + \varepsilon^s \qquad (14)$$

$$\eta = \eta_1 \nu' + \eta_2 \nu'' + \eta^s \qquad (15)$$

$$m = m_1 \nu' + m_2 \nu'' + m^s \qquad (16)$$

These extensive quantities of the dividing surface are determined "partly by the state of the physical system which we are considering, and partly by the various imaginary surfaces by means of which the quantities have been defined " (Gibbs (1928) p.224). It can be seen that by placing the surface KLMN in different positions the value of ν' and ν'' change and in consequence ε^s, η^s , m^s change also.

Once the dividing surface is chosen and its extensive quantities defined as above, the system can be treated as comprising two homogeneous phases extending up to the dividing surface, so that there is only a dividing surface and no transition layer. This treatment was developed with a minimum of hypothesis as to the detailed structure of the transition layer, but it was assumed that all the properties of the layer could be determined from the area and configuration of a particular dividing surface postulated. This treatment has the advantage of providing a general theory which is valid for a wide range of possible kinds of transition layers, including solid-liquid interfaces. This treatment is quite different from the less abstract treatment of the inhomogeneous

layer as a definite physical entity (e.g. Guggenheim (1957) p.46-56.)

The treatment of the fluid-fluid interface is by far the simplest because the fluid atoms are free to move, and consequently the strains are isotropic and uniform distribution of matter occurs. The location of the dividing surface which seemed most advantageous to Gibbs for this type of interface was at the "surface of tension". The dividing surface, in this position is so placed that the dependance of the energy of the dividing surface on curvature, for an infinitesimal virtual change, is zero. For a general infinitesimal change, the change in a spherical dividing surface energy is given by

$$\delta\varepsilon^s = t\delta\eta^s + \gamma\delta s + \mu^s \delta m^s + 2C\delta c \qquad (17)$$

where t = temperature, μ^s = Gibbs potential in the surface, γ = a constant, C = a constant, c=radius of curvature. The surface of tension corresponds to the dividing surface being so placed that $C = 0$,

$$\therefore \quad \delta\varepsilon^s = t\delta\eta^s + \mu^s\delta m^s + \gamma\delta s \qquad (18)$$

It can then be easily shown that for a fluid-fluid surface, μ^s is the same as in the two bulk phases, μ, and that γ is the "surface tension". If we consider a change from one equilibrium state to

another and replace δ in equation (18) by d, to signify a real differential, then

$$d\varepsilon^s = td\eta^s + \mu\, dm^s + \gamma ds \qquad (19)$$

If we integrate equation (19) supposing the area s to increase from zero to a finite value s we have

$$\varepsilon^s = t\eta^s + \mu m^s + \gamma s \qquad (20)$$

This applies to any part of the surface of discontinuity in equilibrium which is of the same nature throughout or in which t, μ, γ are constant, and were constant during the integration.

If we denote superficial densities of energy, entropy and mass by $\varepsilon_s = \varepsilon^s/_s$, $\eta_s = \eta^s/_s$ and $\Gamma = m^s/_s$ respectively, equation (20) becomes

$$\varepsilon_s = t\eta_s + \mu\Gamma + \gamma \qquad (21)$$

Hence $\gamma = \varepsilon_s - t\eta_s - \mu\Gamma = f_s - \mu\Gamma$ (22)

where f_s = Helmholtz free energy density of the surface.

If f^s = total free energy of the surface = sf_s

$$f^s = \gamma s + \mu m^s \qquad (23)$$

It can be seen that f_s and γ are different thermodynamic quantities. However, for two fluids of the same single component where adsorption is not present the value of Γ will be so small that it may be considered zero, and the two quantities will be numerically equal. This equality has often been mistaken for equivalence in thermodynamic treatment of equilibrium involving surfaces and this is not correct.

The above treatment is applicable to a liquid surface because there is a relation between the strain in a fluid and the number of atoms in the surface. Also a liquid cannot support a shear strain, so that on stretching the surface, atoms can move up to give the same configuration as before. This dividing surface has the great advantage of relating the pressure difference between two phases, with a curved interface, to γ and to the principal radii of curvature. For a spherical surface of radius R, concave with respect to phase (1) the relationship :-

$$P_1 - P_2 = \frac{2\gamma}{R} \qquad (24)$$

is exactly true for the surface of tension.

For an interface where one of the phases is solid, however, there is no advantage in locating the dividing surface in this way, since the stresses induced inside a crystal by the surface are, in general, of a complicated nature. Furthermore, there is no relationship between the strains inside the volume and the surface free energy of a solid. The

free energy of a surface is mainly a measure of the change of free energy with a change in the number of atoms in the surface layer. Since in a liquid the compression of the interior implies, on the average, a decrease in the number of atoms in the surface, the strain in the liquid is related to the number of atoms in the surface. Consequently by replacing the surface layer by a dividing surface we can obtain a relation between the two. Differentiating equation (20) completely and substituting equation (19), we obtain

$$d\gamma = -\eta_s dt - \Gamma d\mu \qquad (25)$$

i.e. γ is $\gamma(t,\mu)$

Differentiating equation (22) in a general manner, and substituting for $d\gamma$

$$d\gamma = df_s - \mu d\Gamma - \Gamma d\mu = -\eta_s dt - \Gamma d\mu$$

$$\therefore \quad df_s = -\eta_s dt + \mu d\Gamma$$

$$\text{and } df^s = \eta_s dt + \mu dm^s \qquad (26)$$

i.e. f_s is $f_s(t, \Gamma)$,

the free energy is a function of mass.

The increase in free energy of the surface, at constant temperature, is represented by the increase in the number of atoms in the surface, which is directly proportional to the strain in the interior of the liquid. All

isothermal changes of the liquid are then expressed by the changes in the volume of the interior and the area of the dividing surface. However, in a solid, straining the interior will not change the number of atoms in the surface, because their positions are fixed and consequently the change of the surface free energy and the strain energy, which measures the volume free energy, of a solid, are not related as simply as with liquids.

Gibbs recognised these facts and accordingly proposed that the dividing surface be placed in such a way as to make the superficial density of the solid vanish. i.e. the surface is placed in such a way that m^s in equation (16) is zero. This gives a precise location of the surface, which is much easier to localise relative to other physical characteristics of the interface, than the surface of tension. (Tolman (1949), Kirkwood and Buff (1949)). Then, obtaining the extensive properties of this surface as before, he defined

$$\sigma = \varepsilon_s - t\eta_s \qquad (27)$$

This is the free energy density of the surface, f_s, and measures the free energy difference between the actual system and one in which the two bulk phases extend homogeneously up to the dividing surface.

The properties of this dividing surface are quite different to those of the surface of tension, for now since $m^s=0$ all terms involving μ^s, m^s vanish and consequently its functional form changes.

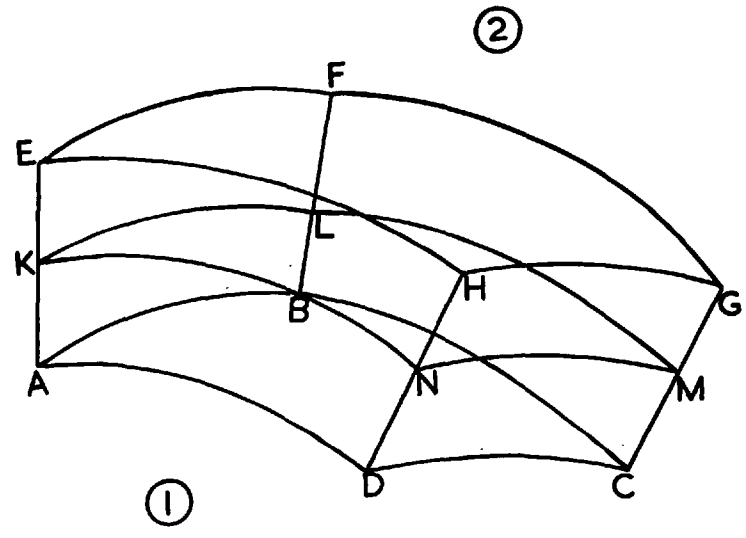

Figure 42. An element of a transition layer between two phases.

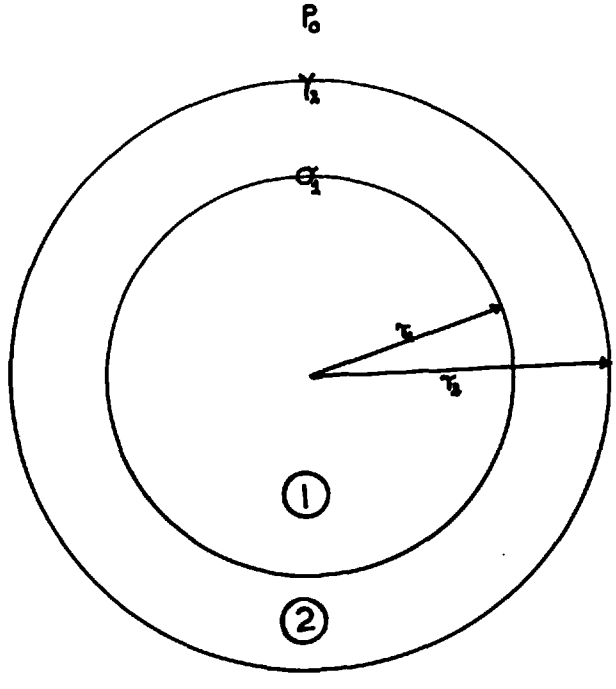

Figure 43. A solid core surrounded by a liquid shell. This is used in the first theoretical model of melting.

2. Surface Free Energy and Surface Stress.

By replacing the fluid-fluid interface by a dividing surface at the surface of tension, Gibbs considered the changes that occurred in the whole system to be represented by the change in the volumes and in the dividing surface. Although this might appear to be a simplification, it is in fact a most rigorous treatment, as Tolman (1949) showed in his more detailed treatment of interfaces between fluid masses. At the time that this theory of capillarity was proposed there was little experimental material pertaining to effects of solid surfaces, so less attention was given to solid-liquid interfaces. The surface free energy was however utilised in the problems where the equilibrium between a solid and liquid with respect to solution was investigated. In the system where we replace the surface of discontinuity by a dividing surface, we must be able to represent all the properties of the system. The case of a liquid surface falls very neatly into this pattern, the variables at constant temperature being the volume and surface area, mass of liquid and mass of dividing surface, and pressure and surface tension, all of which are related. However, in the case of a solid, because the position of the atoms are fixed, no such simple relation is to be expected.

Gibbs was careful to point out the difference, in the case of solids, between surface stress and surface free energy. Surface free energy is a measure of the work necessary to create a surface, whereas the surface stress is a measure of the work necessary to deform a surface. In the

case of a solid there is no such equivalence.

We may define the specific free energy of any crystal surface, in the most general case as $\sigma(n)$. This is the increase in the free energy of the crystal, when a face normal to a unit vector $\underline{n}$ is increased by unit amount, when the internal properties of the specimen and the areas of the other types of face are kept constant. The quantity $\sigma(n)$ will have different values for different crystal faces, because of the different distributions of atoms in the different crystal planes. The free energy of the specimen will then be the volume free energy plus the terms $\int_S \sigma(\underline{n})\, ds$. In the case of a liquid or an isotropic solid, $\sigma(\underline{n})$ will be constant for any part of the surface, and correspondingly the surface free energy will be σs. This definition of $\sigma(n)$ corresponds tc the definition of σ at the $\Gamma = 0$ dividing surface.

The concept of surface tension is a very old one in the theory of liquid capilarity (a historical account is given by Baaker (1928) and Shuttleworth (1950)). The concept was extended to surface stress for solids (Gibbs (1928) and recently a detailed treatment of the stresses for the general case of crystal surfaces has been carried out by Herring (1950 (a)) and by Shuttleworth (1950).

Given an interface and any plane P normal to it, we may define the surface force acting across P as the surface contribution to the total force exerted by the material on one side of P on the material on the other side. The total force is then considered to be composed of

contributions from the dividing surface and bulk phases, according to the method given in the previous section. The force per unit length of the intersection of P with the dividing surface, may be called the surface stress acting across P. In the case of a crystal, as the orientation of P is changed, the surface stress acting across the surface has been shown by Herring (1950), to have the general form:-

the μ th component of the stress is $\sum_{\nu} g_{\mu\nu} \, p_{\nu}$

where $\nu = x,y$ $\mu = x,y,z$, (x,y being the plane of the surface).

$\underline{p}$ is the unit vector normal to P

$g_{\mu\nu}$ is the surface stress tensor.

This general surface stress tensor contains shear components which could not be present in a liquid. However if the surface has greater than threefold rotational symmetry, then $g_{\mu\nu}$ reduces to a multiple of the unit matrix i.e. $g_{\mu\nu} = g\delta_{\mu\nu}$ where $\delta_{\mu\nu} = 0$ if $\mu \neq \nu$, and $\delta_{\mu\nu} = 1$ if $\mu = \nu$. For this type of surface the shear components vanish and the stress becomes isotropic.

Strictly, the surface stress just defined is no exception to the general rule that the division of any quantity into surface and bulk

contributions, depends on the location of the dividing surface. However the product of $\chi\lambda$, where χ is the volume stress and λ is of the order of the thickness of the transition layer, will be negligible compared with the components of $g_{\mu\nu}$, so that to this degree of approximation the surface stress can be considered as independent of the position of the dividing surface.

The numerical components of $g_{\mu\nu}$ for a crystal surface can be calculated directly by summing the forces which the various atoms of the crystal exert on one another, and by finding the unbalance of these forces due to the presence of the free surface. These atomistic calculations have been carried out ((Lennard-Jones and Dent (1928), Orowan (1932), Shuttleworth (1950)) and for certain crystals, such as some of the alkali halides and the rare gases, tensile and not compressive stresses were obtained.

In all cases however, it was found that σ, the surface free energy, was much different from the surface stress. Atomistic calculations have also been made for liquid surface stresses and free energies, and the calculations show that they are equal. MacLellan (1952), Kirkwood and Buff (1949)).

In the treatment of the melting of tin crystallites, we shall treat the surface free energy as having a uniform value σ over the entire surface where $\sigma = \int_s \sigma(\underline{n})\, ds / \int_s ds$. Since the crystallites were

spherical, their shape would only agree with a uniform value of σ - equivalent to a single crystal plane. This would occur if the crystallites were small enough for the atomic forces to be sufficient to smooth out all edges and facets to give a uniform atomic distribution. The surface stress will be treated as being due to a high symmetry face, namely a tensile stress, g, which is isotropic. The crystallite will be considered to have isotropic elastic properties, so that the complex form of its general stresses can be represented as a uniform pressure.

In the following consideration we shall consider the surface free energy and the surface stress to be independent of the curvature. This is permissible when the thickness of the transition layer is very much less than the radii of curvature of the surface. (Herring (1952)). Let us consider the changes of the free energy in the cases of a) a liquid, b) a solid, when they both have a free surface, and c) a solid liquid interface.

(a) Suppose we have a liquid with a free surface and consider the change in free energy when we carry out a virtual arbitrary change. The two dividing surfaces proposed by Gibbs yield the same change in free energy for a single component system in which the adsorption at the surface is zero.

The free energy F of the liquid is $F=F_v+F_s$, where F_v is the free energy of the interior and F_s is the free energy of the surface.

For an infinitesimal change with t constant,

$$(\delta F)_t = (\delta F_\nu)_t + (\delta F_s)_t \qquad (28)$$

The general form of δF for a bulk phase is

$$\delta F = -p\,\delta\nu - \eta\delta t + \mu\,\delta m \qquad (29)$$

(Gibbs p.186)

where p = pressure, ν = volume,

η = entropy, t = temperature,

μ = Gibbs potential, m = mass of the phase.

Therefore for the interior of the liquid which has mass m, potential μ, pressure p, and volume ν

$$(\delta F_\nu)_t = -p\delta\nu + \mu\,\delta m_\nu \qquad (30)$$

When the dividing surface is considered at the surface of tension

$$\delta F_s = \gamma\delta s + \mu^s \delta m^s \quad \text{from equation (23)}$$

$$\therefore\ (\delta F)_t = -p\delta\nu + \mu\,\delta m_\nu + \gamma\delta s + \mu^s\delta m^s \qquad (31)$$

In this change

$-p\,\delta\nu$ represents the external work done by the change in volume, $\gamma\delta s$ represents the work done on the surface by stretching it.

$\mu \delta m_\nu$ represents the change in free energy due to a change of mass in the interior, δm_ν $\mu^s \delta m^s$ represents the change in free energy due to a change of mass in the surface, δm^s, where δm^s and δm_ν are unrelated.

At equilibrium $\mu^s = \mu$, therefore no work is done in transferring matter from the interior to the surface, so that on stretching a surface, the external work done is $\gamma \delta s$, when ν is kept constant. Therefore $\left(\frac{\partial F_s}{\partial s} \right)_{t,\nu,m} = \gamma$, where m is the mass of the liquid. Also for a liquid the strains inside the liquid can be correlated with the surface tension and free energy, so

$$\mu = \mu^s \quad \text{i.e.} \left(\frac{\partial F_\nu}{\partial m_\nu} \right)_{t,\nu} = \mu = \mu^s = \left(\frac{\partial F_s}{\partial m^s} \right)_{s,t}.$$

The same relation exists between the free energy of the interior and its mass, as between the surface and its mass.

If we now place the liquid dividing surface where the mass density of the single component liquid is zero, the term in equation (23) containing m^s vanishes, and consequently the change in the free energy of the surface becomes a function of the mass in the interior- which is now the total mass - and $m_\nu = m$.

The general variation for the liquid is still represented by equation (28). However, since F_s is now σs, $\delta F_s = \delta(\sigma s) = \sigma \delta s + s \delta \sigma$, and from equation (30) $(\delta F_\nu)_t = -p \delta \nu + \mu \delta m$, where m is

the total mass of the liquid, for a general variation

$$\delta\sigma = \left(\frac{\partial\sigma}{\partial s}\right)_m \delta s + \left(\frac{\partial\sigma}{\partial m}\right)_s \delta m \qquad (32)$$

$$\therefore (\delta F)_t = -p\delta v + \mu\delta m + \left[\sigma + s\left(\frac{\partial\sigma}{\partial s}\right)_m\right]\delta s + s\left(\frac{\partial\sigma}{\partial m}\right)_s \delta m \qquad (33)$$

If there is no adsorption, the configuration in the surface remains the same after the stretching, so that the free energy per unit area remains constant, so that $\left(\frac{\partial\sigma}{\partial s}\right)_m = 0$.

Since σ is $\sigma(m,s)$ the derivatives of σ with respect to s and m have the relation

$$\left(\frac{\partial\sigma}{\partial m}\right)_s = -\frac{\left(\frac{\partial s}{\partial m}\right)_\sigma}{\left(\frac{\partial s}{\partial\sigma}\right)_m} = -\left(\frac{\partial s}{\partial m}\right)_\sigma \left(\frac{\partial\sigma}{\partial s}\right)_m \qquad (34)$$

But since $\left(\frac{\partial\sigma}{\partial s}\right)_m = 0$, $\left(\frac{\partial\sigma}{\partial m}\right)_s = 0$, therefore $(\delta F_s)_t = \sigma\delta s$ (35).

The relation for the variation expressed by equation (33) has the

form

$$(\delta F)_t = -p\delta v + \mu\delta m + \sigma\delta s \qquad (36)$$

The more general form which allows for a change in the surface mass due to adsorbable components, also reduces to this simpler form if the configuration in the surface is the same after stretching. If we consider the variation δF_s, in the general form of the surface of tension,

$F_s = f_s s$, where f_s is the free energy per unit area. For constant t

$$(\delta F_s)_t = \delta(f_s s)_t = f_s \delta s + s\delta f_s \qquad (37)$$

But δf_s from equation (26), for t constant is $\mu^s \delta\Gamma$

$$\therefore \quad (\delta F_s)_t = f_s \delta s + s\mu^s \delta\Gamma \qquad (38)$$

If $\delta\Gamma = 0$ i.e. the configuration of the surface is the same although the area has changed, $(\delta F_s)_t = f_s \delta s$, as in equation (35) where $f_s = \sigma$

b) The general change of free energy, for an infinitesimal arbitrary variation, is more complicated in the case of a solid than in the case of a liquid, since the solid has both rigidity and long range order. Shear energy, which cannot exist for a liquid, may be present in the case of the solid and because of the long range order of the solid no rearrangement of atoms can take place in a solid surface. Consequently, after stretching a solid, the configuration of the atoms in the surface will be different and therefore the surface free energy will change. In the case of a liquid when no account of the surface is taken the Gibbs thermodynamic potential is unambigiously defined by $\mu = \left(\frac{\partial F}{\partial m}\right)_{t,\nu}$ where F,m, ν and t, are, respectively, the free energy, mass, volume, and temperature of the liquid. This applies to a liquid because the only way of changing its free energy at constant volume and temperature, is by changing its mass. In the case of solid, however, there is the additional possibility of the presence of shear strain energy. Therefore, the Gibbs thermodynamic potential for a solid is defined by :-

$$\mu = \left(\frac{\partial F}{\partial m}\right)_{t,\nu,\ \text{shear}} \qquad (39)$$

where F,m,ν,t are now, respectively, the free energy, mass, volume and temperature of the solid. This means that to specify the potential of a solid, the change in the free energy must occur at constant shear as well as at constant t and ν (see also Herring (1952)). If the solid is subject to a uniform pressure P amd has no shearing stresses acting on it, then if there are no shear strains subsequently induced in an arbitrary

variation, the change in free energy is represented in the same way as in the case of a liquid i.e. by equation (29).

Consider, single component solid having a free surface and let F_ν, m, ν be respectively the free energy, mass and volume, of the interior when the dividing surface is placed in the position where it has zero mass. The mass, m, is then the total mass of the solid and σ from equation (27) represents the free energy per unit area. If the area of the surface is s, then the free energy of the surface, F_s, is equal to σs. For a solid crystal surface, which has greater than three-fold rotational symmetry, the surface has no shear components, and therefore if there are no external shear stresses applied, the change in the free energy of the interior of the solid, for a variation at constant temperature, will be given by equation (30), and the change of the surface free energy will be $\delta F_s = \delta(\sigma s)$. Thus the total change of free energy can be represented, in the same form as in the case of a liquid, by equation (33). However, because of the long range order and the subsequent change of configuration of the surface due to the variation, equation (33) cannot take the simple form as the case of the liquid. From equations (32) and (34) we have

$$\delta(\sigma s) = \sigma\delta s + s\left(\frac{\partial\sigma}{\partial s}\right)_m \delta s + s\left(\frac{\partial\sigma}{\partial m}\right)_s \delta m$$

$$= \sigma\delta s + s\left(\frac{\partial\sigma}{\partial s}\right)_m \delta s - \left(\frac{\partial s}{\partial m}\right)_\sigma \delta m \qquad (40)$$

and since for a solid, $\left(\frac{\partial\sigma}{\partial s}\right)_m \neq 0$ because of the fixed positions of the atoms, the full equation (40) must be used to represent the change of

free energy of the surface, and hence the full form of equation (33) for the total change. This is because the work done in creating a solid surface is distinguishable from the work done in deforming it.

c) If we consider a solid phase in contact with a liquid phase, the change in free energy of the system in arbitrary variations will include any free energy change in the solid-liquid interface. If we consider a single component solid completely surrounded by its liquid, it will be subject to an isotropic pressure providing there are no shear stress components in the solid-liquid interface. If the solid free surface stress has no shear components, the presence of a liquid cannot create any, and consequently for a surface of sufficiently high symmetry, the changes in the free energies of the solid and the liquid interior will be given by equation (29). Let us replace the solid-liquid interface by the dividing surface which has zero mass, and let σ be the solid-liquid surface free energy per unit area, s the area of the surface, m_1 the mass of the solid, m_2 the mass of the liquid and t the temperature. Then the general form of σ is $\sigma(t, s, m_1, m_2)$ because the surface free energy of an interface between two phases depends on them. However, if the solid does not affect the liquid to the extent of altering the ordering by introducing a long range order, the dependence of the solid-liquid surface free energy on the liquid will have the same form as a liquid surface. Also the dependence of the solid-liquid surface free energy will be a function of the solid mass and the surface area, so that for an infinitesimal variation, at constant t :-

$$\delta\,(s\sigma) = \sigma\delta s + s\left(\frac{\partial\sigma}{\partial s}\right)_{m_1}\delta s + s\left(\frac{\partial\sigma}{\partial m_1}\right)_{s}\delta s \quad . \qquad (41)$$

3). The Effect of Solid-Liquid Interface and Liquid-Air Surface on Thermodynamic Equilibrium.

Let us consider a spherical solid particle in equilibrium with, and completely enclosed by, a liquid shell. Let us replace the solid-liquid transition layer by a dividing surface placed so that the superficial density of solid is zero, and let us replace the liquid air transition layer by a dividing surface in the surface of tension. Let the radii of the two surfaces be r_1 and r_2 respectively (Figure 43) and let the external air pressure be P_o. Since the system is considered in equilibrium, thermal equilibrium condition must be satisfied. Therefore the temperature, t, is constant throughout the system. If we consider the solid to be subject to an isotropic pressure; let the pressure, Gibbs potential and mass in the solid be P_1, μ_1, m_1 and in the liquid P_2, μ_2, m_2, respectively. Let σ_1 = the free energy density of the solid-liquid surface.

γ_2 = the surface tension of the liquid-air surface and μ_2^s, m_2^s its potential and mass.

s_1 = area of the solid-liquid surface

s_2 = area of the liquid-air surface.

For equilibrium, for a general virtual change $(\delta F)_{t,m} = \delta W$ (42) (Gibbs p.89) where F = the free energy of the solid and liquid

δW = the work done on the system

m = total mass = $m_1+m_2+m_2^s$

$$\delta F = \delta F_1 + \delta F_2 + \delta F_{s1} + \delta F_{s2} \tag{43}$$

$$\delta W = -P_o \, \delta \nu \tag{44}$$

where δF_1 = change in solid free energy

δF_2 = change in liquid free energy

δF_{s1} = change in solid-liquid surface free energy

δF_{s2} = change in liquid-air surface free energy

$\delta \nu$ = total change of solid and liquid volume.

$\therefore$ for t constant, from equations (40) and (29)

$$\delta F_1 = -P_1 \delta \nu_1 + \mu_1 \, \delta m_1 \tag{45}$$

$$\delta F_2 = -P_2 \delta \nu_2 + \mu_2 \, \delta m_2 \tag{46}$$

and from equations (41) and (23)

$$\delta F_{s1} = \sigma_1 \, \delta s_1 + s_1 \left(\frac{\partial \sigma_1}{\partial s_1} \right)_{m_1} \delta s_1 + s_1 \left(\frac{\partial \sigma_1}{\partial m_1} \right)_{s_1} \delta m_1 \tag{47}$$

$$\delta F_{s2} = \gamma_2 \, \delta s_2 + \mu_2^s \, \delta m_2^s \tag{48}$$

Therefore from equation (43)

$$(\delta F)_{t,m} = -P_1 \delta v_1 + \mu_1 \delta m_1 \quad -P_2 \delta v_2 + \mu_2 \delta m_2$$

$$+ \sigma_1 \delta s_1 + s_1 \left(\frac{\partial \sigma_1}{\partial s_1} \right)_{m_1} \delta s_1 + s_1 \left(\frac{\partial \sigma_1}{\partial m_1} \right)_{s_1} \delta m_1 \cdot$$

$$+ \gamma_2 \delta s_2 + \mu_2 \delta m_2^s$$

$$= - P_o \delta v \qquad (49)$$

Since $\delta v = \delta v_1 + \delta v_2$, $-P_2 \delta v_2 = -P_2 \delta v + P_2 \delta v_1$ and since s_1 is a function of v_1 and s_2 of v, we can rewrite equation (49) as

$$-P_1 \delta v_1 + P_2 \delta v_1 + \sigma_1 \left(\frac{\partial s_1}{\partial v_1} \right) \delta v_1 + s_1 \left(\frac{\partial \sigma_1}{\partial s_1} \right)_{m_1} \left(\frac{\partial s_1}{\partial v_1} \right) \delta v_1$$

$$-P_2 \delta v + P_o \delta v + \gamma_2 \left(\frac{\partial s_2}{\partial v} \right) \delta v$$

$$+ \mu_1 \delta m_1 + s_1 \left(\frac{\partial \sigma_1}{\partial m_1} \right)_{s_1} \delta m_1 + \mu_2 \delta m_2 + \mu_2^s \delta m_2^s = 0 \qquad (50)$$

But as $s_1 = 4\pi r_1^2$, $v_1 = \frac{4}{3}\pi r_1^3$ and $s_2 = 4\pi r_2^2$ and $v = \frac{4}{3}\pi r_2^3$

$$\left(\frac{\partial s_1}{\partial v_1} \right) = \frac{2}{r_1} \quad \text{and} \left(\frac{\partial s_2}{\partial v} \right) = \frac{2}{r_2} \cdot$$

Since $\delta\nu_1$, $\delta\nu$ are arbitrary changes and since $\delta m_1 + \delta m_2 + \delta m_2^s = 0$, for equation (50) to be satisfied

$$\left[-P_1 + P_2 + \sigma_1 \left(\frac{\partial s_1}{\partial \nu_1} \right) + s_1 \left(\frac{\partial \sigma_1}{\partial s_1} \right)_{m_1} \left(\frac{\partial \sigma_1}{\partial \nu_1} \right) \right] \delta\nu_1 = 0$$

$$\left[-P_2 + P_o + \gamma_2 \left(\frac{\partial s_2}{\partial \nu} \right) \right] \delta\nu = 0$$

$$\left(\mu_1 + s_1 \left(\frac{\partial \sigma_1}{\partial m_1} \right)_{s_1} \right) \delta m_1 + \mu_2 \, \delta m_2 + \mu_2^s \, \delta m_2^s = 0$$

Therefore $$P_1 = P_2 + \frac{2\sigma_1}{r_1} + \frac{2s_1}{r_1} \left(\frac{\partial \sigma_1}{\partial s_1} \right)_{m_1} \qquad (51)$$

$$P_2 = P_o + \frac{2\gamma_2}{r_2} \qquad (52)$$

and $$\mu_1 + s_1 \left(\frac{\partial \sigma_1}{\partial m_1} \right)_{s_1} = \mu_2 = \mu_2^s \qquad (53)$$

But from equation (41) for constant temperature σ_1 is $\sigma_1(s_1, m_1)$ and therefore using equation (34)

$$\left(\frac{\partial \sigma_1}{\partial m_1} \right)_{s_1} = - \left(\frac{\partial s_1}{\partial m_1} \right)_{\sigma_1} \left(\frac{\partial \sigma_1}{\partial s_1} \right)_{m_1} \qquad (54)$$

$\left(\frac{\partial \sigma_1}{\partial m_1} \right)_{\sigma_1}$ represents the change of surface area with mass, when σ_1

remains constant i.e. we imagine the mass increasing by dm_1 and the state of the interior remaining the same, so that $dm_1 = \rho_1 d\nu_1$ and consequently

$$\left(\frac{\partial s_1}{\partial m_1}\right)_{\sigma_1} = \frac{1}{\rho_1}\left(\frac{\partial s_1}{\partial \nu_1}\right) \tag{55}$$

But $\left(\frac{\partial s_1}{\partial \nu_1}\right) = \frac{2}{r_1}$ so

$$\left(\frac{\partial \sigma_1}{\partial m_1}\right)_{s_1} = -\frac{2}{r_1\rho_1}\left(\frac{\partial \sigma_1}{\partial s_1}\right)_{m_1} \tag{56}$$

Consequently equation (53) can be rewritten.

$$\mu_1 - \frac{2 s_1}{r_1 \rho_1}\left(\frac{\partial \sigma_1}{\partial s_1}\right)_{m_1} = \mu_2 = \mu_2^s. \tag{57}$$

Equations (51) and (52) give the conditions of mechanical equilibrium. Equation (52) is the Gibbs-Kelvin relation for the pressure difference across a spherical surface between two fluids, in terms of the surface tension and the radius of curvature. Equation (51) gives the relation for the pressure difference across the solid-liquid surface i.e.

$$P_1 = P_2 + \frac{2}{r_1}\left(\sigma_1 + s_1\left(\frac{\partial \sigma_1}{\partial s_1}\right)_{m_1}\right) \tag{58}$$

If we consider an isotropic surface stress g in a curved solid surface, then for mechanical equilibrium there must be a balance of forces in all directions. Therefore, if we consider a small square element area of a spherical surface of radius R, such that its sides are length l, the resultant normal force inwards on the element, due to surface stress is $2gl.\frac{l}{R}$. For equilibrium this must be balanced by a normal pressure difference across the surface element. If the pressure difference is ΔP, where the pressure is greater inside the spherical surface, the force on the element due to this pressure is $\Delta P l^2$. These forces will balance if $\Delta P = \frac{2g}{R}$. Similarly for a solid-liquid spherical surface, where there is an isotropic surface stress g_1, and radius r_1, the pressure difference $P_1 - P_2$ is given by $\frac{2g_1}{r_1}$. Therefore from equation (58)

$$g_1 = \sigma_1 + s_1 \left(\frac{\partial \sigma_1}{\partial s_1} \right)_{m_1} \qquad (59)$$

so that

$$s_1 \left(\frac{\partial \sigma_1}{\partial s_1} \right)_{m_1} = g_1 - \sigma_1 \qquad (60)$$

Therefore substituting equation (60) in equation (57)

$$\mu_1 - \left(g_1 - \sigma_1\right) \frac{2}{r_1 \rho_1} = \mu_2 \qquad (61)$$

Equation (61) gives the condition of equilibrium in terms of the Gibbs potential, surface stress, and the specific surface free energy. Equation (59) gives the relation of the surface stress in terms of the specific surface free energy. For a crystal with a plane surface, when the external normal stress is zero, in an arbitrary deformation at constant mass which is assumed to change the local state of the surface, and in consequence the surface free energy, we have

$$g_{\mu\nu} = \sigma\delta_{\mu\nu} + \left(\frac{\partial\sigma}{\partial U_{\mu\nu}}\right) \qquad (62)$$

where $g_{\mu\nu}$ = the general surface stress tensor

σ = specific surface free energy.

δ = Kronecker delta.

$U_{\mu\nu}$ = general strain tensor of deformation

μ = x,y,z ν = x,y and x-y is the plane of the surface.

This equation, for a crystal face of greater than 3-fold rotational

symmetry, reduces to

$$g = \sigma + \frac{\partial \sigma}{\partial(\text{strain})} = \sigma + s\left(\frac{\partial \sigma}{\partial s}\right) \qquad (63)$$

which is the relation in equation (59). For a solid, the term $s\left(\frac{\partial \sigma}{\partial s}\right)$ will be appreciable, (of the order of σ), but for a liquid it will vanish because a liquid cannot support a shear strain, and the deformation will result in a transfer of liquid from the interior to the surface or vice-versa, without change of the state of the surface. For a liquid, therefore $\left(\frac{\partial \sigma}{\partial s}\right)_s = 0$ and σ is numerically equal to the surface stress. Consequently when phase (1) is a fluid equation, (61) reduces to $\mu_1 = \mu_2$ because then $\sigma_1 = g_1 = \gamma_1$, which is the normal relation between potentials of fluid phases. (see e.g. Curzon (1960)).

The apparent inequality of the Gibbs thermodynamic potential of a crystal and its liquid in equation (61) arises from the fact that a crystallite contains an additional degree of freedom to temperature and strain, namely the concentration of lattice defects in the form of holes and interstitial atoms. The atoms in the interstitial positions have a different potential from the lattice atoms and the representative potential of the crystal can be considered as: $\bar{\mu} = \mu_a - \mu_i$ (64)
where μ_a = the potential of lattice atoms and μ_i = the potential of interstitial atoms or lattice vacencies in equilibrium with each other.

If we consider a bulk crystal at zero stress, with none of these imperfections, then on decreasing its size the surface stress will induce atoms into the interstitial positions and form corresponding vacancies. If we consider this crystal in equillbrium with its liquid When $\bar{\mu}_1 = \mu_2$, then from equation (61).

$$\bar{\mu}_1 = \mu_1 - \frac{2}{r_1 \rho_1} (g_1 - \sigma_1) = \mu_a - \mu_i \qquad (65)$$

Hence $\mu_a = \mu_1$ where μ_1 is the potential at a pressure P_1 if no changes in the 'ideal' structure occurs, and $\mu_i = \frac{2}{r_1 \rho_1} (g_1 - \sigma_1)$ would be the potential of the imperfections. This is then in agreement with Herring (1950, a).

However, considering the equilibrium in terms of the normal macroscpic variables, in the case of a solid core and liquid shell, we have from equation (61)

$$\mu_1(P_1,T) - \frac{2}{r_1 \rho_1} (g_1 - \sigma_1) = \mu_2 \ (P_2,T) \qquad (66)$$

Since $P_1 = P_o + \frac{2\gamma_2}{r_2} + \frac{2g_1}{r_1}$ and $P_2 = P_o + \frac{2\gamma_2}{r_2}$

from equations (51) and (52)

$$P_1 - P_2 = \frac{2g_1}{r_1} \qquad (67)$$

Therefore equation (66) can be rewritten

$$\mu_1(P_1,T) - \frac{(P_1-P_2)}{\rho_1} + \frac{2\sigma_1}{r_1\rho_1} = \mu_2(P_2,T) \qquad (68)$$

But $$\mu = F_m - p\nu_m = F_m - {}^{P}/_{\rho} \qquad (69)$$

where F_m = free energy per unit mass

$\nu_m = {}^{1}/_{\rho}$ = volume per unit mass.

$$\therefore \quad \mu_1(P_1,T) - \frac{P_1}{\rho_1} + \frac{2\sigma_1}{r_1\rho_1} = \mu_2(P_2,T) - \frac{P_2}{\rho_2} + \frac{P_2}{\rho_2} - \frac{P_2}{\rho_1}$$

so that $$F_{1m}(P_1,T) + \frac{2\sigma_1}{r_1\rho_1} = F_{2m} - P_2\left(\frac{1}{\rho_1} - \frac{1}{\rho_2}\right) \qquad (70)$$

Therefore for equilibrium

$$F_{2m} = F_{1m} + \frac{2\sigma_1}{r_1\rho_1} - P_2 \quad (\nu_{2m} - \nu_{1m}) \qquad (71)$$

When two bulk phases are in equilibrium and no account is taken of the effect of the surface of discontinuity, $p_1 = p_2 = p$ and the condition of equilibrium is, as expected,

$$F_{2m} = F_{1m} - p \quad (\nu_{2m} - \nu_{1m}) \qquad (72)$$

i.e. the difference of free energy per unit mass is equal to the external work done in transferring unit mass from one phase to the other. However, it can be seen from equation (71) the free energy of

the solid is augmented by the term $\frac{2\sigma_1}{\rho_1 r_1}$ when a spherical surface of discontinuity is taken into account.

The equilibrium of a crystallite inside a liquid is unstable. If we consider an actual change where some solid has melted into the liquid and signify the increments occurring by Δ, for the equilibrium condition to be satisfied from equation (68), $\Delta\mu_1 + \Delta\left(\frac{2\sigma_1}{\rho_1 r_1}\right) - \Delta\left(\frac{P_1-P_2}{\rho_1}\right)$ must equal $\Delta\mu_2$ for constant temperature t, and total mass, m. If we suppose the solid transferred to the liquid diminishes the radius of the solid particle by Δr_1, then the shell outer radius increases by Δr_2 because $\rho_1 > \rho_2$

$$\Delta\mu_2 = \left(\frac{\partial\mu_2}{\partial P_2}\right)\left(\frac{\partial P_2}{\partial r_2}\right)\Delta r_2 = \frac{1}{\rho_2}\left(\frac{\partial P_2}{\partial r_2}\right)\Delta r_2 \qquad (73)$$

because $\left(\frac{\partial\mu}{\partial P}\right)_T = 1/\rho$

$$\Delta\mu_1 = \left(\frac{\partial\mu_1}{\partial P_1}\right)\left(\frac{\partial P_1}{\partial r_1}\right) = \frac{1}{\rho_1}\left(\frac{\partial P_1}{\partial r_1}\right)\Delta r_1 \qquad (74)$$

$$\Delta\left(\frac{2\sigma_1}{r_1\rho_1}\right) = -\frac{2\sigma_1}{\rho_1 r_1^2}\Delta r_1 - \frac{2\sigma_1}{\rho_1^2 r_1}\left(\frac{\partial\rho_1}{\partial P_1}\right)\left(\frac{\partial P_1}{\partial r_1}\right)\Delta r_1 \qquad (75)$$

$$\Delta\left(\frac{P_1-P_2}{\rho_1}\right) = \frac{1}{\rho_1}\left(\frac{\partial (P_1-P_2)}{\partial r_1}\right)\Delta r_1 - \frac{(P_1-P_2)}{\rho_1^2}\left(\frac{\partial\rho_1}{\partial P_1}\right)\left(\frac{\partial P_1}{\partial r_1}\right)\Delta r_1$$

(76)

But $-\frac{1}{\nu_m}\left(\frac{\partial \nu_m}{\partial P}\right)_T = \frac{1}{k}$ where k = bulk modulus and $\nu_m = {}^1/\rho$, therefore $d\nu_m = \frac{1}{\rho^2}\, d\rho$ so that

$$\left(\frac{\partial \rho}{\partial P}\right)_T = \rho/k \tag{77}$$

$$\therefore \Delta\mu_1 - \Delta\left(\frac{2\sigma_1}{\rho_1 r_1}\right) - \Delta\left(\frac{P_1-P_2}{\rho_1}\right)$$

$$= \frac{1}{\rho_1}\left(\frac{\partial P_1}{\partial r_1}\right)\Delta r_1 - \frac{2\sigma_1}{\rho_1 r_1^2}\,\Delta r_1 - \frac{2\sigma_1}{\rho_1 r_1}\,\frac{1}{k_1}\left(\frac{\partial P_1}{\partial r_1}\right) - \frac{1}{\rho_1}\left(\frac{\partial}{\partial r_1}(P_1-P_2)\right)\Delta r_1 + \frac{(P_1-P_2)}{\rho_1 k_1}\left(\frac{\partial P_1}{\partial r_1}\right)\Delta r_1 \tag{78}$$

Since from equations (51) and (52) $P_1 = P_o + \frac{2\gamma_2}{r_2} + \frac{2g_1}{r_1}$,

$\therefore P_2 = P_o + \frac{2\gamma_2}{r_2}$ and $P_1 - P_2 = \frac{2g_1}{r_1}$, therefore

$$\frac{\partial(P_1-P_2)}{\partial r_1} = -\frac{2g_1}{r_1^2}, \quad \frac{\partial P_2}{\partial r_2} = -\frac{2\gamma_2}{r_2^2}, \quad \frac{\partial P_1}{\partial r_1} = -\frac{2g_1}{r_1^2}$$

$$\therefore \Delta\mu_2 = -\frac{1}{\rho_2}\left(\frac{2\gamma_2}{r_2^2}\right)\Delta r_2 \tag{79}$$

and

$$\therefore \Delta\mu_1 + \Delta\left(\frac{2\sigma_1}{\rho_1 r_1}\right) - \Delta\left(\frac{P_1-P_2}{\rho_1}\right) = -\Delta r_1\left[\frac{2\sigma_1}{\rho_1 r_1^2} + (g_1-\sigma_1)\,\frac{2}{\rho_1 r_1 k_1} - \frac{2g_1}{r_1^2}\right] \tag{80}$$

Since Δr_2 is positive and Δr_1 is negative, the R.H.S. of equation (80) is positive and the R.H.S. of equation (79) is negative, so consequently these terms cannot be equal and the equilibrium is not maintained.

Also since $\left(\frac{\partial \mu}{\partial T}\right)_P = -\eta_m$, where η_m is the entropy per unit mass, and since the entropy of a liquid is greater than that of a solid, for equilibrium to be maintained on a decrease of the solid, the temperature must be lowered. This means that the solid is in unstable equilibrium with respect to size variation when it is completely surrounded by the fluid. The condition of equilibrium obtained in equation (61) will represent the limiting case of equilibrium when a continuous change of phase is considered.

4. Melting Point Equilibrium of Crystallites.

When bulk solid melts, each step may be considered as a reversible transfer of matter from the solid to the liquid phase, while the intensive properties remain the same. However, in the case of a small solid particle the melting process cannot be considered so simply, since its intensive properties depend on its size. Therefore, when a transfer of matter from the solid occurs, its size decreases and it may no longer be in a state of equilibrium with the phase into which it is changing, as was shown in the previous section. In the experiments carried out, the solid spherical crystallite changed into a liquid spherical drop, and because the amount of both phases present was small, the intensive properties of the liquid would also have changed during the transformation. In the experiments carried out, at some stage the liquid must have been formed from the crystallites. Since the temperature was raised continuously

for the equilibrium conditions to be satisfied, the considered liquid and solid must be at the same temperature. Therefore the simple model of solid and liquid spheres in equilibrium cannot be applied. (Pavlov (1909), Reiss and Wilson (1948)). Also the initial and final state of a tin particle could pass through a series of non-equilibrium states, so that for the condition of thermodynamic equilibrium of melting of small crystallites, we must consider a system where both phases are present at the same temperature. Two models of melting will be considered.

4.1. Uniform Melting - Simultaneous Melting Over Entire Solid Surface.

In this model we consider the crystallite to melt at the surface and form a liquid shell which completely encloses the solid, so that consequently there are only solid-liquid and liquid-air interfaces. As the temperature is raised, the solid begins to change uniformly at its surface since the surface layers of the crystallite are already in a state of higher free energy and greater disorder than the interior. The new phase which is formed cannot be considered to be a liquid with homogeneous bulk properties because of the initial thinness of the shell formed. The condition of local order and long range disorder cannot be satisfied, and furthermore the interatomic forces from the solid in contact with this shell will tend to make this "pseudo liquid" more solid-like. If we assume that thermodynamic properties can be assigned to this layer, we may divide it into a volume, and two dividing surfaces, the solid- "liquid" dividing surface and the outer surface of the "liquid" shell. However if the shell initially formed is

allowed to increase in thickness, its properties tend to become more like those of a bulk liquid, so that at some critical thickness, λ, its properties will be those of a bulk liquid.

Since the properties of the dividing surface depend on the properties of the two phases between which it lies, the free energy of the solid - "liquid" interface and the "liquid" surface will also change with thickness of the shell. Since the shell is more like a solid when its thickness, d, is less than λ, the solid - "liquid" interface free energy $\sigma^*_1(d)$ will be less than σ_1, the free energy of the solid-bulk liquid interface. Similarly, the free energy of the "liquid" surface $\gamma^*_2(d)$ will be greater than that of a bulk liquid, since the free energy of a solid is greater than that of a liquid. The free energies of both the surfaces of the shell will acquire the bulk liquid values when the shell has a thickness λ. The value of $\sigma^*_1(d)$ and $\gamma^*_2(d)$ could be considered to vary with d, the thickness of the shell, as shown in Figure 44. The interfacial solid - "liquid "free energy increases from a very small value, to the bulk-liquid surface free energy when $d = \lambda$. The"liquid"- air free energy, correspondingly decreases from a value very near that of a solid-air free energy to the bulk liquid free energy, which is the liquid surface tension, when $d = \lambda$.

The value of λ at which the shell acquires the properties of a bulk liquid is expected to be of the order of 15 to 20 $\mathring{A}$.

If we therefore consider the "melting" to commence uniformly on the surface, the transfer of solid to "liquid" will commence at a temperature at which the equilibrium between the solid core and the "liquid" is satisfied. The system may be considered as the one shown in Figure 43, except that r_2-r_1 is very small, of the order of a few Angstroms. Because of the "pseudo liquid" state, the equilibrium between the solid and the "liquid" will be stable with respect to further "melting". Both $\sigma_1^*(d)$ and $\gamma_2^*(d)$ increase with increase in d, so that when some solid "melts" the shell increases in thickness. Hence there are extra terms in equation (79) and (80). Increase in d means a decrease in r_1 and an increase in r_2 so new terms will occur in equations (79) and (80) namely $\frac{\partial \gamma_1^*(d)}{\partial r_2} \Delta r_2$ in equation (79) and $\frac{\partial \sigma_1^*(d)}{\partial r_2} \Delta r_1$ in equation (80) where the former is positive and the latter negative. Consequently the condition for stability will be satisfied in the range d=0 to d= λ, because the gradient of $\sigma_1^*(d)$ and $\gamma_2^*(d)$ is large in this region, as may be seen from Figure 43. However when the shell attains the bulk properties of the liquid, the above terms become zero, and the equilibrium becomes unstable. Therefore when the shell reaches the thickness λ, a subsequent temperature rise causes a "catastrophic" change of solid to liquid. The melting point equilibrium must therefore be considered at the temperature at which the "liquid" has just attained the properties of a bulk liquid, namely when the shell thickness is λ, if adequate energy is supplied.

At the melting equilibrium the solid core of radius r_1 is in equilibrium with a liquid shell of radius r_2, where $r_2 = r_1 + \lambda$, (at a temperature T). This was initially a crystallite of radius R_o, and its melting point can be considered as T.

Let us consider a crystallite of radius $R_o + \Delta R_o$, and let its melting point temperature be $T + \Delta T$. At this temperature a solid core of radius $r_1 + \Delta r_1$ is in equilibrium with a shell of thickness λ.

$$\therefore \quad \Delta r_1 = \Delta r_2 \tag{81}$$

From equation (68) for a solid sphere to be in equilibrium with a liquid shell at a temperature T, we must have

$$\mu_1(P_1,T) + \frac{2\sigma_1(T)}{r_1\rho_1} - \frac{(P_1-P_2)}{\rho_1} = \mu_2(P_2,T) \tag{82}$$

Therefore for equilibrium to be satisfied when r_1 increases to $r_1 + \Delta r_1$ and r_2 increases to $r_2 + \Delta r_2$ the system must be at $T + \Delta T$, where P_1 has changed to $P_1 + \Delta P_1$ and P_2 to $P_2 + \Delta P_2$.

$$\therefore \quad \Delta\mu_1 + \Delta\left(\frac{2\sigma_1}{r_1\rho_1}\right) - \Delta\left(\frac{P_1 - P_2}{\rho_1}\right) = \Delta\mu_2 \tag{83}$$

But

$$\Delta\mu_1 = \left(\frac{\partial\mu_1}{\partial P_1}\right)_T \Delta P_1 + \left(\frac{\partial\mu_1}{\partial T}\right)_P \Delta T \tag{84}$$

$$\Delta \mu_2 = \left(\frac{\partial \mu_2}{\partial P_2}\right)_T \Delta P_2 + \left(\frac{\partial \mu_2}{\partial T}\right)_P \Delta T \tag{85}$$

$$\Delta\left(\frac{2\sigma_1}{r_1\rho_1}\right) = \left(-\frac{2\sigma_1}{r_1^2\rho_1}\right)\Delta r_1 + \frac{2}{r_1\rho_1}\left(\frac{\partial \sigma_1}{\partial T}\right)\Delta T$$

$$- \frac{2\sigma_1}{r_1\rho_1^2}\left(\frac{\partial \rho_1}{\partial P_1}\right)_T \Delta P_1 - \frac{2\sigma_1}{r_1\rho_1^2}\left(\frac{\partial \rho_1}{\partial T}\right)_P \Delta T \tag{86}$$

$$\Delta\left(\frac{P_1-P_2}{\rho_1}\right) = \frac{\Delta P_1}{\rho_1} - \frac{\Delta P_2}{\rho_1} - \frac{(P_1-P_2)}{\rho_1^2}\left(\frac{\partial \rho_1}{\partial P_1}\right)_T \Delta P_1$$

$$- \frac{(P_1-P_2)}{\rho_1^2}\left(\frac{\partial \rho_1}{\partial T}\right)_P \Delta T. \tag{87}$$

$\left(\frac{\partial \mu}{\partial P}\right)_T = \frac{1}{\rho}$ - the volume per unit mass (88)

$\left(\frac{\partial \mu}{\partial T}\right)_P = -\eta_m$ - the entropy per unit mass . (89)

$\left(\frac{\partial \rho}{\partial P}\right)_T = \rho/k$ - where k= bulk modulus (90)

$\left(\frac{\partial \rho}{\partial T}\right)_P = -\alpha\rho$ - where α=cubical expansion coefficient (91)

$\left(\frac{\partial \sigma_1}{\partial T}\right) = -\eta_s$ - entropy per unit area of the solid-liquid surface (92)

So substituting equation (84) to (87) in equation (83) and rearranging

$$\left(\frac{\partial \mu_1}{\partial T}\right)_{P_1} \Delta T - \left(\frac{\partial \mu_2}{\partial T}\right)_{P_2} \Delta T + \frac{2}{r_1 \rho_1}\left(\frac{\partial \sigma_1}{\partial T}\right)\Delta T - \frac{2\sigma_1}{r_1 \rho_1^2}\left(\frac{\partial \rho_1}{\partial T}\right)\Delta T$$

$$+ \frac{(P_1-P_2)}{\rho_1^2}\left(\frac{\partial \rho_1}{\partial T}\right)\Delta T$$

$$= \left(\frac{\partial \mu_2}{\partial P_2}\right)_T \Delta P_2 - \left(\frac{\partial \mu_1}{\partial P_1}\right)_T \Delta P_1 + \frac{2\sigma_1}{r_1^2 \rho_1}\Delta r_1$$

$$+ \frac{2\sigma_1}{r_1 \rho_1^2}\left(\frac{\partial \rho_1}{\partial P_1}\right)\Delta P_1 + \frac{\Delta P_1}{\rho_1} - \frac{\Delta P_2}{\rho_1}$$

$$- \frac{(P_1-P_2)}{\rho_1^2}\left(\frac{\partial \rho_1}{\partial P_1}\right)\Delta P_1 \qquad (93)$$

Substituting equations (88) to (92) in equation (93)

$$\left[-\eta_{1m} + \eta_{2m} - \frac{2}{r_1 \rho_1}\eta_s + \frac{\alpha_1}{\rho_1}\left[\frac{2\sigma_1}{r_1} - (P_1-P_2)\right]\right]\Delta T$$

$$= \frac{\Delta P_2}{\rho_2} - \frac{\Delta P_1}{\rho_1} + \frac{2\sigma_1}{r_1^2 \rho_1}\Delta r_1 + \frac{2\sigma_1}{r_1 \rho_1 k_1}\Delta P_1$$

$$+ \frac{\Delta P_1}{\rho_1} - \frac{\Delta P_2}{\rho_1} - \frac{(P_1-P_2)}{\rho_1 k_1}\Delta P_1$$

$$= \frac{2\sigma_1}{r_1^2 \rho_1} \Delta r_1 - \Delta P_2 \left(\frac{1}{\rho_1} - \frac{1}{\rho_2}\right) + \frac{\Delta P_1}{\rho_1 k_1} \left(\frac{2\sigma_1}{r_1} - (P_1 - P_2)\right) \qquad (94)$$

But from equations (51),(52) and (67)

$$P_1 = P_o + \frac{2\gamma_2}{r_2} + \frac{2g_1}{r_1} \quad \therefore \quad \Delta P_1 = \frac{-2\gamma_2}{r_2^2} \Delta r_2 - \frac{2g_1}{r_1^2} \Delta r_1 \; ;$$

$$P_2 = P_o + \frac{2\gamma_2}{r_2} \quad \therefore \quad \Delta P_2 = \frac{-2\gamma_2}{r_2^2} \Delta r_2 \quad \text{and} \quad P_1 = P_2 + \frac{2g_1}{r_1}$$

Since $r_2 = r_1 \pm \lambda$ and $\Delta r_1 = \Delta r_2$ from equation (81)

$$(\eta_{2m} - \eta_{1m}) \Delta T - \frac{2}{r_1 \rho_1} \eta_s \Delta T + \frac{2a_1}{r_1 \rho_1} (\sigma_1 - g_1) \Delta T$$

$$= \frac{2\sigma_1}{r_1^2 \rho_1} \Delta r_1 + \frac{2\gamma_2}{(r_1+\lambda)^2} \left(\frac{1}{\rho_1} - \frac{1}{\rho_2}\right) \Delta r_1 \qquad (95)$$

$$- \frac{2}{r_1 \rho_1 k_1} (\sigma_1 - g_1) \left(\frac{2\gamma_2}{(r_1+\lambda)^2} + \frac{2g_1}{r_1^2}\right) \Delta r_1$$

Therefore if we denote r_1 by r

$$\frac{\Delta T}{\Delta r} = \frac{\frac{2\sigma_1}{r^2 \rho_1} - \frac{2\gamma_2}{(r+\lambda)^2 \rho_1} \left(\frac{\rho_1}{\rho_2} - 1\right) + \frac{2}{r \rho_1 k_1} (g_1 - \sigma_1) \left(\frac{2\gamma_2}{(r+\lambda)^2} + \frac{2g_1}{r^2}\right)}{\eta_{2m} - \eta_{1m} - \frac{2}{r \rho_1} \eta_s - \frac{2a_1}{r \rho_1} (g_1 - \sigma_1)} \qquad (96)$$

where $\eta_2 = \eta_{2m}(P_2,T)$ - the entropy per unit mass of liquid.

$\eta_1 = \eta_{1m}(P_1,T)$ - the entropy per unit mass of solid.

The melting point equilibrium expression obtained above is for a solid core of radius r and shell thickness λ. This expression would represent the gradient of the graphs, shown in Figures 34 and 36, at a point R, T_R when $R = r + \lambda$ and $T = T_R$. This is because the radius indicated in these graphs is the radius of the original crystal, and therefore the radius of the outer surface of the liquid shell. Therefore, the gradient on the melting curve at a point R,T, should be given by

$$\frac{\Delta T}{\Delta R} = \frac{\dfrac{2\sigma_1}{(R-\lambda)^2\rho_1} - \dfrac{2\gamma_2}{R^2\rho_1}\left(\dfrac{\rho_1}{\rho_2} - 1\right) - \dfrac{\tau(g_1-\sigma_1)}{(R-\lambda)_1}\left(\dfrac{2\gamma_2}{R^2} + \dfrac{2g_1}{(R-\lambda)^2}\right)}{\eta_2 - \eta_1 - \dfrac{2\eta_s}{(R-\lambda)\rho_1} - \dfrac{2a_1}{(R-\lambda)\rho_1}(g_1 - q_1)} \qquad (97)$$

The density of the solid crystallites was found to be equal to that of the bulk tin, when the largest crystallites of the order 500 Å, were investigated (Chapter IV Section 4). Subsequent determinations of lattice parameters of smaller crystallites showed no change, to within the experimental accuracy of 0.5%. Since the compressibilities of solid and liquid tin are of the same magnitude, the bulk moduli being 5.25 10^{11} dynes/cm^2, (Bridgman (1925), and 3.1 10^{11} dynes/cm^2, (Kleppa (1950)), respectively, the densities

appearing in equation (97) may be taken as those of bulk tin, at normal pressures i.e. $\rho_1 = 7.184$ and $\rho_2 = 6.98$ grams per centimetre cube. γ_2 for liquid tin in vacuo is 580 dynes/cm (Matuyama (1927)) and its variation with temperature is of the order of 5 dynes per $30^{\circ}C$. Therefore the term in the numerator

$$\frac{2\gamma_2}{R^2\rho_1}\left(\frac{\rho_1}{\rho_2} - 1\right) = \frac{2}{R^2} \quad 15.6 \text{ ergs/gm/cm}^3.$$

The last term of the numerator is much smaller than the first two because of the large value of k_1, the bulk modulus of solid tin.

The estimation of the solid-liquid surface stress from the surface free energy (Turnbull (1950)) make the solid-liquid surface stress much less than the liquid surface tension. This would be expected from the similar packing of atoms in solid and liquid tin. Consequently $\frac{2\gamma_2}{R^2}$ will be much larger than $\frac{2g_1}{(R-\lambda)^2}$, so that if we take $g_1 - \sigma_1 \sim \sigma_1$, the last term may be rewritten, approximately, as

$$\frac{2\sigma_1}{\rho_1 k_1 (R-\lambda)} \cdot \frac{2\gamma_2}{R^2}$$

Therefore the ratio of the 1st term, $\frac{2\sigma_1}{(R-\lambda)^2_1}$, to this is

$$\sim \frac{2\gamma_2}{k_1 R} \sim \frac{2.10^{-9}}{R}$$

Since the smallest value of R studied was ~ 30 Å, the last term would be less than 1% of the first term in the numerator. Thus without any loss of accuracy the last term can be ignored.

No discontinuity in the properties of liquid tin at temperatures below its bulk melting point are expected. (Greenwood (1952)) In the denominator $\eta_{2m}(P_2,T) - \eta_{1m}(P_1,T)$ appears. The pressure P_1 is greater than P_2, but they are both of the order of $\frac{2\gamma_2}{R}$. For a crystal of 100 Å, $P_2 \sim 10^9$ dynes/cm^2. The melting temperature for some crystallites may be as much as 100°C below the bulk melting point of tin. Therefore both these factors, temperature and pressure, should be taken into account when the equilibrium entropy is being considered. However, the entropy difference, $\eta_{2m}(P_2,T) - \eta_{1m}(P_1,T)$, does not differ from the value at bulk melting point, T_B, and both phases at one atmosphere, P_o, by more than 1-2% (as discussed below).

Entropy is a function of temperature and pressure as $d\eta_m = \frac{C_p}{T} dT - \frac{\alpha}{\rho} dP$, where C_p is the specific heat at constant pressure, and α is the coefficient of thermal expansion. If we therefore consider $\eta_{2m}(P_2,T)$, $\eta_{1m}(P_1,T)$ in terms of their values at the melting point, T_B, when the pressure is P_o

$$\eta_{2m}(P_2,T) = \eta_{2m}(P_o,T_B) + \int_{T_B}^{T} \frac{Cp_2}{T} dT - \int_{P_o}^{P} \frac{\alpha_2}{\rho_2} dP \qquad (98)$$

$$\eta_{1m}(P_1,T) = \eta_{1m}(P_o,T_B) + \int_{T_B}^{T} \frac{C_{P1}}{T}\, dT - \int_{P_o}^{P} \frac{\alpha_1}{\rho_1}\, dP \qquad (99)$$

But $\eta_{2m}(P_o,T_B) - \eta_{1m}(P_o,T_B) = \frac{L}{T_B}$, where L = the latent heat of fusion of tin. Therefore subtracting equation (99) from equation (98)

$$\eta_{2m}(P_1,T) - \eta_{1m}(P_1,T) = \frac{L}{T_B} + (\bar{C}_{p2}-\bar{C}_{p1})\log_e \frac{T}{T_B} - \frac{\alpha_2}{\rho_2}(P_2-P_o) + \frac{\alpha_1}{\rho_1}(P_1-P_o) \qquad (100)$$

where $\bar{C}_{p2}$, $\bar{C}_{p1}$ are mean values of the specific heats over the range of integration. When P_o is one atmosphere, $T_B = 505^{\circ}K$ and L=14.5 calories/gram = $6.07\ 10^8$ ergs/gram.

Therefore $\frac{L}{T_B} = 1.12\ 10^6$ ergs/gram/degree.

The specific heat of liquid tin, C_{p2}, is 0.0615 calories per gram (Kleppa (1950)), but the specific heat of solid varies from 0.062 calories per gram, at $505^{\circ}K$, approximately linearly with temperature (Kelly (1949)). The term $(\bar{C}_{p2}-\bar{C}_{p1})$ will not exceed 10^4 ergs/gm/degree in the range of the experiments so that $(\bar{C}_{p2}-\bar{C}_{p1})\log_e \frac{T}{TB} < 1\%$ of $\frac{L}{T_B}$. Similarly since $\alpha_1 = 7.10^{-5}$ and $\alpha_2 = 10^{-4}$, when $P_1, P_2 \sim 10^9$ dynes/cm^2, the last two terms in equation (100) will be less than 1% of $\frac{L}{T_B}$. Therefore the entropy difference $(\eta_{2m} - \eta_{1m})$ is equal to $\frac{L}{T_B}$ to within 1-2%.

The entropy of the solid-liquid surface could not be found in the literature, however this term would be expected to be small. If we consider the variation of the liquid surface tension (Matuyama (1927)) as an order of magnitude although γ_2 is much greater than σ_1, for 100 Å radius crystallite $\frac{2\eta_B}{\rho_1(R-\lambda)} \sim 10^4$ again less than 1% of $\frac{L}{T_B}$. The last term in the denominator is negligible being of the order of 10^2 for a crystallite of radius 100Å. Therefore to within a few percent, equation (97) may be rewritten

$$\frac{\Delta T}{\Delta R} = \frac{\frac{2\sigma_1}{(R-\lambda)^2\rho_1} - \frac{2}{R^2\rho_1} \quad 15.6}{\frac{L}{T_B}}$$

$$= \frac{2T_B}{L\rho_1}\left[\frac{\sigma_1}{(R-\lambda)^2} - \frac{15.6}{R^2} \cdot \right] \qquad (101)$$

For large crystallites, when $R >> \lambda$, this reduces to

$$\frac{\Delta T}{\Delta R} = \frac{2T_B}{L\rho_1}\left(\sigma_1 - 15.6\right) \cdot \frac{1}{R^2} \qquad (102)$$

With this approximation, if we integrate from a temperature T to T_B and from R to ∞, where T_B is the bulk melting point, assuming σ_1

is temperature independent,

$$\int_{T}^{T_B} \Delta T = \frac{2\,T_B}{L\,\rho_1}\left(\sigma_1 - 15.6\right) \int_{R}^{\infty} \frac{\Delta R}{R^2} \qquad (103)$$

$$\therefore \quad T_B - T = \frac{2T_B}{L\rho_1} \left(\sigma_1 - 15.6\right) \frac{1}{R} \,.$$

$$\therefore \quad T = T_B - \frac{2T_B}{L\rho_1} \left(\sigma_1 - 15.6\right) \frac{1}{R} \qquad (104)$$

Therefore the graph of T against $1/R$, when R is large, is a straight line. From the graphs in Figures 35 and 37, the gradient obtained for $R \sim 1000\text{A}^{\circ}$ was $(9\pm1)10^6$.

Therefore the value of σ_1 is given by

$$9.10^6 = \frac{2T_B}{L\rho_1} \left(\sigma_1 - 15.6\right) \pm 10\%$$

$$\therefore \quad \sigma_1 = 55\ (1 \pm 0.1)\ \text{ergs/cm}^2 \qquad (105)$$

This value for the free energy of the solid liquid tin surface is in good agreement with the value obtained by Turnbull (1950), of 54.5 ergs/cm^2, which was calculated from the results of experiments on supercooled liquid tin droplets carried out by Vonnegut (1948).

The linear form of T against $^1/R$ does not hold for the range of crystallite radii studied. The gradient, $\frac{\Delta T}{\Delta R}$, on the graphs of T against R were found to increase much more rapidly than indicated by equation (101) when λ was taken of the order of 20 $\mathring{A}$.

Although the curvature dependence of the specific free energy was not taken into acount the discrepancy between equation (101) and the results obtained is too large to be explained by this alone. When the effects of surfaces are considered in the general theory of capillarity, the interior phases are assumed to retain their bulk properties. The change of free energy of a phase is then expressed by the specific free energy of the surface and the strain energy induced in the interior due to the surface stresses. As shown above, the effect of the strains induced by the surface, in the case of the solid, is much less important than the surface free energy. By decreasing the size of a phase sufficiently, however, as was pointed out in the case of the thin liquid shell around a solid core, the properties of the interior could change from those of the bulk phase.

The surface, in the case of a crystal, terminates the indefinitely extending lattice associated with a bulk crystal. The unbalance of the atomic forces distorts the lattice near the surface, changing the free energy and entropy of the surface layers. This is expressed in the specific free energy of the surface. However, if we make the ratio of surface to volume sufficiently large, the unsaturated atomic bonds at the surface will begin to change the properties of the interior. When

crystallite radii of 20-30 lattice spacings are reached, the number of atoms in the surface layers becomes an appreciable fraction of the total number. For a crystallite of radius of 150Å, the fraction of the total number of atoms which is in the top surface layer alone, is 5%, and when the radius is 30 Å, the fraction is 25%. This would cause a greater change in the interior free energy and entropy then would be predicted by just the surface stress pressure alone. This increase would be expected to depend on the radius.

Since at equilibirum we are considering a thin shell of liquid, its properties, already discussed, will also depend on the radius of the solid core. Its free energy and entropy will depend on both the thickness of the shell and the radius of the core. However, we are assuming a constant thickness, λ , for the shell at the equilibrium,so that the difference between the two phases will depend on the radius of the solid core.

Since the properties of both of the phases change with the radius of their interface, tbe condition of equilibrium given by equation (66)i.e.

$$\mu_1(P_1,T) - \frac{2(g_1-\sigma_1)}{r_1 \rho} = \mu_2(P_2,T)$$

can be modified to

$$\mu_1(P_1,T) - \frac{2(g_1-\sigma_1)}{r_1 \rho_1} + \Phi\ (r_1,T) = \mu_2(P_2,T) \qquad (106)$$

where $\Phi(r_1,T)$ is a potential arising from the change in the difference of the free energies and entropies of the solid and liquid phases, at thier

melting point, on account of their size. This is a function of the temperature and the radius. If g_1, σ_1, γ_2 are assumed to retain the same values as at large curvatures, all the changes from the normal bulk phase behaviour are incorporated in the term $\Phi(r_1,T)$. Since P_1, P_2 are functions of r_1, equation (106) can be expressed in terms of the two variables T and r_1.

If we now consider the melting curves, and consider two neighbouring points, $(T, R,)$ and $(T+\Delta T,\ R+\Delta R,)$ then noting that r_1 is $R-\lambda$, where λ is the thickness of the shell, and that $P_1 = P_o + \frac{2\gamma_2}{R} + \frac{2g_1}{(R-\lambda)}$, $P_2 = P_o + \frac{2\gamma_2}{R}$, then

$$\mu_1\left(P_o + \frac{2\gamma_2}{R} + \frac{2g_1}{(R-\lambda)},\ T\right) - \frac{2(g_1 - \sigma_1)}{\rho_1(R-\lambda)} + \Phi(R-\lambda, T)$$

$$= \mu_2\left(P_o + \frac{2\gamma_2}{R},\ T\right) \qquad (107)$$

and

$$\mu_1\left(P_o + \frac{2\gamma_2}{R+\Delta R} + \frac{2g_1}{(R+\Delta R-\lambda)},\ T+\Delta T\right) - \frac{2(g_1 - \sigma_1)}{\rho_1(R+\Delta R-\lambda)}$$

$$+ \Phi(R+\Delta R-\lambda,\ T+\Delta T)$$

$$= \mu_2\left(P_o + \frac{2\gamma_2}{R+\Delta R},\ T+\Delta T\right) \qquad (108)$$

where g_1, σ_1, γ_2 and ρ_1 are considered to be temperature and radius independent. Noting that $\left(\frac{\partial \mu}{\partial R}\right)_T = \left(\frac{\partial \mu}{\partial P}\right)_T \left(\frac{\partial P}{\partial R}\right)_T$, we can

expand equation (108) to the first order

$$\mu_1\left(P_o + \frac{2\gamma_2}{R} + \frac{2g_1}{(R-\lambda)}, T\right) + \left(\frac{\partial \mu_1}{\partial P_1}\right)_R \left(\frac{\partial P_1}{\partial R}\right)_T \Delta R$$

$$+\left(\frac{\partial \mu_1}{\partial T}\right)_R \Delta T - \frac{2(g_1 - \sigma_1)}{(R-\lambda)\rho_1} + \frac{2(g_1-\sigma_1)}{(R-\lambda)^2 \rho_1} \Delta R + \Phi(R-\lambda, T)$$

$$+\left(\frac{\Delta \Phi}{\Delta R}\right)_{M.C.} \Delta R = \mu_2\left(P_o + \frac{2\gamma_2}{R}\right) + \left(\frac{\partial \mu_2}{\partial P_2}\right)_T \left(\frac{\partial P_2}{\partial R}\right)_T \Delta R$$

$$+\left(\frac{\partial \mu_2}{\partial T}\right)_R \Delta T \qquad (109)$$

where M.C. stands for the melting curve. Although Φ is $\Phi(R,T)$, R is a function of T, because of the expansion along the melting curve. For a given value of R there is a unique value of T, so that $\left(\frac{\Delta \Phi}{\Delta R}\right)_{M.C.} \Delta R$ expresses the change in Φ between the points R,T and R+ ΔR, T+ ΔT. on the melting curve.

Noting that $\left(\frac{\partial \mu}{\partial T}\right)_R = \left(\frac{\partial \mu}{\partial T}\right)_P = -\eta_m$

$$\left(\frac{\partial \mu}{\partial P}\right)_T = \frac{1}{\rho}$$

and subtracting equation (107) from equation (109)

$$\frac{1}{\rho_1}\left(\frac{-2\gamma_2}{R^2} - \frac{2g_1}{(R-\lambda)^2}\right)\Delta R - \eta_{1m}\Delta T + \frac{2g_1}{(R-\lambda)^2\rho_1}\Delta R$$

$$- \frac{2\sigma_1}{(R-\lambda)^2\rho_1}\Delta R + \left(\frac{\Delta\Phi}{\Delta R}\right)_{M.C.}\Delta R = \frac{1}{\rho_2}\left(-\frac{2\gamma_2}{R^2}\right)\Delta R - \eta_{2m}\Delta T \qquad (110)$$

Rearranging equation (110)

$$(\eta_{2m}-\eta_{1m})\Delta T = \frac{2\sigma_1}{(R-\lambda)^2\rho_1}\Delta R - \frac{2\gamma_2}{R^2\rho_1}\left(\frac{\rho_1}{\rho_2} - 1\right)\Delta R$$

$$-\left(\frac{\Delta\Phi}{\Delta R}\right)_{M.C.}\Delta R \qquad (111)$$

Therefore

$$\left(\frac{\Delta T}{\Delta R}\right)_{M.C.} = -\frac{\dfrac{2\sigma_1}{(R-\lambda)^2\rho_1} - \dfrac{2\gamma_2}{R^2\rho_1}\left(\dfrac{\rho_1}{\rho_2} - 1\right) - \left(\dfrac{\Delta\Phi}{\Delta R}\right)_{M.C.}}{\eta_{2m} - \eta_{1m}} \qquad (112)$$

Since $(\eta_{2m}-\eta_{1m})$ was shown to be equal to $\dfrac{L}{TB}$, and σ was found to be 55 ergs/cm^2,

$$\left(\frac{\Delta T}{\Delta R}\right)_{M.C.} = \frac{2T_B}{L\rho_1}\left(\frac{55}{(R-\lambda)^2} - \frac{15.6}{R^2}\right) - \frac{T_B}{L}\left(\frac{\Delta\Phi}{\Delta R}\right)_{M.C.} \qquad (113)$$

This equation gives the relation for $\left(\frac{\Delta T}{\Delta R}\right)_{M.C}$, the gradient of the melting curve at any point (T, R). The gradients of various values of T and R, were measured on the melting curves in Figures 34 and 36, and by trying different forms of $\left(\frac{\Delta\Phi\ (R-\lambda, T)}{\Delta T}\right)_{M.C.}$, the form which gave the most consistent results, was

$$\left(\frac{\Delta\Phi}{\Delta R}\right)_{M.C.} = -\frac{A}{(R-\lambda)^3} \qquad (114)$$

where A is a constant.

If we substitute equation (114) in equation (113) we obtain

$$\left(\frac{\Delta T}{\Delta R}\right)_{M.C.} = \frac{2T_B}{L\rho_1}\left(\frac{55}{(R-\lambda)^2} - \frac{15.6}{R^2}\right) + \frac{T_B}{L}\cdot\frac{A}{(R-\lambda)^3} \qquad (115)$$

$$\therefore\ \Delta T_{M.C.} = \frac{2T_B}{L\rho_1}\left[\frac{55}{(R-\lambda)^2} - \frac{15.6}{R^2}\right]\cdot\Delta R_{M.C.} + \frac{T_B}{L}\cdot\frac{A}{(R-\lambda)^3}\Delta R_{M.C.} \qquad (116).$$

If we consider a point (T,R) on the melting curve, then $\Delta T_{M.C}$, $\Delta R_{M.C.}$ are increments in T and R which have to be added in order to go to a neighbouring point on the melting curve. Therefore, if we make $\Delta T_{M.C.}$, $\Delta R_{M.C.}$ infinitely small, we may integrate equation (116) along the melting

curve from the point (T,R) to (T_B, ∞), where T_B is the bulk melting point, in order to obtain the depression in the melting point of a given radius.

Integrating equation (116)

$$\int_T^{T_B} \Delta T_{M.C.} = \int_R^{\infty} \frac{2T_B}{L\rho_1} \left(\frac{55}{(R-\lambda)^2} - \frac{15.6}{R^2} \right) \Delta R_{M.C.}$$

$$+ \int_R^{\infty} \frac{T_B}{L} \cdot \frac{A}{(R-\lambda)^3} \cdot \Delta R_{M.C.} \qquad (117)$$

Since L, T_B, and λ are constant, and if we treat ρ_1 as constant,

$$T_B - T = \frac{2T_B}{L\rho_1} \left(\frac{55}{(R-\lambda)} - \frac{15.6}{R} \right) + \frac{T_B}{2L} \frac{A}{(R-\lambda)^2} \qquad (118)$$

$T_B - T$ is the depression of the melting point for a crystallite of radius R. From the curves in Figures 34 and 35, the depression $T_B - T = \Delta T_R$, for any given radius R can be obtained.

From equation (118)

$$\frac{2L}{T_B}(T_B - T) - \frac{4}{\rho_1}\left(\frac{55}{(R-\lambda)} - \frac{15.6}{R} \right) = \frac{A}{(R-\lambda)^2} \qquad (119)$$

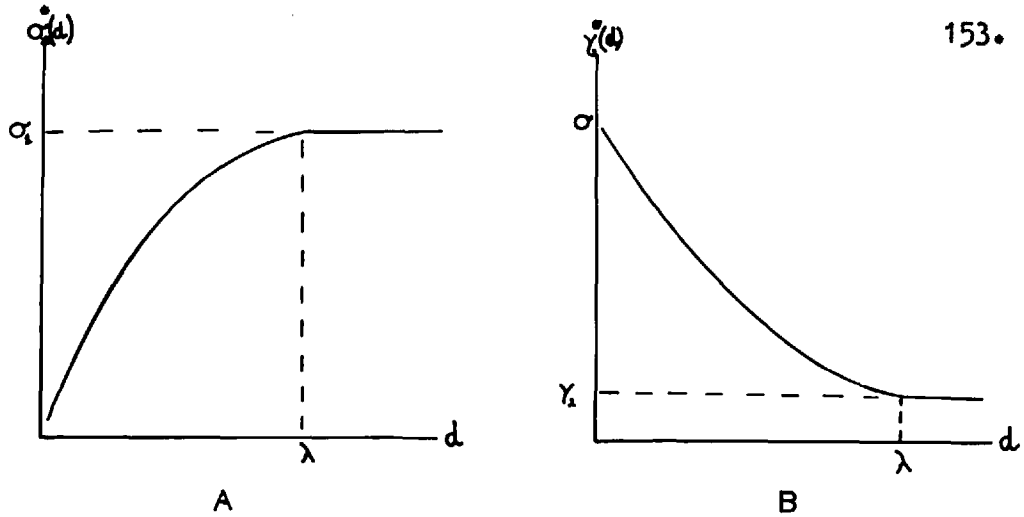

Figure 44. Graphs showing the assumed variation with the shell thickness, d, of: (A) the solid-liquid surface free energy, (B) the liquid-air surface free energy, as used in the first theoretical model of melting.

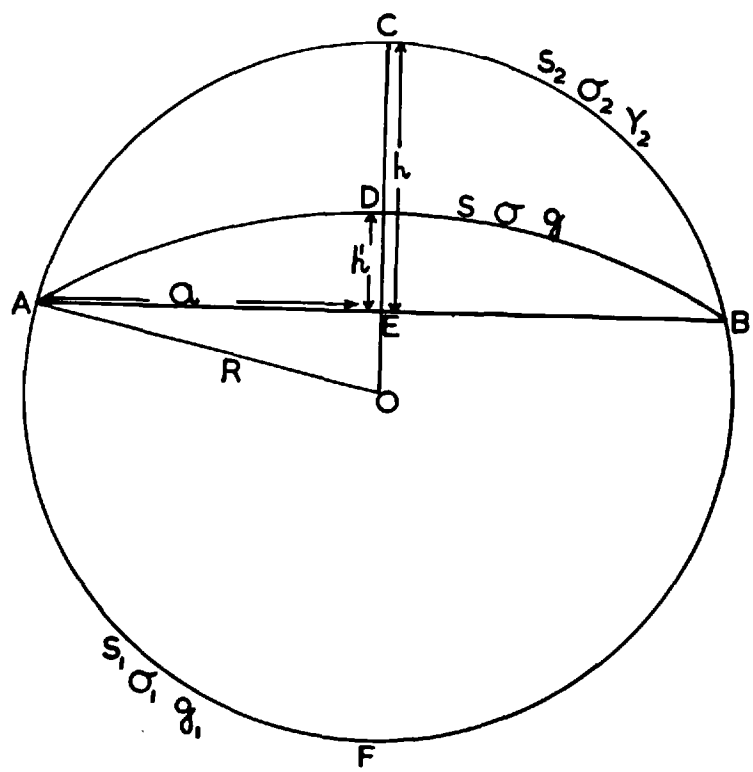

Figure 45. A liquid spherical cap formed from a sperical crystallite as assumed in the second theoretical model of melting.

Therefore plotting $\Psi = \frac{2L}{T_B}(T_B-T) - \frac{4}{\rho_1}\left(\frac{55}{(R-\lambda)} - \frac{15.6}{R}\right)$

against $\frac{1}{(R-\lambda)^2}$ for a series of values of T_B-T and R, when $\lambda = 20\text{A}^{\circ}$, the graph in Figure 46 is obtained. It is a straight line, with a gradient

$$A = 6.85\ (1\pm0.1)\ 10^{-6}\ \text{ergs gm}^{-1}\text{cm}^{2} \qquad (120)$$

Therefore the deviation from the properties of the bulk phases increases as the size of the crystallite decreases. The decrease in the free energy difference between the solid and liquid, when the core radius is 100A°, would be equivalent to an increase in the solid-liquid surface free energy of about 50%.

4.2. Non-uniform Melting- Preferential Melting over part of the Solid Surface.

In the second model, melting will be considered to begin at the point of contact of the crystallite with its substrate. At some stage of the heating, the crystallite begins to melt, and instead of forming a uniform shell on the outside of the solid, forms a spherical cap at the point of contact. This creates liquid-air and solid-liquid surfaces which change on subsequent rise in temperature, as more solid transforms into liquid. If we consider that the liquid and solid are in equilibrium, this equilibrium will be maintained only if the system is stable with

respect to a size variation of either phase. If the equilibrium becomes unstable, at some stage of the melting, this state can be taken as the melting point.

In the last section it was seen that in the crystallites studied the term involving the strain energy in the solid, due to surface stress, was of the order of 1% of that due to the surface free energy. Therefore the equilibrium conditions can safely be assumed to depend on the free energies of the liquid and solid surfaces. To simplify the geometry, since the density difference between solid and liquid tin is only 2.7%, we will consider that the solid and the liquid formed will still retain a total spherical shape with the radius remaining constant. The solid-air surface stress is greater than the liquid-air surface tension, therefore for mechanical equilibrium to occur, the solid-liquid interface must be curved. But since liquid and solid tin have similar atomic packing, the difference is expected to be small so that the radius of curvature of the solid-liquid interface will be much larger than the radius of the crystallite.

Let us consider the system in equilibrium at a temperature t, as in Figure 45, where the liquid formed can be considered to have already attained bulk properties. The crystallite was originally a sphere of radius R. The liquid formed is in the volume ADBC, enclosed by two spherical surface elements, ACB. radius R and ADB of radius R'. The

curvature of the surface ADB is determined by the condition of mechanical equilibrium

$$\frac{2\gamma_2}{R} + \frac{2g}{R'} = \frac{2g_1}{R} \qquad (121)$$

where γ_2 = surface tension of the liquid-air surface

g = surface stress of the solid-liquid surface

g_1 = surface stress of the solid-air surface.

This condition of mechanical equilibrium is obtained on the assumption that the surface stresses are isotropic and that the strains are isotropic throughout. Also if we consider the melting to occur through a series of equilibrium states, since R is assumed constant, R' must be constant to maintain mechanical equilibrium. Consequently when some solid melts, the surface ADB is displaced normally to OC, maintaining constant curvature.

The stability of the system with respect to a continuous change of phase will depend on the change in free energy, when an actual change occurs. If external work must be done to procure the change, the equilibrium will be stable. Since the change in strain energy is ignored in this approximation, the change in free energy is given by the product of the changes in the surface areas and their free energy densities.

Let $\sigma_1, \sigma_2, \sigma$, s_1, s_2 and s be the surface free energy densities and surface areas of the solid-air, liquid-air and solid-liquid surfaces respectively.

If we therefore imagine some solid melting, the area of the solid-air surface decreases by Δs_1 and the liquid-air surface increases by Δs_2. Since we are assuming that the total surface area, AFBC, is constant, then $\Delta s_1 = -\Delta s_2$, and the free energy loss in the outside surface is $(\sigma_1 - \sigma_2)\Delta s_1$. If the change in the solid-liquid surface is Δs, then the gain in free energy at that interface is $\sigma \Delta s$. Since we have assumed that the liquid does not spread over the solid, $(\sigma_1 - \sigma_2)$ must be less than σ, so that in order for the change to occur, external work must be done providing Δs is positive. The equilibrium will therefore be stable as long as there is an increase in the solid-liquid surface on transference of solid to the liquid phase.

In Figure 45, if we consider a plane surface perpendicular to OC, cutting the sphere AFBC, at A and B, in the form of a circle, then AEBC, AEBD are spherical segments of height h,h' respectively, if EC=h and ED=h', and the radii of these spheres are R,R' respectively. The area of the solid-liquid surface, is

$$s = 2\pi R' h' \qquad (122)$$

because s is the area of the curved surface, ADB, of the spherical segment of height h' and radius of sphere R'.

If EC is equal to a,

$$a^2 = R'^2 - (R'-h')^2 \qquad (123)$$

because a is the radius of the base of this segment.

Similarly for the spherical segment ACB of height h, and the sphere radius R

$$a^2 = R^2 - (R-h)^2 \qquad (124)$$

Combining equations (123) and (124)

$$h' = R' - (R'^2 - R^2 - (R-h)^2\ )^{\frac{1}{2}} \qquad (125)$$

Substituting equation (125) in equation (122)

$$s = 2\pi R' (.R' - (R'^2 - R^2 - (R-h)^2)^{\frac{1}{2}} \qquad (126)$$

$$\therefore \quad \frac{\partial s}{\partial h} = \frac{4\pi R' (R-h)}{(R'^2-R^2- (R-h)^2)^{\frac{1}{2}}} \qquad (127)$$

The right side of equation (127) is positive when $h < R$, and negative when $h > R$. Therefore s will increase with increase in h, which occurs when some solid melts, until $h=R$. Then there is a decrease in s on further melting, and consequently the limiting condition of equilibrium occurs at this point. It may be noted that δs at this point is zero, to the first order, because $\frac{\partial s}{\partial h} = 0$ when $h= R$, from equation (127).

We may obtain the condition of equilibrium at this point, if we are ignoring the change in strain energy of the solid due to surface changes, in an analogous way to that used by Gibbs to obtain solid liquid equilibrium with respect to solution. Let us consider the crystal can be treated as an isotropic solid, and suppose that in an infinitesimal virtual change, the solid is unchanged except that an infinitseimal portion is dissolved at the surface, where the solid meets the liquid. If we consider the system enclosed in a rigid adiabatic sheath, the condition of equilibrium is given by

$$(\delta\varepsilon)_{\eta,\nu,m} = 0 \qquad (128)$$

where ε = total energy of the system

η = total entropy of the system

m = total mass of the system

ν = total volume of the system

Let the energy, entropy, and mass per unit volume of the solid and liquid be $\varepsilon_{1\nu}$, $\varepsilon_{2\nu}$, $\eta_{1\nu}$, $\eta_{2\nu}$, ρ_1 and ρ_2 respectively. Let the energy and entropy densities of the solid-air, liquid-air and solid-liquid surfaces be ε_{s1}, ε_{s2}, ε_s, η_{s1}, η_{s2}, and η_s respectively, where the dividing surfaces are placed so that their mass densities are zero.

The increments of energy, entropy and mass in the vicinity of the solid-liquid surface are represented by

$$(\varepsilon_{1\nu} - \varepsilon_{2\nu}) \quad s\,\delta h \quad + \xi_s \quad \delta s \tag{129}$$

$$(\eta_{1\nu} - \eta_{2\nu}) \quad s\,\delta h \quad + \eta_s \delta \, s \tag{130}$$

$$(\rho_1 \quad - \rho_2 \quad) \quad s\,\delta h \tag{131}$$

Where $-s\,\delta h$ is the volume of solid dissolved and δs is the change in the solid-liquid surface area. It was seen that at the point at which the equilibrium is considered $\delta s = 0$, so that the terms containing δs vanish. The entropy and mass represented by equations (130) and (131) we may suppose to be derived from the rest of the system, because the total mass and entropy are constant.

The change in energy in the rest of the system will be given by

$$\varepsilon_{s1} \quad \delta s_1 \quad + \varepsilon_{s2} \quad \delta s_2 \quad + \quad \delta \varepsilon_2 \tag{132}$$

where $\delta\varepsilon_2$ is the change in the energy of the liquid already present. Since its volume is assumed constant,

$$\delta\varepsilon_2 = t\delta\eta_2 + \mu_2 \delta m_2 \qquad \text{(Gibbs p.63)} \tag{133}$$

where $\delta\eta_2$, δm_2 are the changes in the entropy and mass which occur in this volume, and μ is the Gibbs potential of the liquid.

However, since the total entropy and mass are constant

$$(\eta_{1\nu} - \eta_{2\nu})\ s\delta h + \delta\eta_2 + \eta_{s1}\ \delta s_1 + \eta_{s2}\ \delta s_2 = 0 \qquad (134)$$

and $$(\rho_1 - \rho_2)\ s\,\delta h + \delta m_2 = 0 \qquad (135)$$

The total change of energy in this change is

$$\delta\varepsilon = (\varepsilon_{1\nu} - \varepsilon_{2\nu})\ s\delta h + \delta\varepsilon_2 + \varepsilon_{s1}\,\delta s_1 + \varepsilon_{s2}\,\delta s_2 \qquad (136)$$

But from the fundamental equation $\varepsilon = t\eta - P\nu + \mu m$, for unit volume

$$\varepsilon_{2\nu} = t\eta_{2\nu} - P_2 + \mu_2\rho_2 \qquad (137)$$

Therefore from equations (137), (132) and (133)

$$\delta\varepsilon = (\varepsilon_{1\nu} - t\eta_{2\nu} + P_2 - \mu_2\rho_2)\ s\delta h + t\delta\eta_2 + \mu_2\,\delta m_2 + \varepsilon_{s1}\,\delta s_1 + \varepsilon_{s2}\,\delta s_2 \qquad (138)$$

Substituting in equation (138) from equations (134) and (135), and rearranging

$$(\delta\varepsilon)_{\eta,m,\nu} = (\varepsilon_{1\nu} - t\,\eta_{1\nu} - \mu_2\rho_1 + P_2)\ s\delta h + (\varepsilon_{s1} - t\eta_{s1})\,\delta s_1 + (\varepsilon_{s2} - t\eta_{s2})\,\delta s_2 \qquad (139)$$

But $\varepsilon_s - t\eta_s = \sigma$ from equation (27), and since the total outer surface area is constant, $\delta s_2 = -\delta s_1$, for equilibrium

$$(\varepsilon_{1\nu} - t\eta_{1\nu} - \mu_2\rho_1 + P_2)\, s\delta h - (\sigma_1 - \sigma_2)\, \frac{\partial s_1}{\partial h}\, \delta h = 0 \tag{140}$$

But $$\varepsilon_{1\nu} - t\eta_{1\nu} = f_{1\nu} = f_{1m}\rho_1 , \tag{141}$$

where f_{1m} is the Helmholtz free energy of the solid per unit mass, and since $\mu_2 = f_{m2} + P_2/\rho_2$, where f_{m2} is the Helmholtz free energy of the liquid, per unit mass, equation (140) will be satisfied if

$$f_{1m} - f_{2m} + P_2\left(\frac{1}{\rho_2} - \frac{1}{\rho_1}\right) - \frac{(\sigma_1 - \sigma_2)}{\rho_1} \cdot \frac{1}{s}\left(\frac{\partial s_2}{\partial h}\right) = 0 \tag{142}$$

Therefore equation (142) represents the melting point condition of equilibrium. At this point, since $R' >> R$ we may, to a first approximation, consider the solid-liquid interface as plane, so that its area s is equal to πR^2. Therefore since $s_2 = 2\pi Rh$, $\frac{\partial s_2}{\partial h} = -2\pi R$

$$\frac{1}{s}\left(\frac{\partial s_2}{\partial h}\right) = -\frac{2}{R} \tag{143}$$

Substituting equation (143) in (142) the equilibrium condition becomes

$$f_{2m} - f_{1m} = \frac{2(\sigma_1 - \sigma_2)}{R\rho_1} + \frac{P_2}{\rho_2}\left(\frac{\rho_2}{\rho_1} - 1\right) \tag{144}$$

The form of equation (144) is identical to that of equation (71), except that in place of the solid-liquid surface free energy, there is now present the difference between the solid-air and the liquid-air surface free energies, $\sigma_1 - \sigma_2 = \bar{\sigma}$.

We may obtain in exactly the same way as in Section 4.1 of this Chapter, the relation between the equilibrium conditions of two crystallites of radius R, R+ΔR at their melting temperature T,T + ΔT. This yields the expression

$$\frac{\Delta T}{\Delta R} = \frac{\frac{2\bar{\sigma}}{R^2 \rho_1} - \frac{2\gamma_2}{R^2 \rho_1}\left(\frac{\rho_1}{\rho_2} - 1\right)}{\frac{L}{T_B}} \qquad (145)$$

as the pressure $P_2 = p_o + \frac{2\gamma_2}{R}$, where p_o is the external pressure. Equation (145) has exactly the same form as equation (101), for the uniform melting model, except that in the surface free energy term, $\bar{\sigma}$ is present in place of the solid-liquid surface free energy, and R in place lf R-λ. Since we may consider all terms in equation (145) as constant, except T and R, then integrating from T to T_B, and T to ∞ .

$$\int_T^{T_B} \Delta T = \frac{2T_B}{L\rho_1} (\bar{\sigma} - 15.5) \int_R^{\infty} \frac{\Delta R}{R^2} \qquad (146)$$

$$\therefore \quad T_B - T = \frac{2T_B}{L\rho_1} \quad (\bar{\sigma} - 15.6) \quad \frac{1}{R} \qquad (147)$$

Equation (147) predicts a straight line for the graph of T against $^1/R$. However the graphs in Figures 35 and 37 have already been seen to be non linear except for large values of R. When R is taken $\sim$ 1000 $\mathring{A}$, the value obtained for $\bar{\sigma}$ is

$$\bar{\sigma} = 55\ (1 \pm 0.1)\ \text{ergs/cm}^2 \qquad (148)$$

This is the same value as obtained for the solid-liquid surface free energy in equation (105).

In order to correlate the experinental results with the melting point equilibrium conditions of this model we have to introduce an intrinsic potential, as in the previous section. By considering adjacent points on the melting curve, we obtain a term of the form $\left(\frac{\Delta\Phi}{\Delta R}\right)_{M.C.}$, where Φ is dependent on the difference in the properties of these small phases from their bulk properties. However, Φ is now $\Phi\ (R,t)$ and not $\Phi\ (R-\lambda, T)$ as in the previous section, so that the relation for the melting curve becomes

$$\left(\frac{\Delta T}{\Delta R}\right)_{M.C.} = \frac{\frac{2}{R^2\rho_1}\ (\bar{\sigma} - 15.6) - \left(\frac{\Delta\Phi}{\Delta R}\right)_{M.C.}}{\frac{L}{T_B}} \qquad (149)$$

Substituting $\bar{\sigma}$ = 55 ergs/cm^2 in equation (149) a relation is obtained for the gradient, $\left(\frac{\Delta T}{\Delta R}\right)_{M.C.}$, in Figures 34 and 36 at different values of R. It was found that replacing the expression for $\left(\frac{\Delta \Phi}{\Delta R}\right)_{M.C.}$, obtained in the previous section i.e. $\left(\frac{\Delta \Phi}{\Delta R}\right)_{M.C.} = -\frac{A}{(R-\lambda)^3}$, by $\frac{A'}{R^3}$ did not yield the correct results. The gradients predicted by this form were too small, so a term in the form of a series expansion was tried. The type of expression which was consistent for the range of R studied was

$$\left(\frac{\Delta \Phi}{\Delta R}\right)_{M.C.} = -\frac{A'}{R^3} - \frac{B'}{R^4} \qquad (150)$$

If we substitute equation (150) in equation (149)

$$\left(\frac{\Delta T}{\Delta R}\right)_{M.C.} = \frac{2T_B}{L\rho_1} \cdot \frac{39.4}{R^2} + \frac{T_B}{L} \cdot \frac{A'}{R^3} + \frac{T_B}{L} \cdot \frac{B'}{R^4} \qquad (151)$$

Integrating equation (151) in exactly the same way as equation (115) the expression for the depression of the melting point of a crystallite is given by

$$T_B - T = \frac{2T_B}{L_1} \frac{39.4}{R} + \frac{T_B}{2L} \frac{A'}{R^2} + \frac{T_B}{2L} \frac{2}{3} \frac{B'}{R^3} \qquad (152)$$

where T is the melting temperature of a given crystallite and R its radius. From equation (152)

$$\frac{2L}{T_B}(T_B-T)R^2 - \frac{4}{\rho_1}\,39.4\,R = A' + \frac{2}{3}\,\frac{B'}{R} \qquad (153)$$

Obtaining T_B-T from Figures 34 and 36, and plotting from equation (153), $\Psi' = \frac{2L}{T_B}(T_B-T)R^2 - \frac{4}{\rho_1}\,39.4\,R$ against $1/R$, the graph shown in Figure 47 is obtained. This is a straight line where the intercept

$$A' = 1.45 \pm 0.05\ 10^{-5} \text{ ergs gm}^{-1} \text{ cm}^2 \qquad (154)$$

and the gradient

$$\frac{2}{3}\,B' = 5.3\,(1\pm 0.1)\ 10^{-12} \text{ ergs gm}^{-1} \text{ cm}^3 \qquad (155)$$

$$\therefore \quad B' = 7.95\,(1 \pm 0.1)\ 10^{-12} \text{ ergs gm}^{-1} \text{ cm}^3. \qquad (156)$$

Therefore the deviation from the properties of the bulk phases increases as the size of the crystalite decreases. The decrease in the free energy difference between the solid and liquid, when the solid crystallite has a radius 100 Å, would be equivalent to an increase of ~12% in the solid-air surface free energy, if the liquid surface free energy is assumed constant.

Figure 46. Graph of Ψ against $1 / (R - \lambda)^2$, obtained from the first theoretical model of melting, where R is the outside radius of the liquid shell and λ = 20 Angstroms.

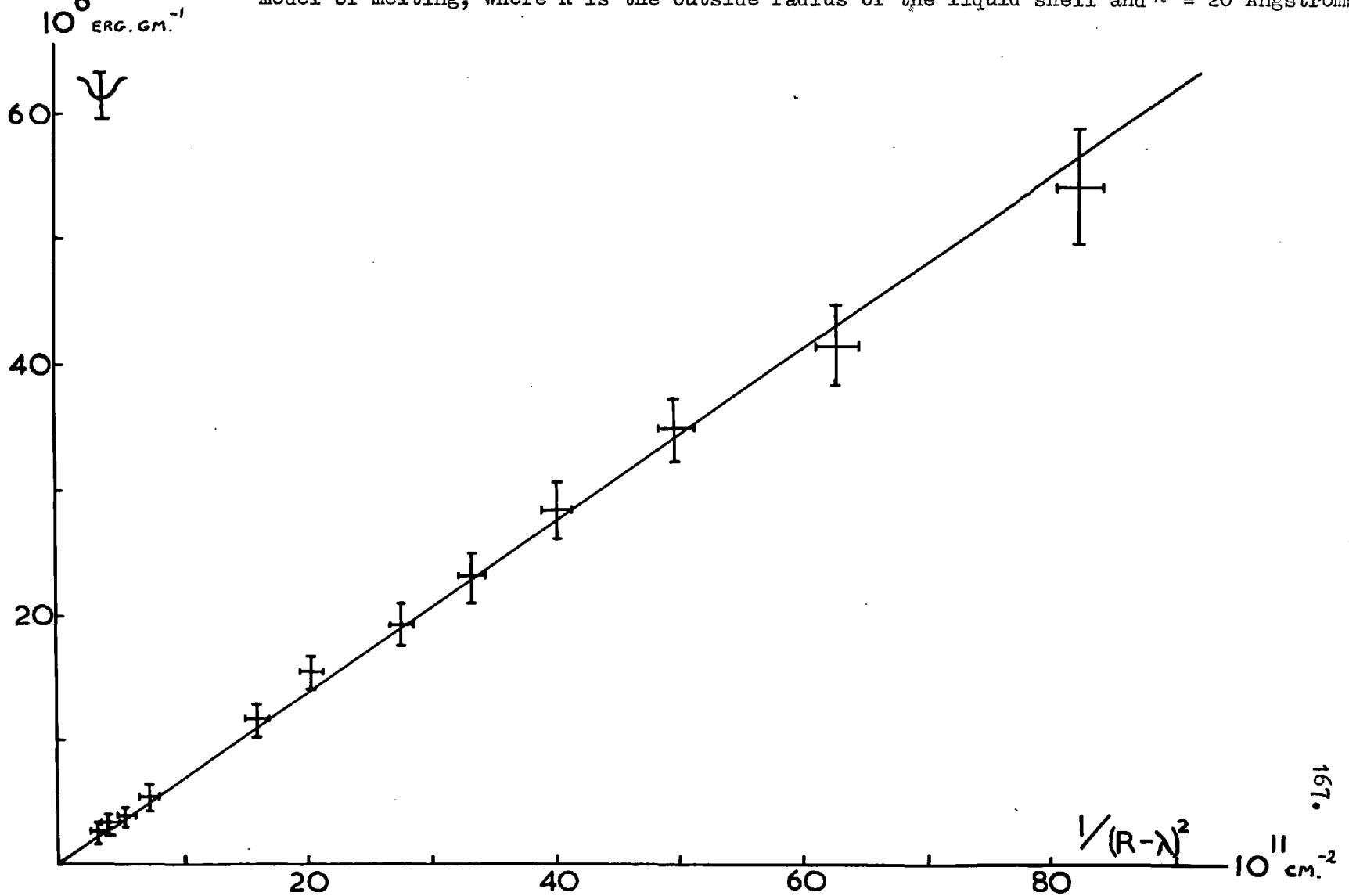

Figure 47. Graph of Ψ' against 1/R, obtained from the second theoretical model of melting, where R is the radius of the crystallite.

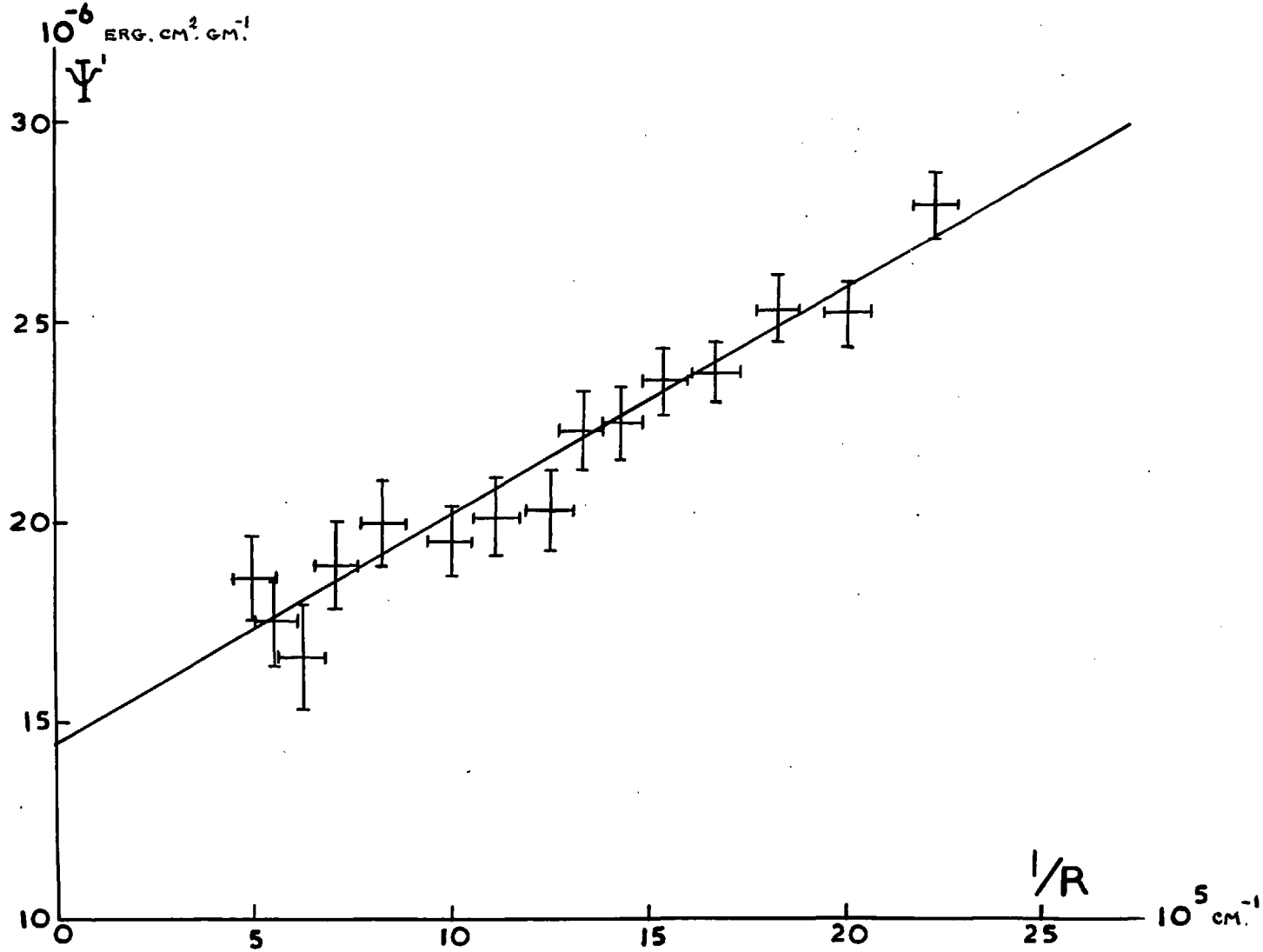

5. Discussion of the Theoretical Treatment of the Experimental Results.

The above considerations have shown that the results of the experiments may be interpreted in terms of two different theoretical models. In the development of these theories it has been assumed that the substrates have no effect on the results. This appears reasonable since the experimental results for tin crystallites on silicon monoxide and on carbon substrates are the same, within the experimental error. This would not have been likely if the substrate had had a significant influence on the behaviour of the crystallites.

Since each crystallite was spherical, its area of contact with the base was small in comparison with its total area and it is reasonable to suppose that the substrate did not, in fact, have any effect on the melting of the tin. In this case a theory based on spherical symmetry may be used. This is the basis of the first theoretical model. However, the point of contact with the base represents a small break in the symmetry of the crystallite, and its possible that the melting commences at the point of contact with the base. This is the underlying assumption of the second model. In both models the transfer of matter from one phase to the other reaches a limiting equilibrium condition, after which there is a catastrophic collapse of solid to liquid. This limiting condition of equilibrium is taken to be the melting point.

In the first model, the temperature T_R, obtained from the experiments, corresponds to the melting point of the solid core of radius $R-\lambda$, where λ is the thickness of the shell at the melting point equilibrium. The

contribution of this shell to the diffraction patterns from which T_R is calculated were neglected because of the thinness of the shell, and in addition the temperature range over which this shell exists is expected to be small. Therefore the presence of the shell does not affect the measurement of T_R. The value of the parameter λ occuring in this model was found, by the method indicated in section 4.2. of this chapter, to be 20 Å. As this is of the order of seven atomic layers, the assumption that the liquid had acquired bulk properties at this thickness would seem to be justifiable. The theoretical results from this model expressed in terms of the solid-liquid surface free energy can be obtained from the gradient of the melting curve at large values of R. The value obtained was 55 ± 5 ergs/cm^2, which is in good agreement with the value obtained by Turnbull.

In the second model the temperature T_R obtained from the experiments, corresponds simply to the melting point of a crystallite of radius R. In the calculation based on this model the strain energy was omitted and the geometry simplified by neglecting the density change on melting. The strain energy may be omitted since it has been shown to be small compared with the surface free energy. Although there is no justification for ignoring the change in density, the form of the equilibrium condition would be very similar to that already obtained, since this density difference is very small. This model has the advantage of representing the melting point curve in terms of a single parameter. The term that appears in the condition for melting equilibrium contains, in this case,

the difference between the solid-air and liquid-air free energies. If the solid-liquid surface free energy, σ, is very nearly equal to the difference between the solid-air and liquid-air surface free energies, $\bar{\sigma}$, the melting point, or limiting, equilibrium will be reached very soon after the liquid nucleus has formed. Because of the rapidity of this transformation from solid to liquid, it will be difficult to obtain diffraction patterns which show features consistent with a partly solid and partly liquid state. The value of the difference between the bulk solid-air and liquid-air surface free energies, can be calculated from the melting curve. The value obtained was again 55 ± 5 ergs/cm^2. This indicates that the assumption of the near equality of σ and $\bar{\sigma}$ is justified, but the error is too large to estimate the value of the difference between σ and $\bar{\sigma}$.

CONCLUSION

The experiments described in this thesis enable the melting point of a spherical tin crystallite to be related to its size. The dependence of the melting point of a crystallite on its size can be explained by the effect of its surface properties on the interior. The depression of the melting point calculated by the normal macroscopic free energy methods is not in agreement with the experimental results, and to explain this it has been necessary to postulate a change from the bulk properties of tin for particles whose radii are less than 200 Å. This change can be represented by an extra term in the equilibrium condition in the form of an intrinsic potential. This term represents all changes from the bulk thermodynamic properties which occur in the solid and liquid phases consequent to the reduction of the particle size; for example free energy per unit mass, latent heat per unit mass and surface free energy per unit mass.

The effect of this additional potential on the melting point has been considered in the two models used. In both the models this potential gives rise to a further term, in addition to the bulk surface free energy, in the expression for the depression of the melting point as a function of radius, and this term is found to be a function of the radius measured along the melting curve. In the first model this term was of the form $\frac{A}{(R-\lambda)^2}\frac{T_B}{L}\,^{o}C$, where $A = 6.85\ (1\pm0.1)\ 10^{-6}$ erg. gm.$^{-1}$ cm.^{2}

and $\lambda = 20$ Å. In the second model the additional terms, were of the form $\left(\frac{A'}{R^2} + \frac{2C'}{3R^3} \right) \frac{T_B}{2L}$, where $A' = 1.45\ (1\pm0.4)\ 10^{-3}$ erg. gm.$^{-1}$ cm.^{2}, and $C' = 5.3\ (1\pm0.1)\ 10^{-12}$ erg. gm.$^{-1}$ cm.^{3}

Good agreement with the experimental results was obtained in both cases, but there is not enough experimental evidence to indicate which of these two models represents the true melting mechanism. There is strong experimental evidence, however, to suggest that there is a fundamental change in the free energies of particles whose radii are below ~150 Å, which cannot be explained by stress effects, as the corresponding density change would have been observed experimentally, nor by the effect of the normal bulk surface free energy. Since the results obtained using silicon monoxide and carbon substrates are the same, it is also concluded that an amorphous base does not influence the melting point of spherical tin crystallites.

A C K N O W L E D G E M E N T S

The author would like to express his extreme gratitude to Professor M. Blackman for his most valuable advice, guidance and criticisms concerning this work which was performed at his suggestion, and under his supervision. The author would also like to thank all the members of the Electron Diffraction Group at Imperial College, and in particular Dr. N.D. Lisgarten and Dr. A.E. Curzon for their interest, help and useful discussions, and Mr. T.E. Gallon for assistance in the preparation of this thesis. In addition to the above, thanks are due to Mrs. M.E. Aviss for the help given in the typing of this thesis and the Department of Scientific and Industrial Research for a maintenance award.

Finally the author wishes to express his gratitude to Miss L.M. Verbeek for her constant help and encouragement in all phases of this work.

§§§§§§§§§§§§§§§§§§§§§§

REFERENCES

APPLEYARD, E.T.S., 1937, Proc. Phys. Soc., Lond., Extra part 49., 118.

BAKKER, G., 1928, Hand. der. Expt. phys., 6, (Leipzig: Akad. Verlog).

BASSET, G.A., Menter, J.,W., and PASHLEY, D.,W., 1959,
"Structure and Properties of Thin Films".
(Proc. of Int.Conf. held in New York, Wiley and Sons) 11..

BIJL, A.J., (1918) (See Bijl,A.,J., and KELKEMEIJER, N.,H.,)

BIJL, A.J. and KELKMEIJER N.H.,
1918, Chem. Wekblad, 15, 1264
1919,a, Proc. Acad.Sci. Amsterdam, 21, 405
1919,b, Proc. Acad.Sci. Amsterdam, 21, 501

BLACKMAN,M., and CURZON A.E., 1959,
"Structure and Properties of Thin Films".
(Proc. of Int. Conf. held in New York, Wiley and Sons) 217.

BONFLIGLIOLI,G., FERRO,A, and MONTALENTI G., 1952,
Paris Conference of Phase Changes.

BORN, M., 1939, J. Chem. Phys., 7, 591

BRADLEY, D.E., 1954, Bri. J. App. Phys., 5, 65.

BRIDGMAN, P.W., Proc. Am. Acad. Arts.
Sci., 60, 305.

BUBLIK, A.I., and PINES B., Ya., 1952,
Dokl. Akad. Nauk. S.S.S.R., 87, 215.

COSTER and VAN LANTEN, 1939, Physica, 6, 17.

CURIE, P., 1885, Bull. Soc. min. de France, 8, 145.

CURZON, A.E., 1960, (See Curzon, A.E., 1959).

CURZON, A.E., 1959, Ph.D. Thesis, London.

FRANK, F.,C., 1939, Proc. Roy. Soc., A, 170, 182.

FOWLER, R.H., and GUGGENHEIM, E.A., 1939,
"Statistical Thermodynamics" (C.U.P.).

FURTH, R., 1941, Camb. phil. Soc., 37, 34, 177.

GIBBS (see GIBBS J.W., 1928).

GIBBS, J.W. 1875-78. (see GIBBS J.W., 1928).

GIBBS, J.W., 1928. "The Collected Works of J.Willard Gibbs". 1. (New York: Longmans Green and Co. 55-353) Sp. pp. 219-331.

GUGGENHEIM, E.,A., 1957, "Thermodynamics" (Nth.Hol.Pub.Co., Amsterdam)

GREENWOOD, 1952, Proc. Roy. Soc., 215, 47.

HART, R.K., 1952, Proc. Phys. Soc., 13, 65, 955.

HEDGES, E.S., and HIGGS, J.V., 1952, Nature 169, 621

HERRING, C., 1950, (See HERRING,C., 1950,a).

HERRING, C., 1950,a, "Surface Tension as a Motivation for Sintering", in "The Physics of Powder Metallurgy", ed. Kingston, W.E., (New York: McGraw-Hill Book Co).

HERRING,C., 1952, "The Use of Macroscopic Concepts in Surface Energy Problems" in "Structure and Properties of Solid Surfaces". ed. Gomer,R., and Smith,C., (Univ. of Chi. Press).

HOLLAND,L., 1956, "Vacuum Deposition of Thin Films" (Lond.Chap. and Hall Co.).

JENKINS, R.,O., 1935, Proc. Roy.Soc., 47, 109

JETTE,E.R., and FOOTE,F., 1935, J.Chem.Phys. 3, 605.

JEVINS,A., STRAUMANIS,M., and KARLSONS,K., 1938, Z. Phys. Chem., 40B, 347.

KELLY,K., 1949, U.S. But. Mines. But., 383.

KEHOE, R.,B., 1956, Ph.D. Thesis, London.

KEHOE,R.,B., Newman, R.,C., and PASHLEY,D.,W., 1954, J.Sci.Inst., 31, 399.

KESITA, Mem. Coll. KEYATO. Univ., 17, 32.

KIRKWOOD, J.,G., and BUFF,F.,P., 1949, J.Chem. Phys., 17, 338.

KLEPPA, O.,J., 1950, J. Chem. Phys., 18, 1331.

KOSLAPOV, G.,F., and Trapeznikov, A.,K., 1936,
Zeit. f. Krist., 94A, 53.

KUNSDEN,M., 1909, Ann. Phys. Lp2., 28, 999.

LANGMUIR, I., 1917, Proc. Nat. Acad. Sci. Wash., 3, 141.

LENNARD JONES, J.E., and DENT, B.,M., 1928,
Proc. Roy. Soc., A, 121, 247.

LENNARD JONES,J.E., and DEVONSHIRE, A.F.,
1939a, Proc. Roy.Soc., A, 169, 317.
1939b, Proc.Roy.Soc., A, 170, 464.

LENNARD JONES, J.E., 1937, Proc. Phys. Soc.,
Lond., Extra part 49; 140.

LINDEMANN,A., F., 1910, Phys. Z., 11, 609.

MACLELLAN, A.,G., 1952, Proc. Roy. Soc., A213, 274.

MATUYAMA, 1927, Sci. Rep. Tohaku. Imp. Univ. 16, 555.

MEISSNER, F., 1920, Zeit.f. anorg. und. allg. Chem., 110, 169.

NEWMAN, R.,C., 1955, Ph.D. Thesis, London.

NICOLSON, M.,M., 1950, (See Shuttleworth, R., 1950).

OROWAN, E., 1932, Zeit. f. Physik., 79, 573.

PAVLOV,P., 1909, Z. physik. Chem., 65, 1.

PINSKER, Z.,G., 1953, "Electron Diffraction", (London: Butterworths).

RICHTER, H., 1943, Phys. Z., 44, 406.

REISS, H., and WILSON,I.,B., 1948, J.Colloid.Sci., 3, 551.

SAYAMA, Y., 1941, Proc.Phys.- Math.Soc., Japan, 23, 869.

SENNET, R.,S., MCLAUCHLAN, T.,A., and SCOTT, G.,D., 1952, Canad. J. Phys., 30, 370.

SHUTTLEWORTH, R., 1950, Proc. Phys. Soc., A63, 444.

SMAKULA,A., and KALNAJAS,J., 1955, Phys. Rev., 99, 1737.

STAHL, H.,A., 1949, J.Appl. Phys., 20, 1.

TAKAGI, M., 1954., J. Phys. Soc. Japan, 9, 359.

TEMPERLEY, H.,E.,V., 1956, "Changes of State", (Cleaver Hume Press, Lond.).

THOMSON, G.,P., and COCHRANE,W., 1939, "The Theory and Practice of Electron Diffraction". (London: Macmillan & Co., Ltd.).

TOLMAN, R.,C., 1948, J. Chem. Phys., 16, 758.

TOLMAN, R.,C., 1949, a, J. Chem. Phys., 17, 118.

TOLMAN, R.,C., 1949,b, J. Chem. Phys., 17, 333.

TURNBULL, D., 1950, J. Appl. Phys., 21, 1022.

VONNEGUT,B., 1948, J. Colloid. Sci., 3, 563.

WAGNER,S., and STAHL,H., 1943, Z.Tech.Phys., 24, 280.

WINKELMANN,A., 1956, Z. agnew. Phys., 8, 218.

WOOD, R.,W., 1915, Phil. Mag., 30, 300.

WOOD. R.,W., 1916, Phil. Mag., 32, 364.

WULFF,G. 1901, Zeits.f. Kristallog., 34, 449.

WYCKOFF, R.,W.,G., 1948, "Crystal Structures", Section I (New York : Interscience Publishers Inc).